Combustion Optimization in a Hydrogen-Enhanced Lean Burn SI Engine

by

Joshua A. Goldwitz

B.S., Mechanical Engineering
Massachusetts Institute of Technology, 2002

Submitted to the Department of Mechanical Engineering
in Partial Fulfillment of the Requirements for the Degree of
Master of Science in Mechanical Engineering

at the

Massachusetts Institute of Technology
[June 2004]
May 7, 2004

Signature of Author .....
Department of Mechanical Engineering
May 7, 2004

Certified by .....
John B. Heywood
Sun Jae Professor of Mechanical Engineering
Thesis Advisor

Accepted by .....
Ain A. Sonin
Professor, Department of Mechanical Engineering
Chairman, Department of Graduate Committee

(This page was intentionally left blank.)

Combustion Optimization in a Hydrogen-Enhanced Lean Burn SI Engine

by

Joshua A. Goldwitz

Submitted to the Department of Mechanical Engineering
on May 7, 2004 in Partial Fulfillment of the
Requirements for the Degree of Master of Science in
Mechanical Engineering

Abstract

Lean operation of spark ignition (SI) automotive engines offers attractive performance incentives. Lowered combustion temperatures inhibit NO_x pollutant formation while reduced manifold throttling minimizes pumping losses, leading to higher efficiency. These benefits are offset by the reduced combustion speed of lean mixtures, which can lead to high cycle-to-cycle variation and unacceptable engine behavior characteristics. Hydrogen-enhancement can suppress the undesirable consequences of lean operation by accelerating the combustion process, thereby extending the "lean limit." Hydrogen can be produced onboard the vehicle with a plasmatron fuel reformer device.

Combustion optimization experiments focused on three key areas: the ignition system, charge motion in the inlet ports, and mixture preparation. The ignition system tests compared a standard inductive coil scheme against high-energy discharge systems. Charge motion experiments focused on the impact of turbulence patterns generated by conventional restrictor plates as well as novel inlet flow modification cones. The turbulent motion of each configuration was characterized using swirl and tumble flow benches. Mixture preparation tests compared a standard single-hole pintle injector against a fine atomizing 12-hole injector. Lastly, a further series of trials was also run to investigate the impact of high exhaust gas recirculation (EGR) dilution rates on combustion stability.

Results indicate that optimizations of the combustion system in conjunction with hydrogen-enhancement can extend the lean limit of operation by roughly 25% compared against the baseline configuration. Nearly half of this improvement may be attributed to improvements in the combustion sys[illegible]. An inductive ignition system in conjunction with a high tumble-motion inlet configuration leads to the highest levels of combustion performance. Furthermore, hydrogen enhancement affects a nearly constant absolute improvement in the lean misfire limit regardless of baseline combustion behavior. Conversely, the amount of improvement in the point of peak engine NIMEP output is inversely related to the level of baseline performance.

Thesis Advisor: John B. Heywood
Title: Sun Jae Professor of Mechanical Engineering

(This page was intentionally left blank.)

Acknowledgements

Thinking back on the past two years, I am struck by just how many people have generously contributed their time, support, and resources toward helping me complete this thesis.

Firstly, I would like to thank Prof. John B. Heywood for his advising and guidance. In taking Prof. Heywood's internal combustion engines course as a MIT undergrad, I came to appreciate his extensive technical knowledge and became interested in further study within the field. Working alongside Prof. Heywood as a MIT graduate, I have been most touched by his professional integrity and deliberate demeanor. I hope to carry these same ideals with me as I now embark on my own career.

My other colleagues at MIT Sloan Lab have also contributed toward a tremendous experience. I am grateful for the friendship and camaraderie I shared with Ziga Ivanic. From trying to get the EGR system to work to hanging out at the beach, there are too many memories to count. Mike Gerty and Jenny Topinka also made the plasmatron experience enjoyable; we really did make for an interesting group of characters. Special thanks to Ed Tully- besides laying the groundwork for my engine experiments, he has provided me with a lot of guidance and continued friendship. To all of the other Sloan Labbers too numerous to mention, thanks for everything…

Further appreciation goes to the MIT Plasma Science Fusion Center staff- Leslie Bromberg (I really thought the Mexican food in Albuquerque was pretty good,) Dan Cohn, and Alexander Rabinovich. ArvinMeritor has provided essential funding and support for this project and it will be very interesting to see how the firm takes plasmatron technology out of the lab and onto the roads. Our contacts at Arvin, including collaborators Rudy Smaling and Navin Khadiya, have provided us with vital "real world" perspective. A big debt of gratitude goes to Chris Thomas, Cliff Kratzet, and Tim Connolly (and Jeff and Ed) at the DaimlerChrysler Technical Center. I had a great time during my visit and the flow bench data I obtained has immeasurably contributed toward my final conclusions. Ed Van Dyne of Adrenaline Research has been very generous in providing me with the use of one of his ignition systems and I also enjoyed our conversations on entrepreneurship and the business side of the auto industry. Carilee Cole of Delphi was kind in providing me with a fine-atomizing fuel injector. Her contribution came about through my participation in the MIT Engine and Fuels Research Consortium; I feel very fortunate to have participated in such a unique collaboration between academia and industry.

In addition to all those aforementioned that rendered professional assistance, I am so lucky to have had the support of some of the best family and friends anybody could ever ask for. To my parents and sister, thank you for your unwavering love and guidance. My girlfriend Claire Lévy has also brightened these past two years in so many ways. Out of all the friends I have made in six years at MIT, the word "friend" probably doesn't do justice to Grant Kristofek, Karl McLetchie, Miguel Ferreira, Vijay Divi, and the Castigliones. And to my guys from back home in Brooklyn- Anthony Capalbo, Jared Jagdeo, Jen Yim, Mike Stein, Petros Benias, Seth Rakoff, and Victor Buonocore, thanks for everything. We have had many great years and I look forward to many more to come.

(This page was intentionally left blank.)

Table of Contents

(This page was intentionally left blank.)

List of Tables

(This page was intentionally left blank.)

List of Figures

(This page was intentionally left blank.)

Chapter 1: Introduction and Background

1.1 Advanced Automotive Powerplants

After more than 100 years of research and development, the internal combustion engine (ICE) remains the powerplant of choice for nearly all automobiles on the road. Based upon the spark ignition (SI) Otto cycle or the compression ignition (CI) Diesel cycle, the ICE has proven to be a reliable and efficient choice with unmatched power to weight efficiency.

In recent years, there has been a shift toward exploring new technologies that will bring greater fuel efficiency with reduced emissions. The need for such developments has taken on a greater sense of urgency in light of tightening emissions regulations (Euro V / EPA 2007) and the double-digit growth of automobile sales in developing markets such as China. Some powertrain concepts, such as hydrogen-powered fuel cells, represent a fundamental paradigm shift. Others, such as hybrid-electrics, clean Diesels, or the hydrogen-enhanced lean burn SI (HLSI) system to be explored in this thesis leverage established ICE technology.

HLSI is a unique solution that addresses the competing demands of future vehicle powerplants. By coupling the efficiency of a lean burn SI operating cycle with the emissions benefits of homogeneous lean combustion, it is possible to achieve low consumption and minimized environmental impact. Most importantly, HLSI is a realistic near-term solution that builds upon mature engine technology, utilizes the existing gasoline infrastructure, and is completely transparent to the vehicle operator.

1.2 Hydrogen-Enhanced Lean Burn SI (HLSI) Concept

HLSI merges familiar powerplant technology with a new type of hydrogen reforming device to deliver high efficiency with low emissions. The system combines several attributes to address relevant technological challenges and successfully meet high-level performance goals.

1.2.1- Homogeneous Charge Lean Burn Cycle

The HLSI system is built around a homogeneous charge lean burn cycle. A homogeneous mixture (typical of a SI engine,) encourages more complete and uniform combustion, minimizing unburned hydrocarbon emissions (*HC*). Lean burn provides further benefits by reducing peak combustion temperatures. This discourages the highly temperature-dependent NO_x formation mechanism, helping to further curb emissions. Additionally, a lean cycle (typical of a CI engine) provides a cycle efficiency benefit by reducing pumping losses [1]. This comes from the fact that lean engines admit higher amounts of air to combust a given amount of fuel, requiring a corresponding increase in inlet manifold air pressure (MAP).

Combustion of a lean air-fuel mixture presents several challenges. There is a marked decrease in the laminar flame speed of a typical hydrocarbon at high lambda values. At a certain lambda value, the mixture will reach a point of inflammability and a spark discharge will no longer be able to initiate a propagating flame kernel. CI engines and stratified charge SI engines address this issue by initiating combustion in locally rich pockets within an inhomogeneous mixture that is globally lean. The problem with this approach is that NO_x formation rates will still be high in the areas of rich combustion and incomplete combustion of the rich pockets encourages *HC* emissions. In order to preserve the NO_x-inhibiting characteristics of true lean combustion, it is necessary to combust a homogeneous mixture. This can be facilitated through the use of hydrogen enhancement.

1.2.2- Hydrogen Enhancement

Hydrogen has a fast laminar flame speed and can be used to enhance the combustion characteristics of lean hydrocarbon-air mixtures. As early studies have clearly indicated [2, 3], hydrogen addition offsets the slow burning tendencies of lean mixtures (Figure 1.2.2), promoting greater combustion speed and stability. Hydrogen enhancement makes it possible to operate a lean burn engine at higher lambda values than can be achieved with non-enhanced mixtures. Hydrogen can be generated onboard the vehicle in a plasmatron fuel reformer device. Inside this reformer, a continuous plasma arc is used to partially oxidize a rich gasoline-air mixture.

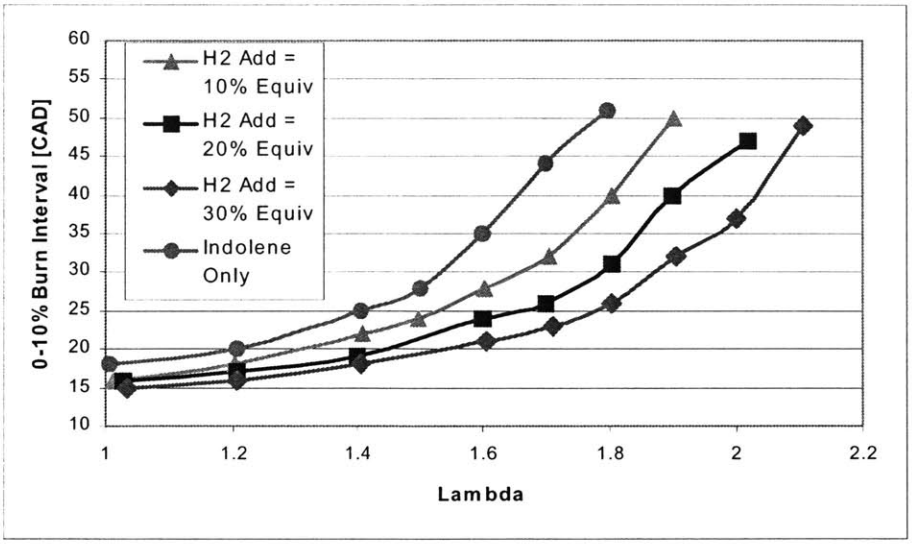

Figure 1.2.2- 0-10% Lean Mixture Burn Speed with Different Fractions of H_2 Addition [4]

1.2.3- High Compression Ratio/ Boosted Operation

Hydrogen enhancement provides a further benefit to the HLSI system. Research at MIT [5] has demonstrated that hydrogen addition has a knock-inhibiting effect, promoting a higher effective fuel octane rating. Enhancement with 15% of the gasoline reformed roughly corresponds to an effective octane number increase of 10 over the baseline hydrocarbon. This could allow for an increase of roughly two compression ratio units. Furthermore, this knock resistance makes the enhanced engine ideally suited to inlet boosting. The combination of a boosted manifold and/or a higher compression ratio could allow for a more efficient, downsized displacement engine [6].

1.2.4- Optimized Combustion System

In order to extract the full potential of the HLSI system, optimization of the combustion system is necessary. This thesis explores various types of ignition systems, inlet port motion control devices, and fuel injectors to determine the best performing parameters. As the results will show, combustion system design complements hydrogen enhancement by affecting large changes in the lean misfire limit and combustion speed.

1.2.5- High EGR Tolerance

High concentration (> 20%) exhaust gas recirculation (EGR) can provide many of the same benefits as lean operation. EGR reduces *HC* exhaust emissions by allowing for further oxidation

of unburned *HC* while also lowering combustion temperatures to inhibit NO_x formation. Additionally, EGR increases the mass flow rate through the cylinder, reducing pumping losses. However, high concentrations of recirculated exhaust can also drastically slow combustion speed, similar to the excess air dilution of lean operation. The improved flame speeds that accompany hydrogen enhancement offset this tendency, increasing EGR tolerance.

1.2.6- Performance Summary

A table has been prepared to summarize the performance goals of the HLSI system and which specific attributes address each goal (Table 1.2.6).

Table 1.2.6- Summary of HLSI Parameters

Goal	*Design Feature*
High Efficiency	Lean Cycle, Possible Downsizing/ Boosting, High EGR Tolerance
Extended Lean Limit	Hydrogen Enhancement, Optimized Combustion System
Low *HC* Emissions	Homogeneous Charge, High EGR Tolerance
Low NO_x Emissions	Lean Stoichiometry, Homogeneous Charge, High EGR Tolerance
Knock Resistance	Hydrogen Enhancement

1.3 Plasmatron Fuel Reformer

The plasmatron fuel reformer is the key new technology in the HLSI system. The device is being developed at the MIT Plasma Science and Fusion Center (MIT PSFC). It uses a continuous plasma arc discharge to partially oxidize a rich hydrocarbon-air mixture in an exothermic reaction (Equation 1.3.1).

$$C_mH_n + \frac{m}{2}(O_2 + 3.773N_2) \rightarrow mCO + \frac{n}{2}H_2 + \frac{m}{2}\cdot 3.773N_2 \qquad (1.3.1)$$

This reaction represents the theoretical ideal; in actual operation, there are small amounts of H_2O and CO_2 also present in the reformate gas (Table 1.3.1).

Table 1.3.1- Ideal and Typical Plasmatron Characteristics

Parameter	*Ideal Plasmatron*	*Typical Plasmatron*
H_2	25%	20%
CO	26%	22%
N_2	49%	51%
CO_2	0%	2%
H_2O	0%	4%
HC	0%	< 1%
Fuel Conversion Efficiency	84%	76.5%

It is important to note the presence of significant quantities of CO in the reformate gas. Although CO does not have a very fast laminar flame speed (Table 1.3.2), it does have desirable octane enhancing effects similar to hydrogen [5].

Table 1.3.2- Combustion Characteristics of Different Fuels [7]

Fuel	*Flame Speed (100°C, 1 atm)*		*Spontaneous Ignition Temp. [°C]*
	Stoichiometric	*Maximum*	
Isooctane	57.8	58.2	447
N-Heptane	63.8	63.8	247
Hydrogen	170.0	325.0	572
Carbon Monoxide	28.5	52.0	609

The plasmatron reformer will require an energy supply to power the plasma discharge. Consumption should be on the order of 5-6 MJ/kg H_2. Much work is being undertaken to improve the energy conversion efficiency, η_{plas}, of the reformer (Equation 1.3.2) as this parameter directly impacts the overall energy conversion efficiency of the aggregate system.

$$\eta_{plas} = \frac{\dot{m}_{H_2} \cdot LHV_{H_2} + \dot{m}_{CO} \cdot LHV_{CO}}{\dot{m}_{indolene} \cdot LHV_{indolene}} \tag{1.3.2}$$

where $\dot{m}_x$ indicates mass flow rate and LHV_x indicates lower heating value.

1.4 HLSI System Architecture

In the HLSI system, the majority of the gasoline (typically 70-90%) is injected into the inlet ports much as it would be in a conventional SI powertrain. The balance is routed through the plasmatron reformer device where it is converted to hydrogen-rich reformate gas. This reformate is then introduced into the engine intake system several critical lengths upstream of the inlet ports to assure homogeneous mixing. Typically, hot reformate will pass through a plasma intercooler en route to the inlet manifold to help maintain charge efficiency. In this system schematic (Figure 1.4), a turbocharger and charge intercooler are also depicted. This is representative of the probable downsized and boosted implementation.

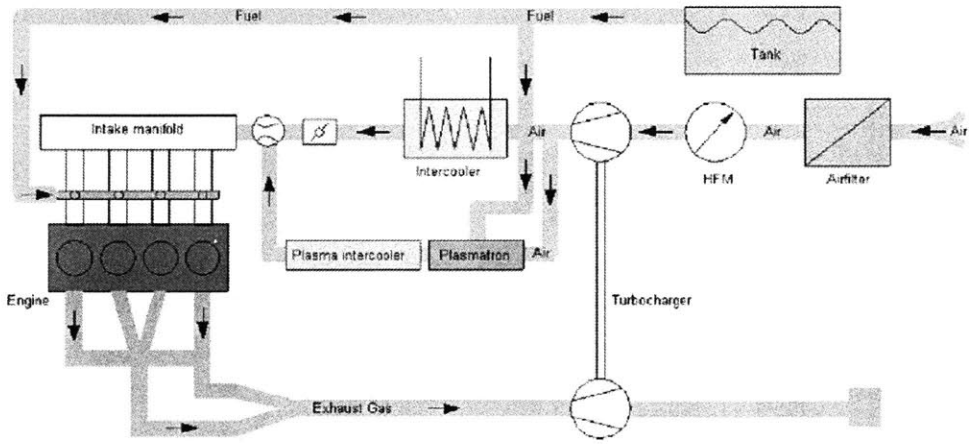

Figure 1.4- Boosted HLSI System Schematic

1.5 Combustion Optimization

By improving the combustion performance of the HLSI system as much as possible, the greatest emissions and efficiency benefits will result. There are a number of techniques available for improving combustion performance and several will be explored in this thesis.

1.5.1- Benefits of Optimized Combustion

As discussed earlier, reliable combustion of lean air-fuel mixtures is difficult because of problems with inflammability and low laminar flame speed. An optimized combustion system is one that addresses these challenges as effectively as possible and may be characterized by:

- Reliable Combustion- Low incidence of misfire or partial burn cycles
- Low Variability- Acceptably low fluctuation of cycle to cycle NIMEP (low COV)
- Fast Burning- Short mass fraction burned intervals (ex- 0-10%, 10-90%)
- Extended Lean Limit- Peak of NIMEP and misfire limits occur at high lambda values

Each of these characteristics is required, respectively, to achieve:

- Compliance with emissions standards
- Acceptably smooth engine performance and drivability
- High efficiency and consequent output (faster burn approaches constant-volume ideal)
- Maximized benefits of lean operation

In particular, within the lean operating regime, the properties of an optimized combustion system help to offset the slow burning and difficult to ignite tendencies of lean mixtures. This complements and extends the effects of hydrogen enhancement.

1.5.2- Ignition System

In a SI engine, the ignition system is needed to initiate a propagating flame kernel within the air-fuel mixture. This is accomplished by means of an electrical breakdown, which heats a small region of mixture to a plasma state (~ 60,000 K), initiating reaction chemistry. The high voltage needed to accomplish this breakdown is usually generated through an inductive coil. In some

specialized systems, a more efficient capacitor-based circuit topology may be used. The discharge characteristics of these two systems is somewhat different; capacitor based systems are able to achieve higher peak discharge currents and voltages while inductive systems tend to have longer discharge time constants. Some capacitor-based "multistrike" ignition systems are able to discharge more than one spark per engine cycle. Careful consideration must be given to the geometry of the spark plug electrodes. A higher number of electrodes provides more breakdown paths to ground (although only one is taken per discharge event,) however, these also provide more pathways for heat loss.

Prior research [8, 9] has suggested that lean combustion performance is best when a platinum-tipped thin-electrode "J" type plug is used in combination with an inductive coil ignition. This has been attributed to the minimized heat-losses of a thin-electrode plug [10] and the longer spark duration of coil ignitions, which is required to ignite lean mixtures [11].

1.5.3- Charge Motion Control

In-cylinder flow behavior of the air-fuel charge has a large impact on combustion performance. This impact is magnified under difficult high-dilution combustion conditions, where localized turbulence near the spark plug gap impacts flame kernel initiation [12] and broader turbulence characteristics affect laminar flame speed [13]. In-cylinder charge motion may be broadly characterized as either swirling or tumbling (Figure 1.5.3). Swirl motion describes rotation of the flow about an axis along the cylinder bore and is encouraged by introducing the charge with a tangential velocity component. Tumble is a barrel rolling flow pattern that tends to roll from the inlet ports down to the piston crown; introducing the charge with a large velocity component perpendicular to the cylinder axis may encourage this. One study [14] found that tumble motion generates higher levels of turbulent intensity than swirl, although excessive tumble could also lead to flame extinction in localized areas. Prior work at MIT has shown that enhanced charge motion can stabilize combustion in the lean regime [2]. Other lean combustion studies have reached similar conclusions, with swirl and/or tumble motion being used to extend the lean misfire limit [15, 16]. Enhanced charge motion can also improve stoichiometric combustion and various techniques have been employed in production engines [17, 18] to effectively generate turbulent flow behavior. Inlet valve deactivation schemes and asymmetrical inlet port geometry

promote swirl while high-included angle combustion chambers and active charge motion control plates promote tumble.

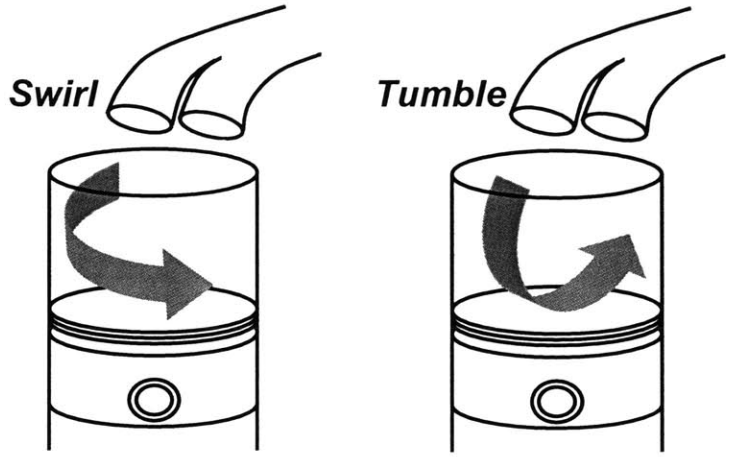

Figure 1.5.3- Swirl and Tumble In-Cylinder Motion

1.5.4- Mixture Preparation

Although the HLSI system is designed to work with homogeneous mixtures, a perfectly homogeneous mixture cannot be attained in real-world conditions. The challenge of evaporating and diffusing the injected gasoline becomes even more critical in the lean regime. One of the most difficult conditions for creating a homogeneous mixture is during cold start, when the engine ports are far below steady state operating temperature. In this case, liquid gasoline does not evaporate as readily and small liquid droplets will persist, leading to high levels of unburned *HC* emissions. One of the most effective solutions is to create finer droplets of fuel spray. In direct injection fuel systems, this can be accomplished by increasing injection pressure. In low-pressure port-injected combustion systems such as HLSI, the approach is to use fine-hole injectors that replace a single pintle hole with as many as twelve laser-drilled orifices. While the benefits of fine-atomizing injectors under startup conditions are clear, the advantages at steady state are less certain. Earlier research [19] has suggested that fuel atomization may not be a limiting factor of steady state lean combustion performance.

1.6 Mixture Characterization

In working with diluted air-fuel mixtures, it is important to characterize the level of dilution with an appropriate parameter. Two different approaches, excess air ratio (lambda) and thermal dilution parameter (TDP), are used in the course of this thesis.

1.6.1- Excess Air Ratio (Lambda)

Lambda is a widely used parameter that describes the relative richness or leanness of an air-fuel mixture (Equation 1.6.1).

$$\lambda = \frac{(A/F)_{actual}}{(A/F)_{stoichiometric}} \tag{1.6.1}$$

where *A/F* is the ratio of air and fuel mass flow rates. Stoichiometric operation is the condition where there is precisely enough air present to allow for complete oxidation of the fuel. In lean operation, there is a surplus of air in the air-fuel mixture, thus $\lambda > 1$. Lambda is easily measured using a universal exhaust gas oxygen (UEGO) sensor.

Each fuel has a unique stoichiometric *A/F* ratio (AFR). For pure indolene (a type of gasoline,) this ratio is 14.6. In a mixture of air and several different fuels, the stoichiometric AFR of the overall mixture is the weighted average of the AFR values of the constituents. Adding plasmatron reformate to air-indolene mixtures lowers the overall stoichiometric AFR because the reformate gas component has a lower stoichiometric AFR than indolene.

1.6.2- Thermal Dilution Parameter (TDP)

TDP (Equation 1.6.2.1) was developed [2] to characterize the thermal properties (Equation 1.6.2.2) of air-fuel mixtures diluted by diluents such as plasmatron reformate or recycled exhaust. Since thermal properties largely govern combustion behavior, TDP is an effective means for comparing different dilute mixtures. In particular, it should be noted that lambda does not effectively describe EGR diluted mixtures since operating conditions may be stoichiometric. Conversely, TDP provides a useful measure of EGR dilution:

$$TDP = \frac{\Delta T_{all\_indolene,stoichiometric}}{\Delta T_{diluted\_mixture}} \tag{1.6.2.1}$$

where,

$$\Delta T = \frac{\sum_i \dot{m}_i \cdot LHV_i}{\dot{m}_{total} \cdot \overline{C}_v} \tag{1.6.2.2}$$

ΔT is the chemical energy per unit heat capacity (dilution) of the mixture, i is a species in the diluted air-fuel mixture, LHV represents lower heating value (energy density) and C_v is the molar heat capacity.

1.7 Project Objectives

This thesis focuses on the combustion improvement aspect of the HLSI system. A series of experiments is conducted to evaluate the impact of different ignition systems, charge motion control devices, and fuel injectors on HLSI combustion performance. In particular, by combining flow bench data with combustion data, it is possible to achieve new understanding of the impact of tumble and swirl motion on combustion performance. Additionally, tests are run at very high EGR rates to examine the effects of hydrogen enhancement on an alternate high-dilution approach. By correlating EGR dilution with lean dilution using the TDP parameter, it is possible to extrapolate the lean combustion system results to very dilute EGR operation.

Subsequent chapters in the thesis will describe the engine and testing apparatus used in the experimental program, followed by details of the testing procedure. Then, the results of both the flow bench and engine based tests will be presented and discussed. Finally, a series of concise conclusions will highlight the key findings and recommendations. The results of this thesis will help HLSI to achieve the leanest possible operation, reducing emissions while maximizing efficiency.

(This page was intentionally left blank.)

Chapter 2: Engine Setup and Test Apparatus

2.1 Engine Overview

Experiments were conducted in the MIT Sloan Automotive Laboratory using a specially prepared single-cylinder research engine (Table 2.1). The block is a Ricardo Hydra MkIII while the head is a modified Volvo B5254 (a single cylinder segment of an original inline five cylinder head.) The Volvo head has four valves with a centrally located spark plug and pentroof combustion chamber geometry (Figure 2.1). The engine cranks an Eaton 6000 series air-cooled dynamometer. During startup, the dynamometer motors the engine; then the fuel is triggered, at which point the unit automatically transitions to a power-absorbing mode.

Table 2.1- Ricardo/Volvo Engine Specifications

Displacement [cm^3]	487
Clearance Volume [cm^3]	54
Bore [mm]	83
Stroke [mm]	90
Connecting Rod Length [mm]	158
Compression Ratio	10.1
Valvetrain	DOHC, 4V
Inlet Valve Timing	IVO 0° ATDC, IVC 60° ABDC
Exhaust Valve Timing	EVO 68° BBDC, EVC 8° ATDC

Engine control is accomplished with a MoTeC M4 engine control unit (ECU) model 9806. The ECU is connected to a computer running the MoTeC engine management program v. 4.22. This software allows for real-time adjustment of spark timing with single crank angle degree (CAD) resolution and fuel injection pulse-width adjustment with 0.03 msec precision.

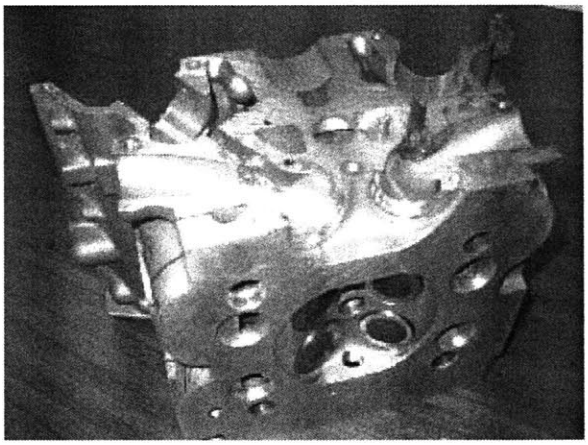

Figure 2.1- Modified Volvo B5254 Head (note pressure transducer hole drilled through side of combustion chamber)

A thermostat-regulated coolant circuit provides thermal management of the engine. During startup, the coolant is run through a heating circuit that brings the coolant up to steady state operating temperature (~ 88 °C). Once the coolant has reached this operating temperature, the thermostat selectively engages a water-water heat exchanger circuit that uses city water to chill the coolant as needed.

The test engine is also equipped with an exhaust gas recirculation (EGR) system (that the author helped to fabricate and test) as well as a compressor-fed induction system to allow boosted operation (not used for this thesis.)

2.2 Fuel System

The HLSI engine is equipped with two types of fuel systems; one for liquid gasoline and the other for plasmatron reformate gas.

2.2.1- Indolene System

The chosen liquid gasoline blend used for this project is indolene (UTG-96), a standard research fuel (Table 2.2.1). A constant 40 psi supply pressure is maintained in the fuel lines. Indolene injection occurs in the inlet port with the fuel injector spraying downward toward the valves. The end of the injection pulse is timed to 385 CAD BTDC.

Table 2.2.1- Chevron Phillips UTG-96 Specifications [20]

Lower Heating Value [MJ/kg]	43.1
Molar H/C Ratio	1.93
Carbon Weight [%]	86.5
Hydrogen Weight [%]	13.5
Research Octane Number	96.1
Motor Octane Number	87
Anti-Knock Index (R+M)/2	91.6

2.2.2- Reformate Gas System

In the absence of a working plasmatron reformer, bottled reformate gas mixed to the ideal plasmatron outlet specification by BOC Gases (Table 1.3.1) was used. Reformate mass flow is metered using a critical flow orifice [4] operating in a choked condition. The reformate gas is introduced into the inlet manifold several critical lengths upstream of the inlet valves, assuring homogeneous mixing.

Reformate gas concentration is measured in terms of a "plasmatron fraction" or "enhancement fraction" (i.e.- 0%, 10%...) This is defined as the amount of reformate gas that would be generated by diverting the said mass fraction of indolene through the reformer device (Figure 2.2.2). Thus, a 20% plasmatron fraction indicates the amount of reformate gas that would be generated by routing 20% of the indolene flowing out of the tank through the plasmatron reformer device. Assuming 80% energy conversion efficiency in the reformer, this means that 4% of the total indolene energy flow extracted from the tank is lost. Thus, comparing 0% plasmatron operation with 20% plasmatron operation, there is less indolene injected at the 20% operating point because some of the indolene is substituted for by an equivalent amount of reformate gas.

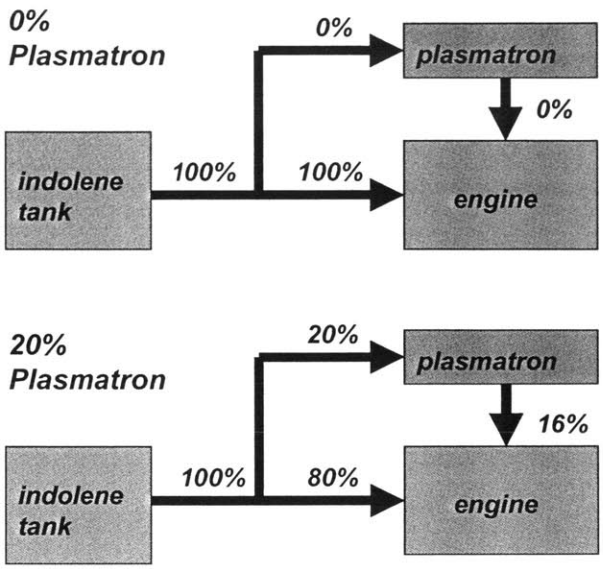

Figure 2.2.2- Plasmatron Energy Flow Schematic (Assumes 80% Plasmatron Energy Conversion Efficiency)

2.3 EGR System

An external EGR system (Figure 2.3) was designed and installed to allow for testing of high EGR dilution operating points. This system is fabricated from temperature resistant ¾ in flexible steel piping. Exhaust gas is tapped 8 in downstream of the cylinder head and reintroduced to the inlet manifold 17 in upstream of the cylinder head. A gate valve allows regulation of the pressure drop through the pipe, providing control of EGR flow rate. Provision is also made for insertion of a series of custom made orifices that allow further restriction of EGR flow rate. Although no EGR heating or cooling system is fitted, a pair of thermocouples monitoring exhaust gas temperature through the line provide assurance that temperatures remain high enough to prevent condensation.

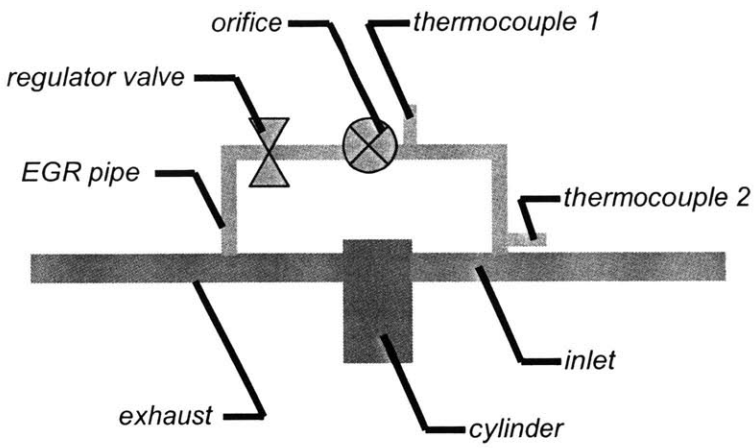

Figure 2.3- EGR System Schematic

2.4 Ignition Systems

A series of three different ignition systems was tested to evaluate HLSI combustion response. These systems cover the spectrum from a typical OEM-spec inductive coil based ignition to a high-energy capacitor based plasma discharge scheme.

2.4.1- Denso 580

The Denso 580 system represents a typical high quality OEM ignition. This coil near plug design is used on the LS1 V8 engine that powers the Chevrolet Corvette. The coil is triggered directly from the MoTeC ECU by a 5 V TTL falling trigger signal with 5.1 msec dwell. The Denso system is used in conjunction with a fine tip Bosch platinum spark plug with standard "J" geometry. Gap width on the stock plug is 0.035 in, however tests were also run with a modified plug that is opened up to a 0.070 in gap (and corresponding increase in TTL trigger signal dwell to 5.8 msec.)

2.4.2- Adrenaline Research Plasma

This system was provided by Adrenaline Research, Inc. and is actually an early prototype of their patented SmartFire ignition. SmartFire is capable of providing ionization-sensing combustion feedback, however this feature was not used. The Adrenaline system is based on a dual-capacitor circuit topology (Figure 2.4.2) and is capable of three modes of operation. Low-

energy CD mode discharges a single capacitor to provide output similar to a coil ignition. High-energy DE mode discharges both capacitors to provide a strong plasma discharge characteristic. A multi-strike MS mode discharges both capacitors at 1 ms intervals, providing multiple sparks and delivering the greatest amount of energy. The system uses a custom coil that mounts directly on the spark plug. The electronics unit is triggered from the MoTeC ECU by a 5 V TTL rising trigger signal with 5.1 msec dwell and is connected to the coil with a custom multicore MIL-spec wiring harness. Customized Champion resistor-less projected-gap type spark plugs are used, with a central electrode surrounded by four grounding electrodes.

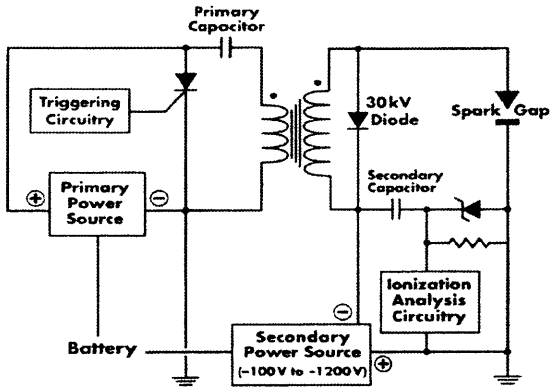

Figure 2.4.2- Adrenaline Research Plasma Ignition Circuit Topology [21]

2.4.3- MSD Digital 7Plus

Digital 7 Plus is a high-performance capacitive discharge ignition system primarily targeted for racing applications. The controller unit incorporates a IGBT coil driver and can deliver 520-535 V to the primary side of the ignition coil. Spark energy is up to 190 mJ and the system operates in a multistrike mode below 3300 rpm (tests for this thesis were run at 1500 rpm) with a 20 CAD interval between discharges. The MoTeC ECU triggers the controller with a 5 V TTL falling trigger signal with 2.9 msec dwell and this in turn drives a MSD HVC II ignition coil. This coil is capable of delivering 45 kV peak voltage and 2 A peak current and is connected to the spark plug using a custom-fabricated Magnecor wire. The MSD ignition is used in conjunction with the same Bosch platinum J-plugs as the reference Denso ignition at standard 0.035 in and 0.07 in widened gaps.

2.5 Charge Motion Control Devices

This thesis required methods for creating substantial variations in charge motion with minimal modifications to the baseline research engine. The necessity of quick changes to different configurations and the reality of simultaneous engine sharing with other students precluded any alterations to the head or valvetrain. Instead, two inlet port-based solutions were used to provide both major modifications to in-cylinder flow as well as ease of use.

2.5.1- Restrictor Plates

Ed Tully, who ran the initial series of experiments exploring the potential of hydrogen enhanced lean burn operation [2], started work with restrictor plates. The purpose of a restrictor plate is to partially obstruct the inlet ports to enhance turbulence. This can largely be attributed to two mechanisms:

- Flow must accelerate through the restriction, leading to increased velocity and turbulent intensity
- Geometry of obstruction can help direct the flow into a particular region of the inlet port, encouraging swirl and/or tumble

Movable restrictor plates are already used in certain production engines (Figure 2.5.1.1), however they are opened up at higher load/speed conditions to maximize flow rate and reduce the penalty on volumetric efficiency. For simplicity, the restrictor plates used in this project are fixed and held into place when the inlet pipe is bolted onto the head. All test points run for this thesis were conducted at the low load/speed conditions where restrictor plates are most effective. Ed Tully tested three different restrictor plate geometries (Figure 2.5.1.2) and settled on a 2/3 obstructed asymmetrical plate as the best performer. The lower portion of the port is blocked off to encourage flow high in the port, which can lead to increased tumble. The asymmetry might also lead to a differential in flow rate through the left and right inlet valves, introducing some amount of swirl motion. The placement of the plate does not impinge on the fuel injector spray cone.

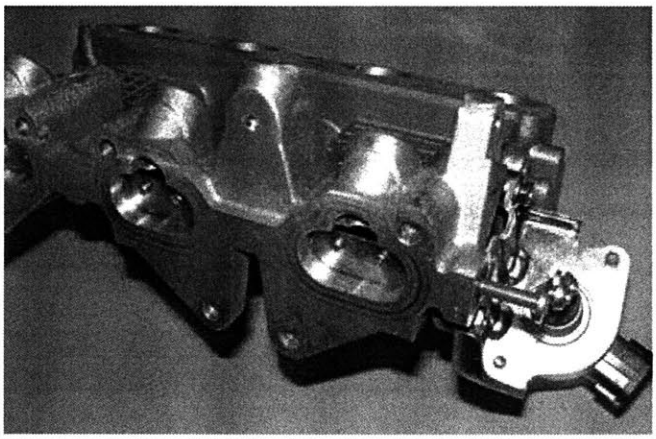

Figure 2.5.1.1- Inlet Restrictor Plates (Closed Position) on Inlet Manifold of Nissan 1.8L I-4 Engine (Note Servo Motor Connected to Actuation Shaft)

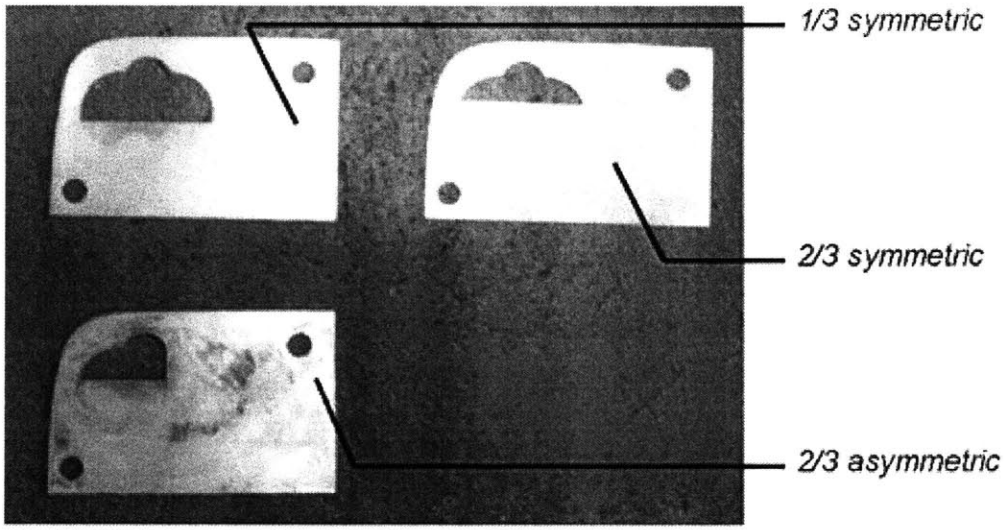

Figure 2.5.1.2- Inlet Port Restrictor Plates

2.5.2- Inlet Port Cones

While restrictor plates are easy to design and simple to fabricate, there are limitations to the amount of flow control they can provide. The flow must still travel several inches to reach the inlet ports after passing through the restrictor and this would make it impossible to, as an example, reliably send all of the flow through a single inlet valve. The inlet port cone device was created to allow even more precise flow management without sacrificing the ease of use of a restrictor plate. Fabricated from cut and rolled stainless steel, the cones plug into the inlet ports through the side of the head and effectively reshape the internal geometry of the inlet ports. The

cones are held in place by a flange that wraps around the edge of the cone inlet opening, which gets clamped to the head when the inlet pipe is bolted on.

Four different cones were created (Figures 2.5.2.1-4):

- Extreme Turbulence- All flow is directed through the left valve, moderately high and as far outside in the port as possible. Intended to generate extreme swirl and high tumble.
- Moderate Turbulence- All flow is directed through the left valve, very high and close to the outside. Intended to generate moderate swirl and high tumble.
- Port Deactivation Cone- Designed to simulate a valve deactivation scheme, this cone brings all of the flow through the left port but does not try to restrict the flow any further.
- Tumble Cone- Brings flow through both valves with equal horizontal port dispersion but directed as high in the port as possible. Intended to create pure tumble without swirl.

As flow bench testing would reveal, the actual turbulent behavior of some of the cones turned out to be quite different from what was intended.

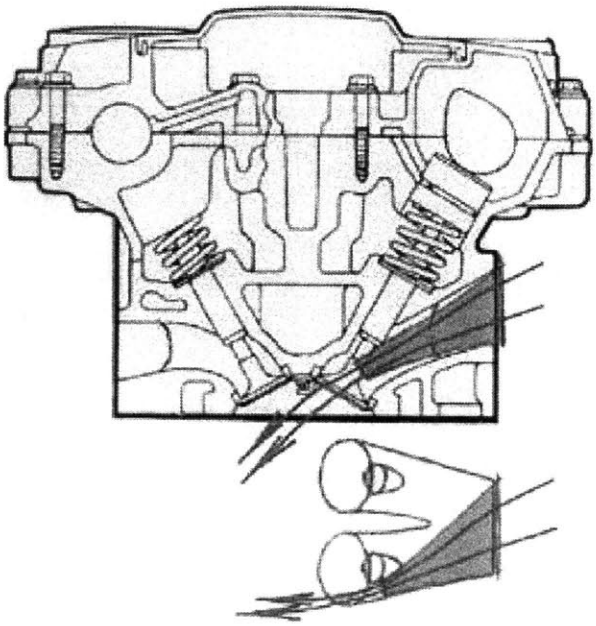

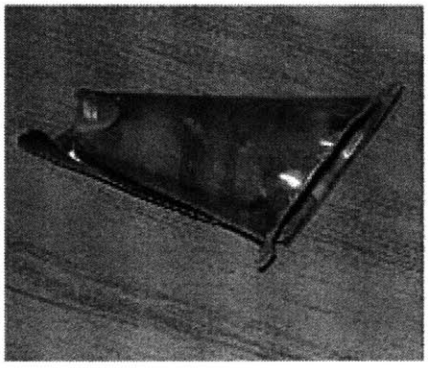

Figure 2.5.2.1- Extreme Turbulence Inlet Port Cone

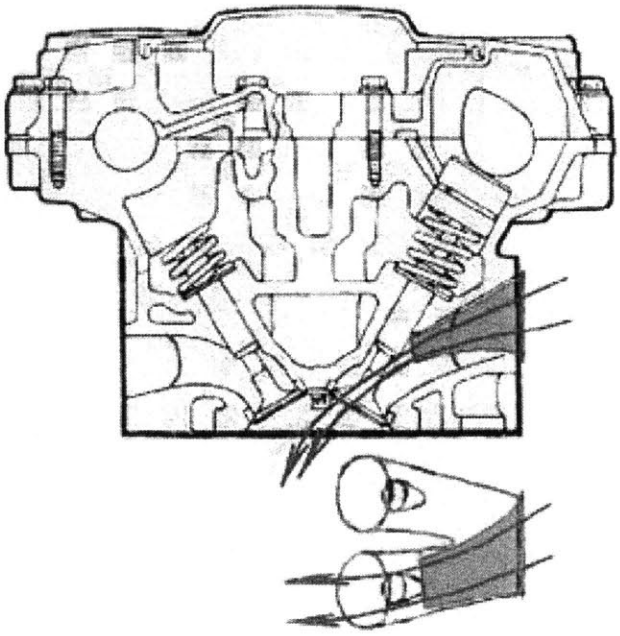

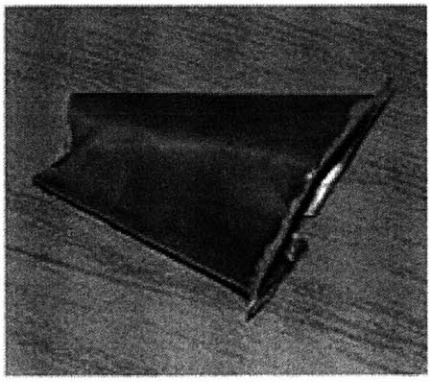

Figure 2.5.2.2- Moderate Turbulence Inlet Port Cone

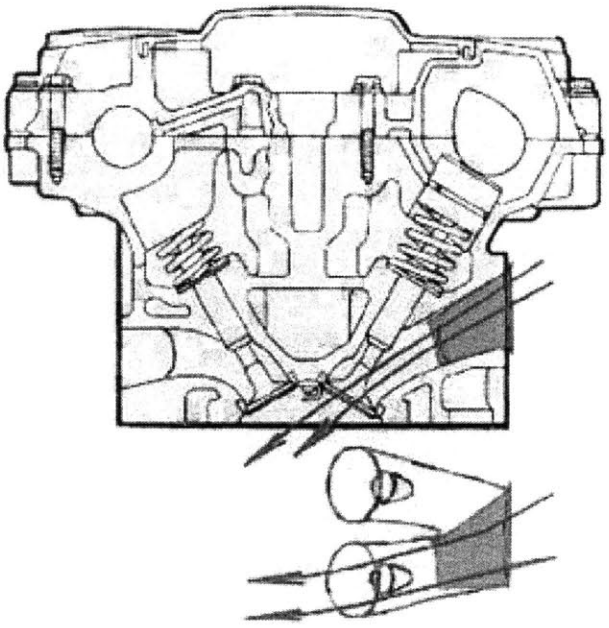

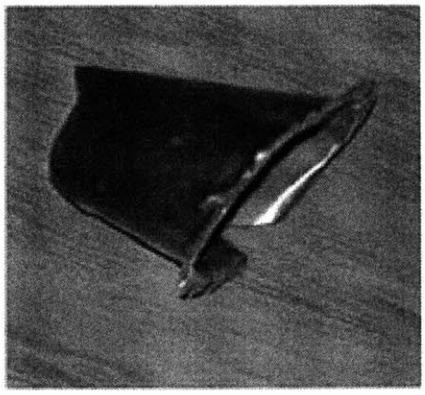

Figure 2.5.2.3- Port Deactivation Inlet Port Cone

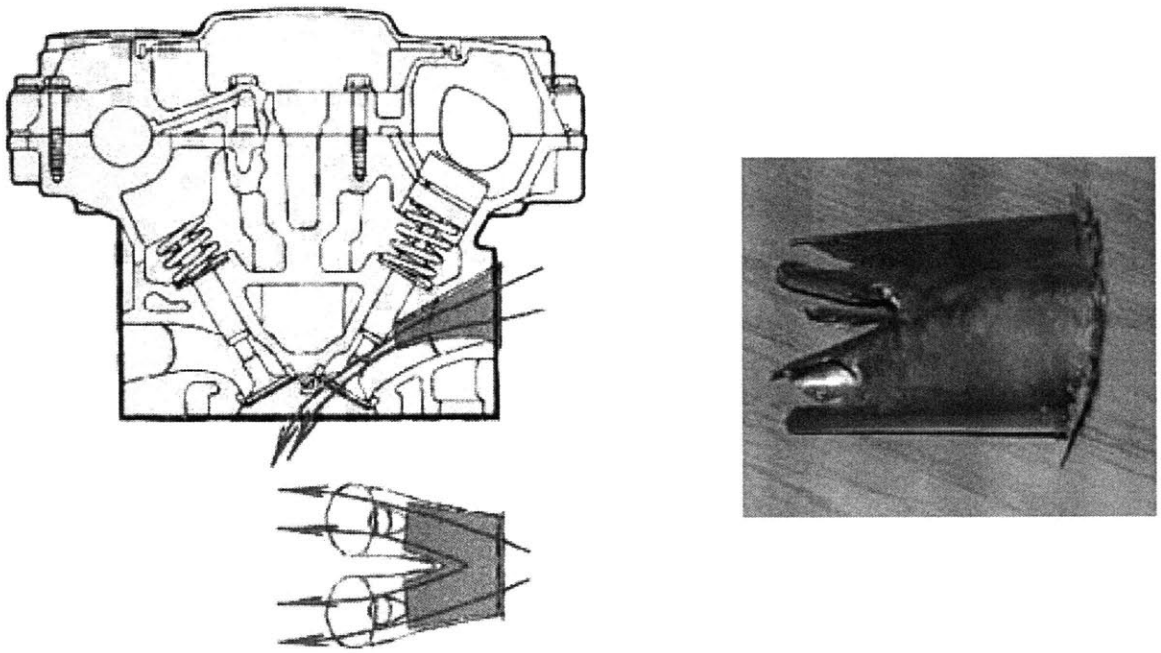

Figure 2.5.2.4- Tumble Inlet Port Cone

In an effort to try to minimize the aforementioned velocity effects of a restriction device, three of the cones maintain a roughly 6 : 1 area reduction ratio (inlet area : outlet area). In contrast, the port deactivation cone has a 2.5 : 1 ratio that is naturally defined by the geometry of the Volvo head, which has the same reduction from the large single opening in the side of the head down to the smaller entry to either of the two inlet ports. By minimizing flow velocity effects, it is possible to focus on the geometry of each cone and how this influences in-cylinder motion.

2.6 Fuel Injectors

Two different fuel injectors were used during the course of experiments. The reference injector is a Bosch EV 1.3a single-hole pintle type injector. This injector is characterized by a conical spray pattern that captures 90% of the flow within a 30° cone. As an alternative, a prototype 12-hole Delphi injector was used. The finer holes of this injector lead to finer fuel atomization. Similar to the Bosch reference injector, the Delphi injector delivers 90% of the flow within a 29° cone. It is also worth noting that the smaller end-diameter of the Delphi injector causes it to sit roughly 1 cm deeper into the inlet pipe injector fitting, although the end of the injector does not protrude deeply enough to impinge on the inlet flow stream. Both injectors were calibrated in-house using

the MoTeC ECU injector calibration mode, which fires the injector for several hundred pulses to allow accurate weighing of the fuel mass injected at different pulse widths.

2.7 Test Cell Configuration

A schematic (Figure 2.7) indicates the layout of critical systems in the test cell.

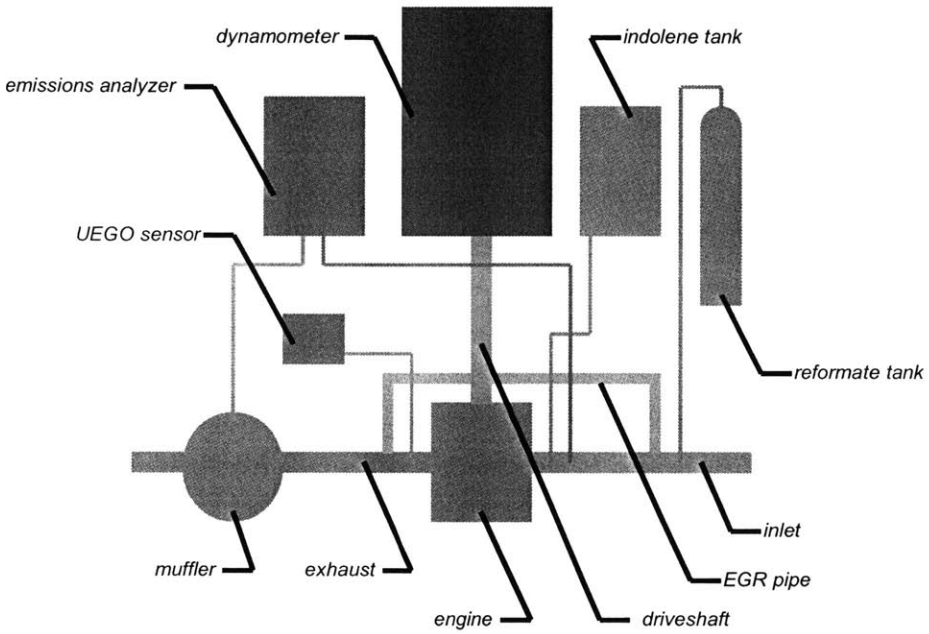

Figure 2.7- Ricardo/Volvo Engine Test Cell Schematic

2.8 Engine Data Acquisition

A number of sensing and detection systems were used to monitor various engine parameters and provide the data necessary to drive the Sloan Laboratory burn rate analysis program, which in turn provides combustion results.

2.8.1- Airflow Measurement

Air volume flow rate is measured by an Omega PX 140 differential pressure sensor, which measures the flow pressure drop through a Ricardo Viscous Flow Meter Model #280-150779.

This measurement is taken upstream of the stepper motor controlled throttle. Downstream of the throttle, an Omega PX 176 device (0-50 psi range) measures manifold air pressure (MAP).

2.8.2- Lambda Measurement

A Horiba MEXA-110λ wideband universal exhaust gas oxygen (UEGO) analyzer is used to provide real-time measurement of the excess air ratio (lambda). The sensing probe is located roughly 8 in downstream of the exhaust valve seats. As a check, lambda values are also calculated based upon measured air and fuel flow rates and typical agreement is within 3%.

2.8.3- In-Cylinder Pressure Measurement

In-cylinder pressure data is obtained from a Kistler Model 6125A piezoelectric pressure transducer, mounted in a hole drilled through the side of the cylinder combustion chamber. The transducer is protected by a flame-arrestor and is calibrated using a dead weight tester. Signal level amplification is provided by a Kistler Type 5010 charge amplifier, which provides enough gain to match the sensitivity of the data acquisition system. Real-time monitoring of the pressure trace is provided by a Tektronix TDS310 digital oscilloscope or custom LabVIEW application.

2.8.4- EGR Measurement

Two different techniques are used to monitor EGR flow rate. Both operate on the principle of measuring the concentration of exhaust gas species in the inlet manifold. Both NO_x and CO_2 are found in high concentrations in the exhaust gas but nearly zero concentrations in fresh inlet air. By measuring NO_x or CO_2 concentrations in both the inlet manifold (downstream of EGR introduction, to allow time for mixing) and the exhaust muffler, it is possible to determine the fraction of EGR (Equation 2.8.4)

$$EGR_{\%} = \frac{NO_{x,inlet}}{NO_{x,exhaust}} \cdot 100 \qquad \text{or,} \qquad EGR_{\%} = \frac{CO_{2,inlet}}{CO_{2,exhaust}} \cdot 100 \tag{2.8.4}$$

At higher load test conditions (5.2 bar NIMEP), NO_x measurement using a California Analytical Instruments Model 400-HCLD chemiluminescent analyzer is used to evaluate EGR fraction. At low load points (3.5 bar NIMEP), the 3.85 psig sample pressure of the NO_x analyzer makes inlet

sampling impossible because the manifold vacuum exceeds 3.85 psig. For these tests, a Horiba MEXA-554JU automotive emissions analyzer connected in series with a Varian type 949-9451 booster pump is used to measure CO_2 concentrations.

2.8.5- Temperature Measurement

A number of Omega K-type thermocouples are installed at various locations around the engine to allow for thermal sampling of key working fluids including:

- Inlet Air
- Exhaust
- Coolant
- Oil
- Recycled Exhaust Gas

2.8.6- Engine Position Sensing

The engine is equipped with three different devices to sense positional information. A crank angle encoder produces a square wave with each pulse corresponding to 1 CAD rotation (360 pulses/ complete crank revolution.) An additional sensor mounted along the axis of the crankshaft provides a pulse every time the piston passes through BDC. Finally, half of the circumferential edge of one of the camshaft sprockets is widened to intermittently pass through an optical sensor. Depending upon whether or not the sensor is obstructed, the device indicates if the crank is rotating through the first or second rotation of a given engine cycle.

2.8.7- Data Acquisition

A customized interface box designed by Prof. Wai K. Cheng of the MIT Sloan Automotive Laboratory is used to integrate engine position information with the in-cylinder pressure signal. The box suppresses the BDC signal at the start of the exhaust stroke and passes the BDC compression signal onwards, also superimposing this 5V step onto the pressure trace. The BDC compression, pressure, and cranxk angle traces are then interfaced to the data acquisition computer using a National Instruments BNC-2090 interface board. On the computer, data acquisition is managed by National Instruments LabVIEW v5.1 (later v6.1) software. Pressure

data is sampled once per CA (360 samples/ revolution = 9 kHz @ 1500 rpm), triggered by the crank angle signal. The BDC compression signal is used to signal the start of each engine cycle.

2.9 Analysis Software

The MIT Sloan Automotive Laboratory burn rate analysis code is used to post-process engine pressure data in order to calculate key engine operating parameters. Inputs for the code include the recorded pressure trace, engine geometry data, heat transfer coefficients, and ambient atmospheric conditions. The algorithm recognizes the start of each new engine cycle by the BDC compression signal that is superimposed on the pressure trace. By integrating the P-V data, the code outputs both gross and net indicated mean effective pressure (GIMEP and NIMEP) as well as information on peak cycle pressure and the crank position at peak pressure. Furthermore, the code monitors engine stability by calculating COV (Equation 2.9.1) of each of the calculated parameters and noting any occurrences of misfires or partial burn cycles (where peak cycle pressure does not exceed 20% of the average for a complete sample set.) Additionally, a heat transfer model [22] allows for the calculation of burn rate and mass fraction burned profiles.

$$COV_{parameter} = \frac{\sigma_{parameter}}{(\sum_{i} parameter_i)/n} \tag{2.9.1}$$

where $\sigma_{parameter}$ is the standard deviation of the parameter over the entire sample set, $parameter_i$ is the parameter value for the i^{th} cycle, and n is the total number of cycles in the sample set. At each measurement point, a 300 cycle sample set of pressure data is recorded. Each of these cycles is then processed individually. The recorded value for each combustion parameter is the mean of the values for each of the individual cycles in the sample set. NIMEP (Equation 2.9.2) is the preferred parameter of engine output as it incorporates the cycle pumping losses.

$$NIMEP = GIMEP - PMEP \tag{2.9.2}$$

where *GIMEP* is the combustion work per cycle and *PMEP* is the pumping work per cycle.

2.10 Flow Bench Testing

The various charge motion control devices used in this experimental program were constructed using informed assumptions. Each one was rendered based upon a best guess of what type of geometry would induce the desired amounts of turbulent motion. In order to provide a rigorous assessment of the actual charge motion that each device generated, flow bench testing was conducted at the DaimlerChrysler Technical Center in Auburn Hills, MI. This facility has a dedicated flow-testing lab equipped with benches to measure both swirl and tumble. Most importantly, highly knowledgeable experts with decades of combined experience were on hand to provide valuable insight and guidance.

2.10.1- Fixturing

The head used in the flow tests is a Volvo B5254 identical to the one fitted on the Ricardo research engine at the Sloan Laboratory. To adapt the head to the SuperFlow flow benches, a custom 86 mm diameter bore adapter was machined from aluminum. This adapter has holes drilled to exactly match the bolt pattern of the Volvo head. The inlet port was fitted with a flared horn (Figure 2.10.1) normally used for testing the DaimlerChrysler 2.4L I-4 engine because the section of this horn is a nearly perfect match to the section of the Volvo port. The horn bolts onto the head using the same bolt pattern as the normal inlet manifold. The restrictor plates and inlet cones are held in place by the compression of the bolted horn, much as they are held in place by the compression of the bolted inlet pipe on the research engine.

In order to actuate the valves during flow tests, the stock valve springs are replaced with lighter springs. A custom fixture holding two micrometers is then bolted onto the head such that the micrometers are positioned to directly depress the valves. In this way, the lift of each valve may be independently adjusted with thousandth inch accuracy.

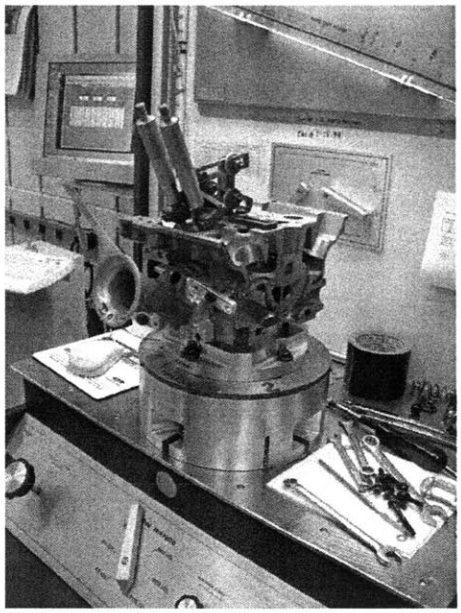

Figure 2.10.1- Volvo B5254 Head Fixtured on SuperFlow 1020 Swirl Bench (Note Flared Inlet Horn and Valve Actuation Micrometers)

2.10.2- Swirl Bench

A stock SuperFlow 1020 swirl bench was used to evaluate swirl turbulence. This bench provides a suction that draws air through the inlet ports into the combustion chamber. The flow travels down the bore adapter and passes through a hexagonal screen that is connected to a torque sensor. Any swirling motion in the flow will exert a torque on the screen, which can be measured as an indication of swirl intensity. Furthermore, the bench provides an indication of the flow rate through the head.

2.10.3- Tumble Bench

A customized SuperFlow bench was used to evaluate tumble motion. This bench operates similarly to the swirl bench, drawing air into the ports and down through a hexagonal screen. A tumble moment is determined, although the exact tumble measurement methodology is proprietary.

(This page was intentionally left blank.)

Chapter 3: Experimental Structure

The experimental program can broadly be divided into three series of experiments. The first involves testing of the various charge motion configurations on a flow bench. These tests helped to characterize the turbulent flow behavior generated by different restrictor plates and inlet port cones. The second series of experiments involves running the Ricardo/Volvo research engine to study the effects of different ignition, charge motion, and mixture preparation systems on lean operation. These tests collected real-time performance data to provide direct insight on lean combustion performance. The final series of tests examines the impact of hydrogen enhancement on very high EGR dilution engine operation. Using the TDP parameter, this data can be correlated to the combustion results of the lean dilution experiments.

3.1 Flow Bench

Flow testing involves two separate benches, one designed for measuring swirl and the other for measuring tumble. For each test, a sweep of eight different test points is measured at valve lifts mapped from 0.050 – 0.400 in, taken at 0.050 in intervals. For comparison, the intake valve lift of the Ricardo/Volvo test engine is 8.45 mm (0.333 in). Both benches apply a 25 in H_2O (6.22 kPa) suction through the inlet ports, held constant at all valve lifts. This is the standard pressure drop used for measurements at the DaimlerChrysler flow lab. All tests were conducted on the same day, with ambient conditions at 71 °F and 28.51 in Hg atmospheric pressure.

3.1.1- Test Configurations

A total of ten different charge motion configurations were tested:

- Baseline- Stock Volvo B5254 head without modifications, full lift map on both valves
- Baseline Deactivation- Designed to emulate a valve deactivation scheme; stock head, left valve does a full map of lifts while the right remains cracked at 0.050 in lift (this is done in valve deactivation schemes to allow fuel to drain from deactivated port)
- Extreme Turbulence- Head with extreme turbulence cone, full map on both valves

- Extreme Turbulence Deactivation- Designed to verify the effect of right valve actuation even when all flow is ported through left valve (as on actual test engine;) head is equipped with extreme turbulence cone, full map of on left valve while the right remains cracked at 0.050 in lift
- Moderate Turbulence- Head with moderate turbulence cone, full map on both valves
- Port Deactivation- Head with port deactivation cone, full map on both valves
- Tumble Turbulence- Head with tumble cone, full map on both valves
- 2/3 Asymmetric Plate- Head with 2/3 blocked asymmetric restrictor plate (found to be best performer by Ed Tully), full map on both valves
- 2/3 Symmetric Plate- Head with 2/3 blocked symmetric restrictor plate, full map on both valves
- 1/3 Symmetric Plate- Head with 1/3 blocked symmetric restrictor plate, full map on both valves

3.1.2- Swirl Tests

Both swirl torque and volume flow rate measurements were recorded at each test point. Positive values of torque indicate clockwise flow rotation while negative values indicate counterclockwise rotation. Since swirl torque scales with volume flow rate, it is useful to define a normalized swirl torque that indicates torque per unit volume flow (Equation 3.1.2):

$$NormalizedSwirlTorque = \frac{SwirlTorque}{VolumeFlowRate} \cdot 1000 \tag{3.1.2}$$

where the scaling factor of 1000 is included to provide convenient values when swirl torque is expressed in [in oz] units and volume flow rate is expressed in [cfm].

3.1.3- Tumble Tests

Measurements were recorded indicating the tumble moment, which provides a relative indication of the amount of tumble motion being generated.

3.2 Engine Test Conditions

A series of standardized engine test conditions ensures consistent and comparable data.

3.2.1- Lean Operation

All lean engine data is taken at 1500 rpm with a constant *equivalent* indolene flow rate of 0.17 g/sec (i.e.- for runs with plasmatron addition, a fraction of this indolene is replaced by plasmatron reformate.) This corresponds to a load of roughly 3.4 bar NIMEP at stoichiometric conditions ($\lambda = 1.00$) and a peak load of approximately 3.9 bar NIMEP near $\lambda = 1.70$. Control of lambda is accomplished by varying the throttle setting to adjust air flow rate. Each lambda sweep data series would begin with a sample point at stoichiometric conditions. From this point, the throttle was opened in steps to progressively increase MAP and consequently lambda. Points of data were recorded at increments of 0.2 lambda ($\lambda = 1.00, 1.20, 1.40\ldots$) until the misfire limit was reached (although no datum are taken right at that limit.) The misfire limit point can generally be pinpointed to within 0.01 lambda and becomes evident by an unstable in-cylinder pressure trace as well as indication of misfires and/or partial burns in the burn rate analysis code output. For the final point of each data series, the lambda value was backed off from the misfire limit by approximately 0.01 lambda so that a data point could be recorded without the incidence of a single misfire or partial burn in the 300 sampled cycles.

3.2.2- EGR Operation

All EGR experiments were also run at 1500 rpm, although this time with constant engine load as opposed to constant fuel flow. Two load setting were used; 3.5 bar NIMEP and 5.2 bar NIMEP. At all points, the air and fuel flow were adjusted to maintain the desired load as well as stoichiometric mixture conditions. For each EGR sweep, the EGR fraction was progressively increased in roughly 10% increments starting from zero concentration (EGR = 0, 10 %, 20 %...) until the misfire limit was reached, at which point one last data point was taken.

3.3 Reference Engine Configuration

As different experiments were planned to evaluate the impact of combustion system modifications, it became necessary to settle upon a reference engine setup that would serve as a

starting point. The chosen reference configuration is the same one that Ed Tully used in his early trials to map out HLSI performance. This configuration is a good reference because it utilizes standard components or designs that are already widely used in production engines. The reference specifications are:

- Ignition- Denso 580 coil with Bosch platinum J-plug, 0.035 in gap
- Charge Motion- 2/3 asymmetric restrictor plate
- Mixture Preparation- Bosch single hole pintle injector

3.4 Lean Experiments

A series of experiments in the lean regime mapped out the impact of varied combustion system modifications on lean operation. The first test series evaluated the reference configuration. For each subsequent series of tests, one system was modified from the reference setup. The exception is one composite configuration where both the charge motion and mixture preparation systems were modified from the reference to evaluate whether or not there are any combined effects. For each combustion system configuration, a pair of lambda sweeps was run, one without plasmatron enhancement and the other with 20% enhancement.

3.4.1- Ignition Tests

Modified ignition system tests were run using the following configurations:

- Denso 580 coil with Bosch platinum J-plug, 0.070 in gap
- Adrenaline Research Plasma, CD mode, Champion projected gap plug
- Adrenaline Research Plasma, DE mode, Champion projected gap plug
- MSD Digital 7 Plus, Bosch platinum J-plug, 0.035 in gap
- MSD Digital 7 Plus, Bosch platinum J-plug, 0.070 in gap

3.4.2- Charge Motion Control Tests

Modified charge motion tests were run using the following configurations:

- Stock head without any restriction (plate or cone)
- Extreme turbulence cone
- Moderate turbulence cone
- Port deactivation cone
- Tumble cone

3.4.3- Mixture Preparation Test

A modified mixture preparation test was run using the following configuration:

- Delphi 12-hole injector

3.4.4- Composite Test

A composite test was run with *two* modifications from the reference system to evaluate any possible combined effects:

- Extreme turbulence cone with Delphi 12-hole injector

3.5 EGR Experiments

A series of EGR sweeps was conducted to map out the boundaries of very dilute EGR operation in conjunction with hydrogen enhancement. Tests were run at two different loads, both 3.5 bar (comparable to the load of the lean burn experiments) as well as 5.2 bar. At each load, an EGR sweep was run without plasmatron reformate and then with 15% and 30% addition fractions. The engine was equipped with the reference combustion system (2/3 asymmetric restrictor plate, Denso ignition, Bosch injector) during all EGR trial runs.

(This page was intentionally left blank.)

Chapter 4: Results and Discussion

4.1 Flow Bench

The flow bench test results proved to be very interesting in that the actual turbulent flow patterns generated by some of the inlet port cones and restrictor plates are quite different from what had been expected. Furthermore, some of the inlet port cones and restrictor plates, while very different in geometry, create very similar in-cylinder flow motion. Full data for all flow bench trials are listed in the Appendix (Table A.1).

4.1.1- General Observations

A series of plots showing the results for one particular flow motion configuration (moderate turbulence cone) helps to illustrate some of the key phenomena observed during the flow bench tests. The volume flow rate chart (Figure 4.1.1.1) indicates a rapid jump in flow rate as the valves are opened from the initial 0.050 in setting to 0.100 in. By 0.200 in of lift the flow rate has nearly stabilized at just over 40 cfm; further increases in valve lift have no impact on flow. This behavior can be explained because beyond 0.200 in of valve lift, the diameter of the inlet cone outlet becomes the limiting restriction, not the available valve area. Similar behavior is evident with the other restricted inlet port configurations. The maximum flow rate at choking scales with the minimum sectional area of the restriction. The unrestricted head allows for the highest flow rate while the most restricted extreme turbulence cone allows the lowest flow (Figure 4.1.2).

The swirl torque chart (Figure 4.1.1.2) presents a couple of noteworthy points. Not surprisingly, the absolute amount of swirl torque increases with increasing valve lift. The predominant swirl torque is positive, indicating a clockwise rotation as would be expected from introducing the flow through the left inlet port. When the swirl torque is normalized against flow rate, the relationship with valve lift is still direct. This shows that at high valve lift, each unit of air flowing through the valves is creating higher levels of swirl motion. Finally, at the lowest valve lift setting, the swirl torque is negative, indicating *counterclockwise* rotation. According to the experts at the DaimlerChrysler flow lab, this is not unusual. At very low valve lift settings, the

flow tends to be unstable and the direction of swirling motion can easily be shifted in different directions by the flow adhering to anomalies along the port wall, etc.

Lastly, the plot of tumble torque moment demonstrates a weak dependency on valve lift (Figure 4.1.1.3). Although there is a slight increasing trend, the tumble torque moment tends to remain fairly constant with valve lift. Keep in mind that the tumble moment is inherently normalized to flow rate. Furthermore, tumble moment is somewhat nonlinear as evidenced by the bump at 0.150 in valve lift. Other inlet configurations show similar localized variations. This contrasts with the highly linear behavior of volume flow rate and normalized swirl torque.

4.1.2- Swirl Findings

We begin by examining the inlet configurations that are not intended to bias the flow in any particular direction, which would generate swirl. These include the baseline head, tumble cone, 2/3 symmetric restrictor plate and 1/3 symmetric restrictor plate. In all of these cases, the swirl torque is negative and nearly zero, demonstrating that the head has a very slight tendency toward counterclockwise swirl (Figure 4.1.2). Similarly, in those configurations that direct all flow through the left inlet valve, there are high amounts of positive, clockwise swirl. As expected, the extreme turbulence cone (with the most pronounced left-directed geometry) created the highest level of swirl. The unexpected result is that the 2/3 asymmetric restrictor plate, with a left-biased cut that would seem to divert most of the flow through the left port, generated the lowest magnitude swirl of any configuration. Apparently, airflow resists mechanical diversions so despite being biased toward the left port at the head entrance, the flow tends back toward a symmetric distribution in the space between the outlet of the restrictor plate and the splitting of the inlet port.

4.1.3- Tumble Findings

The baseline unmodified head demonstrates a low tumble moment (Figure 4.1.2). This belies the steep included valve angle characteristic of the Volvo B5254 head, which tends to promote tumble. Unexpectedly, the tumble cone that was intended to create large amounts of tumble barely creates any more tumble motion than the baseline head. This is probably because the flow coming out of the outlets of the tumble cone is able to redistribute evenly across the sectional

area of the port before reaching the valves, effectively creating a flow pattern that is similar to the baseline head. Comparing the different configurations, tumble moment seems to scale with the amount of restriction. Consider, for example, the similar levels of tumble generated by the high restriction (low flow) extreme turbulence cone, moderate turbulence cone, and 2/3 asymmetric restrictor plate. The geometric dissimilarity between these devices suggests that the increased tumble is primarily caused by the acceleration of flow through the restriction, although each one also biases the flow toward the top of the inlet port. This bias may not have a big impact because the swirl behavior of the 2/3 asymmetric plate and the tumble behavior of the tumble cone both demonstrate that the flow will tend toward an even distribution after exiting a restriction. Lastly, it should be noted that the 2/3 asymmetric plate that Ed Tully found to have the best combustion performance [4] out of the three restrictors also generates the most tumble out of these three configurations.

4.1.4- Valve Deactivation Emulation Analysis

Results indicate that the port deactivation cone does a fairly good job of emulating the type of valve deactivation scheme that would be implemented on a production engine. This is based upon comparison of the baseline deactivation configuration and the port deactivation cone configuration. Both setups exhibit similar flow rate behavior although the cone is nearly 20 cfm more restrictive at maximum valve lift (Figure 4.1.4.1). The swirl (Figure 4.1.4.2) and tumble (Figure 4.1.4.3) measurements are in even closer agreement with the cone registering slightly higher values of each. This matches the trend seen with other configurations, whereby higher levels of restriction tend to increase turbulent motion. The only major disparity is seen in tumble behavior at low valve lifts. The cone first generates a very high moment at the initial 0.050 in lift point and then a lower reading at 0.100 in before joining the more stable deactivated valve trace at 0.150 in. This further highlights the erratic flow behavior that is often seen at low valve lifts.

4.1.5- Active Valve Impact Analysis

Tests to evaluate the impact of both valves actuating even when all of the flow is diverted through the left valve compared the extreme turbulence cone configuration against the extreme turbulence deactivation configuration. Results show nearly zero effect on flow rate (Figure 4.1.5.1) and normalized swirl torque (Figure 4.1.5.2). A small increase in tumble moment is

measured in the case of both valves active compared with the right deactivated in a 0.050 in lifted condition (Figure 4.1.5.3). In both cases, the behavior of the tumble moment trace is very similar, with a peak near 0.250 in lift. These results suggest that running the test engine with an unmodified valvetrain that lifts both inlet valves should not be a cause for concern, even when the chosen inlet configuration routes all flow through just a single valve.

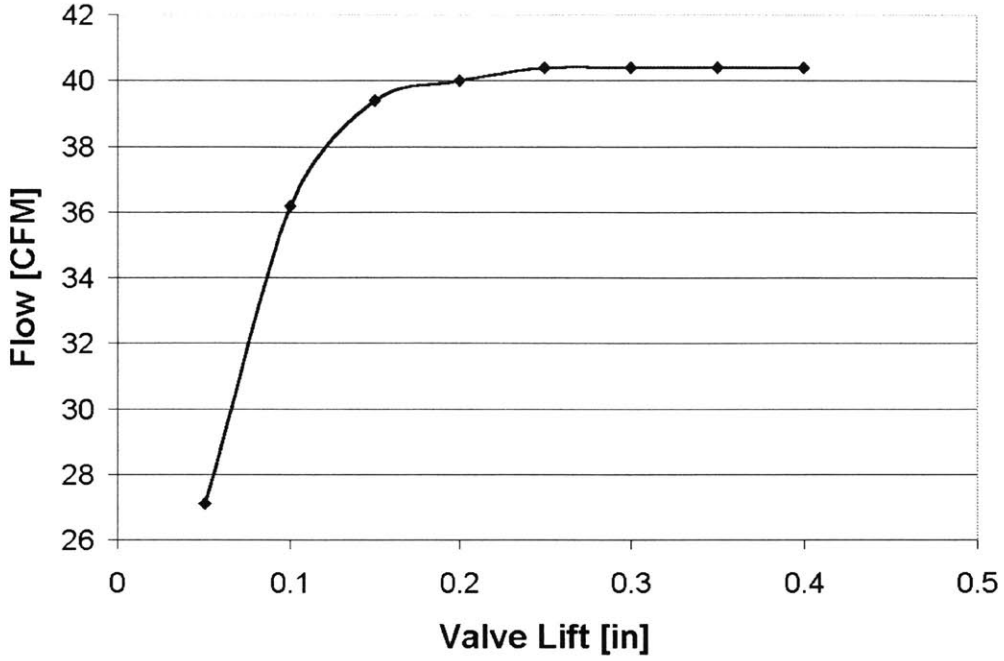

Figure 4.1.1.1- Inlet Port Flow Rate vs. Valve Lift with Moderate Turbulence Cone

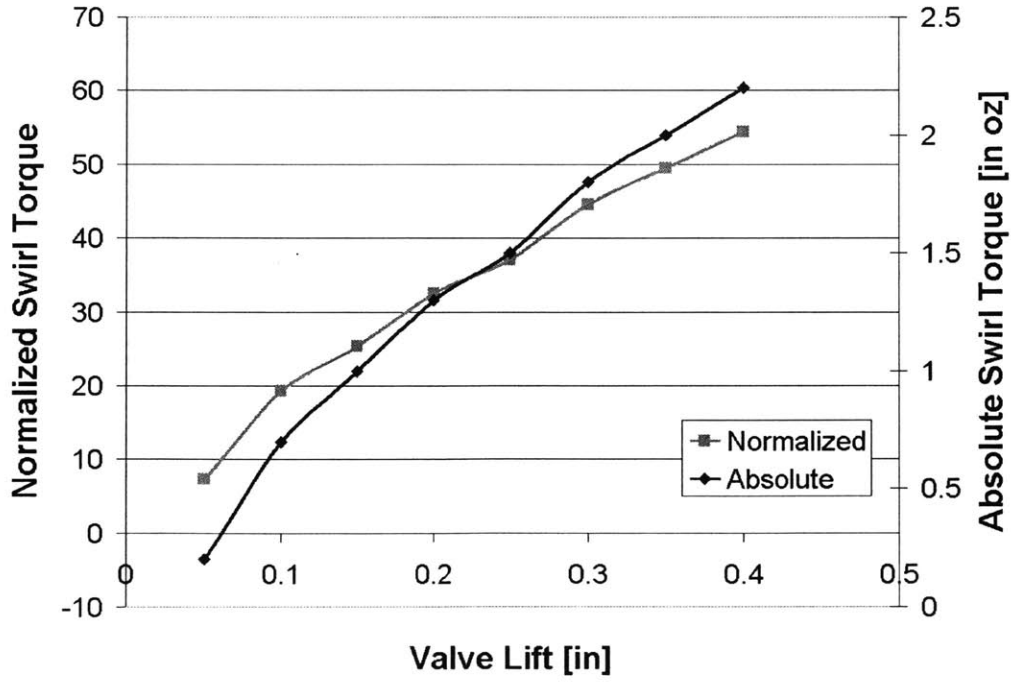

Figure 4.1.1.2- Normalized (to Flow Rate) and Absolute Swirl Torque vs. Valve Lift with Moderate Turbulence Cone

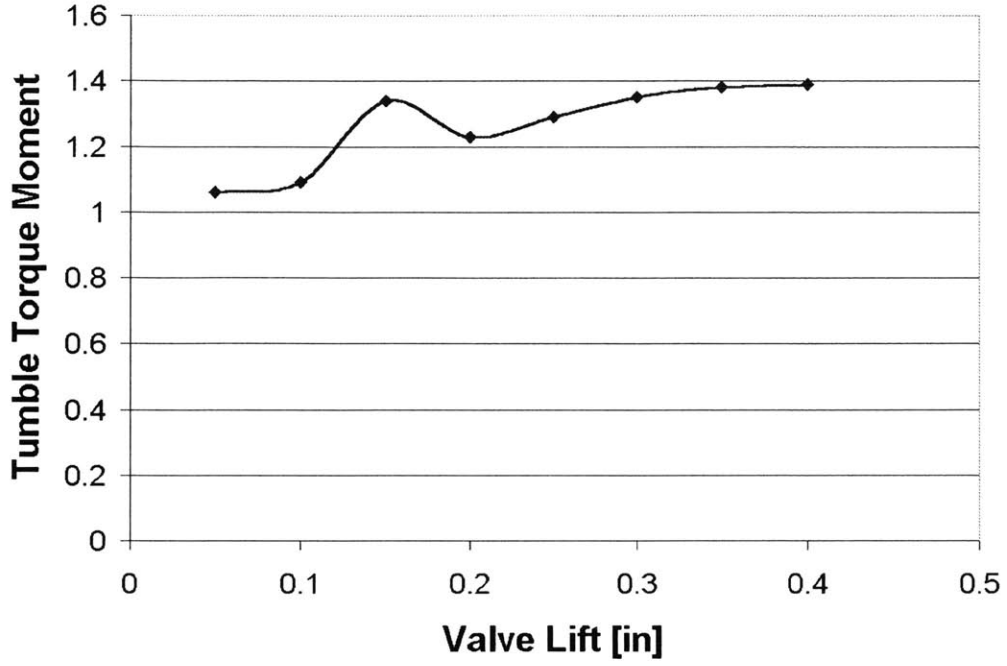

Figure 4.1.1.3- Tumble Torque Moment vs. Valve Lift with Moderate Turbulence Cone

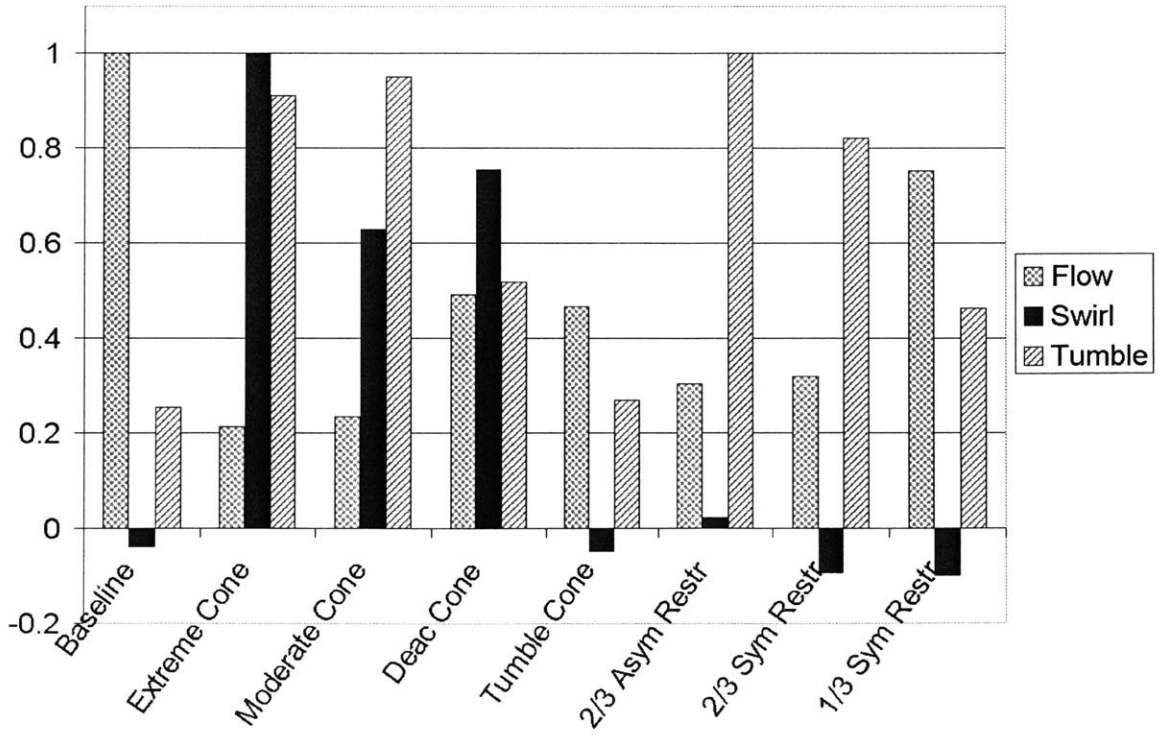

Figure 4.1.2- Inlet Port Flow Rate, Normalized (to Flow Rate) Swirl Torque, and Tumble Torque Moment Plotted on a Normalized Scale for Various Inlet Configurations (0.350 in Valve Lift)

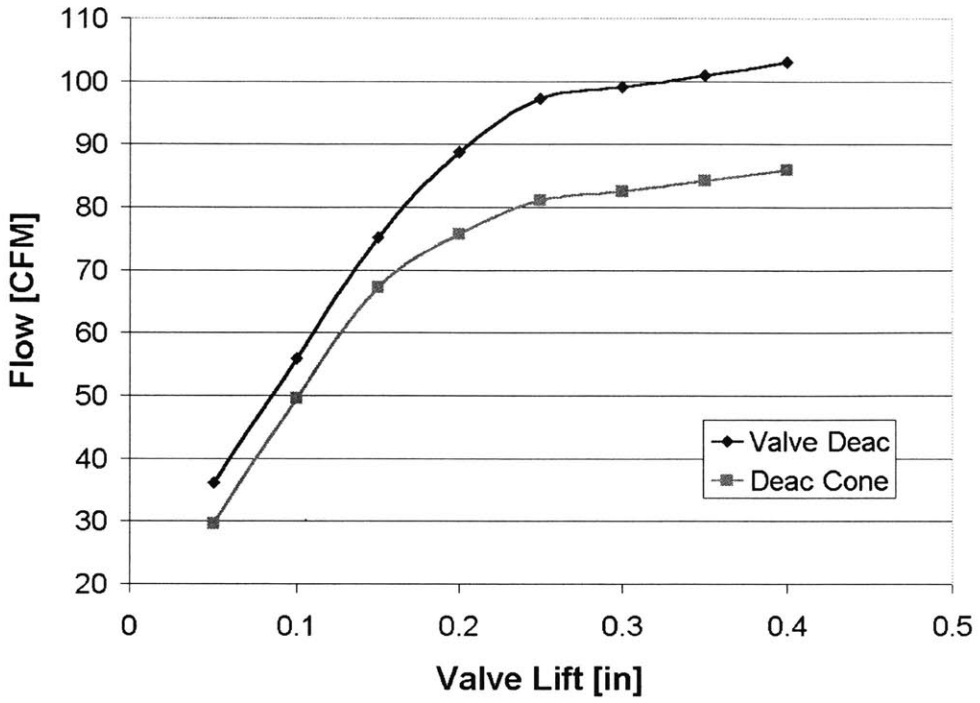

Figure 4.1.4.1- Inlet Port Flow Rate vs. Valve Lift with Baseline Head and Right Valve Deactivated vs. Port Deactivation Cone and Both Valves Active

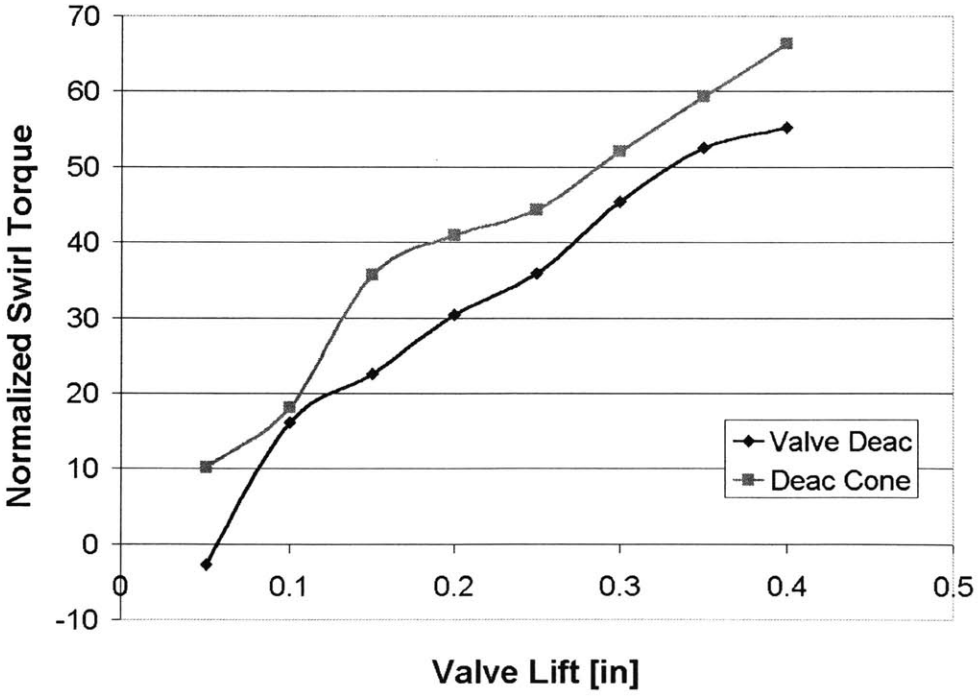

Figure 4.1.4.2- Normalized Swirl Torque vs. Valve Lift with Baseline Head and Right Valve Deactivated vs. Port Deactivation Cone and Both Valves Active

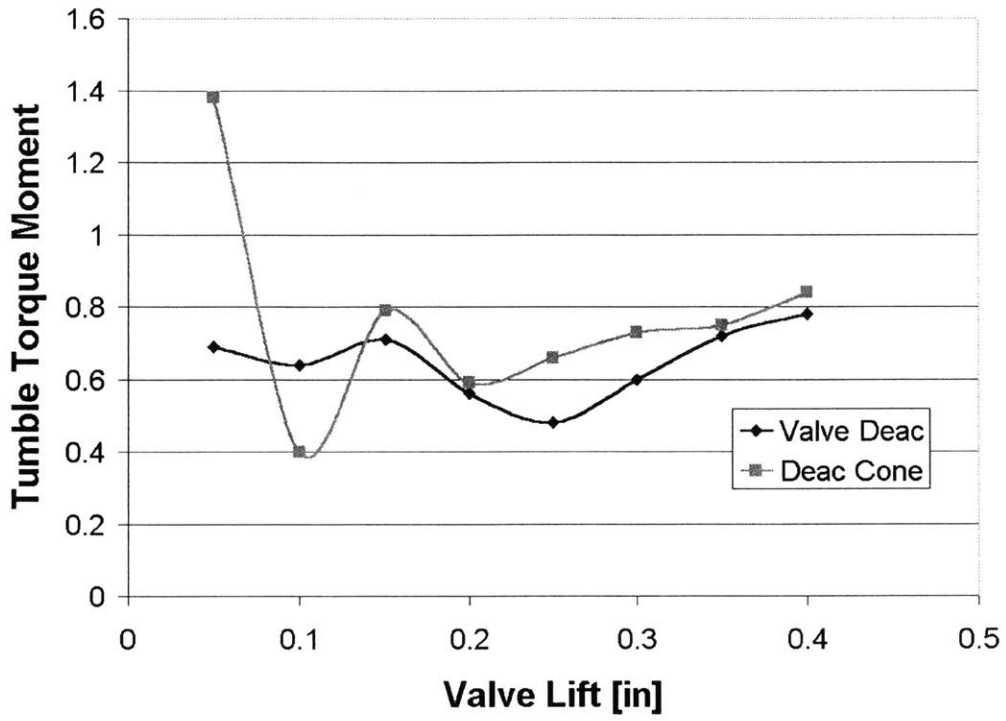

Figure 4.1.4.3- Tumble Torque Moment vs. Valve Lift with Baseline Head and Right Valve Deactivated vs. Port Deactivation Cone and Both Valves Active

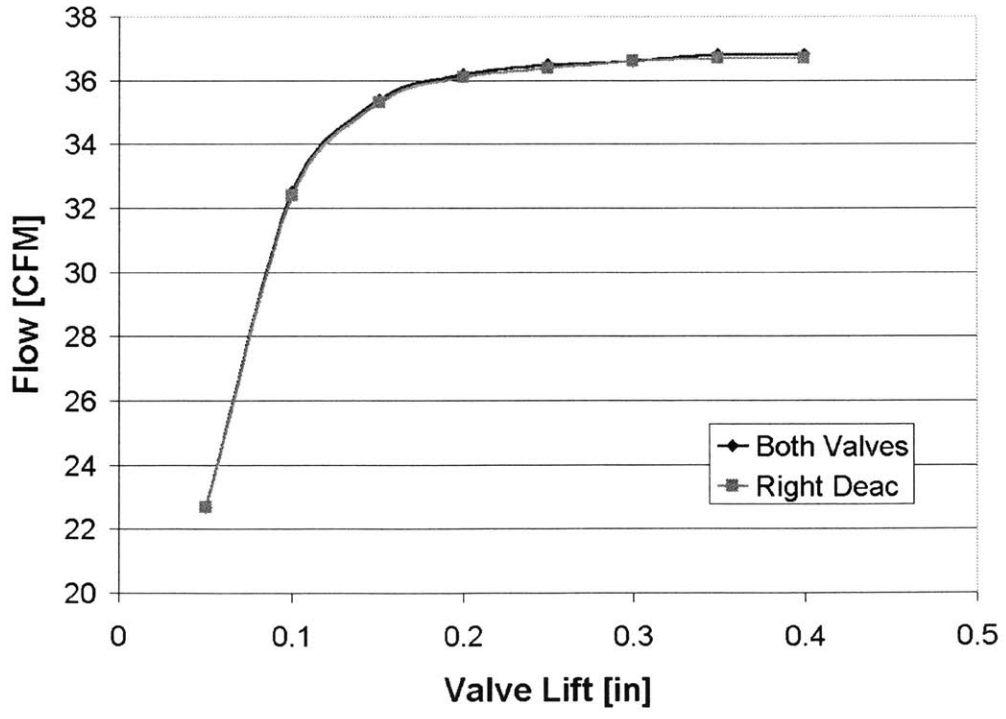

Figure 4.1.5.1- Inlet Port Flow Rate vs. Valve Lift with Extreme Turbulence Cone Comparing Both Valves Active vs. Right Valve Deactivated

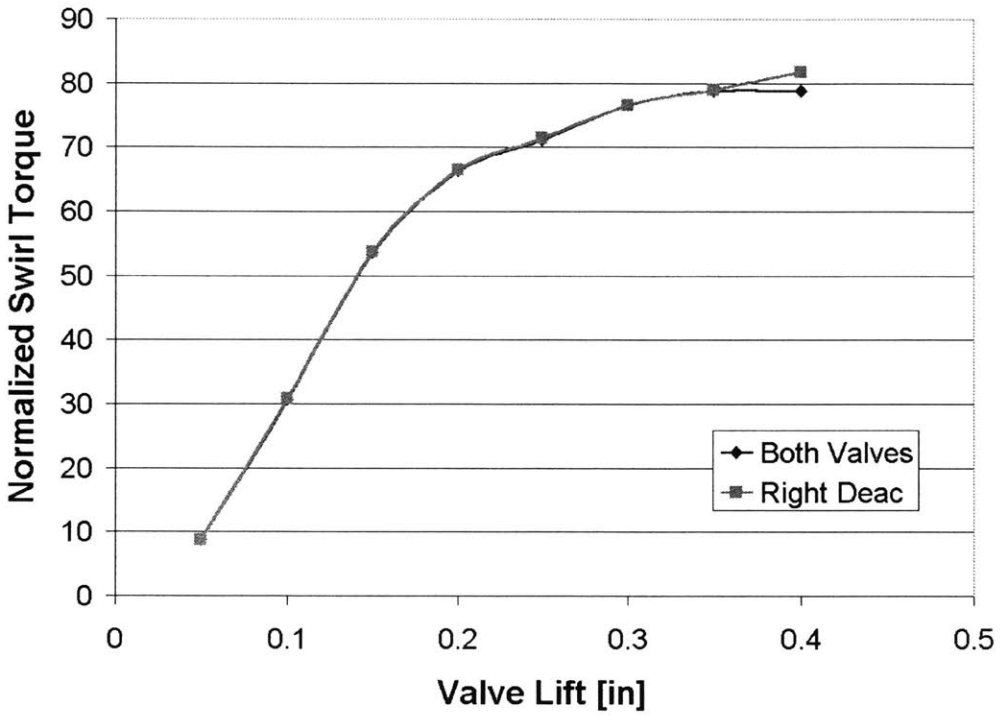

Figure 4.1.5.2- Normalized Swirl Torque vs. Valve Lift with Extreme Turbulence Cone Comparing Both Valves Active vs. Right Valve Deactivated

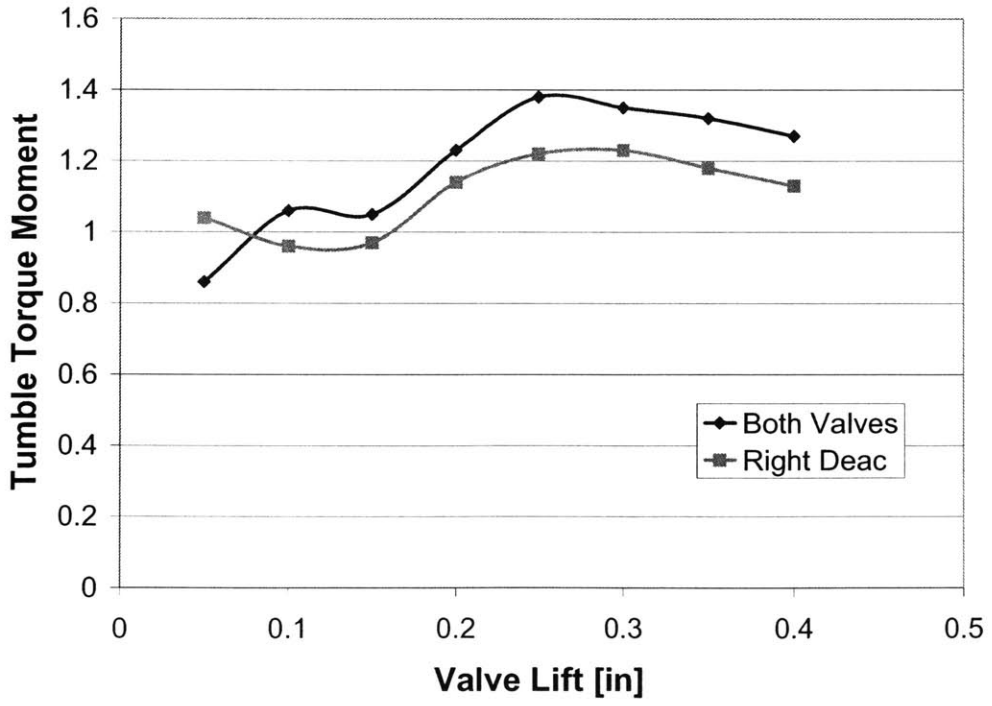

Figure 4.1.5.3- Tumble Torque Moment vs. Valve Lift with Extreme Turbulence Cone Comparing Both Valves Active vs. Right Valve Deactivated

4.2 Dilution Limits

In evaluating the relative performance of different combustion systems under highly diluted lean or EGR operation, it is useful to talk about certain performance limits. This section will clarify the precise definition and significance of each of these limits.

4.2.1- Misfire Limit

For most combustion systems, the misfire limit represents the most diluted possible state of sustainable operation. The misfire limit is the most diluted point of operation at which no misfires or partial burns should be expected to occur in a very high sample set of engine cycles. Looking at a typical lean burn NIMEP trace (Figure 4.2), we see a pronounced roll-off in engine torque at the lean misfire limit. The upturned COV of NIMEP trace shows a dramatic corresponding degradation in engine stability. Moving to a leaner lambda value would bring the immediate onset of misfires and partial burns, causing the COV trace to shoot nearly straight up.

4.2.2- COV Limit

Although it may be possible to operate an engine at the misfire limit without misfires or partial burn cycles, the COV of NIMEP may be unacceptably high for a production application. Many automakers [16] cite 2% as the practical limit for COV of NIMEP. Beyond this point, NVH levels exceed customer expectation. Accordingly, we may designate a COV-limited dilution level by marking the operating point where the COV of NIMEP trace climbs above 2% (Figure 4.2). Since a 2% COV level indicates smooth engine operation and stable combustion, the corresponding NIMEP value is higher than it is at the misfire limit.

4.2.3- Peak NIMEP Limit

While the 2% COV threshold indicates an operating point that could be suitable for a production application, the corresponding NIMEP is still somewhat lower than the peak value. For this reason, it may be desirable to operate at the peak NIMEP limit, which is the dilution level corresponding to peak NIMEP output (Figure 4.2). At this point, the engine is producing maximum torque output for a given amount of fuel flow, while the COV of NIMEP should be at or below 2%. This operating state may represent the best compromise if it requires only a slight reduction in dilution from the COV limit.

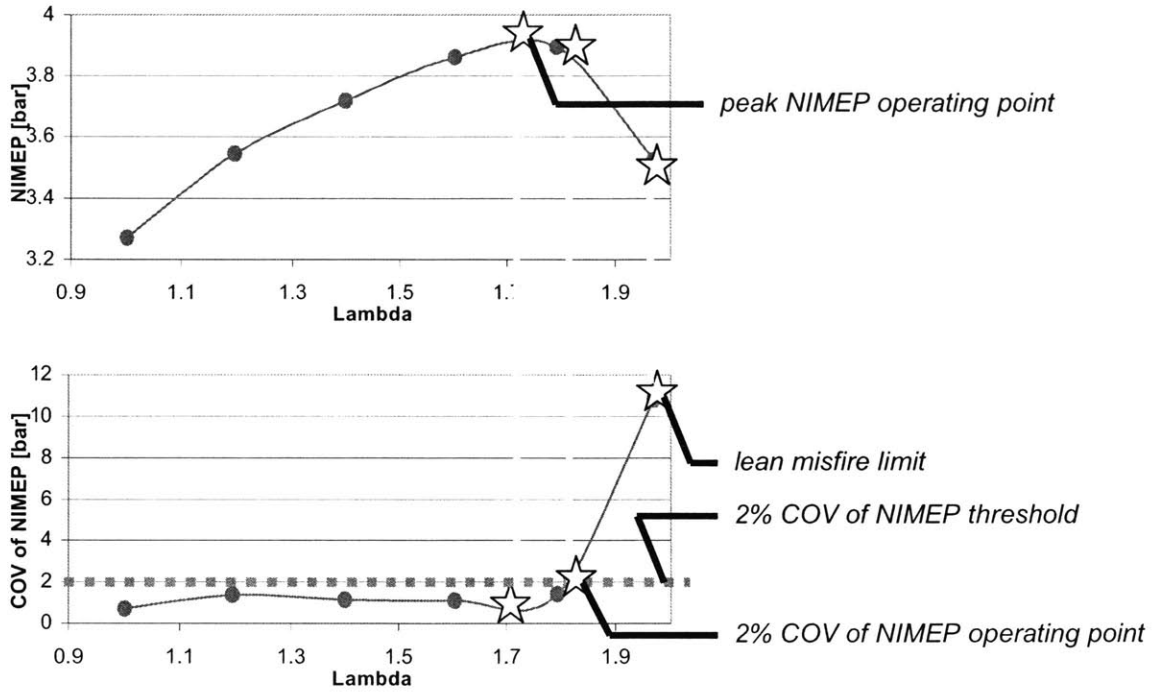

Figure 4.2- Three Critical Lean Limit Operating Points Depicted on NIMEP and COV of NIMEP vs. Lambda Plots (Extreme Turbulence Cone with 20% Enhancement)

4.3 Lean Experimental Results

The lean combustion experiments have been successful in evaluating the impacts of different combustion system modifications and clearly demonstrate which characteristics improve diluted operation and which are detrimental. Furthermore, by examining the overall trends of how combustion system modifications and plasmatron enhancement affect lean operation, two interesting correlations emerge.

4.3.1- Ignition Findings

We begin by comparing the reference combustion system (with a Denso 580 ignition) against the Adrenaline Research Plasma ignition system operating in both low energy (CD) and high energy (DE) modes. First, it should be noted that NIMEP output at $\lambda < \sim 1.6$ is lower with 20% plasmatron enhancement than without (Figure 4.3.1.1). This can largely be attributed to the loss of 4% of the overall fuel energy due to plasmatron inefficiencies. Without enhancement, the Adrenaline DE mode posts the strongest NIMEP output through to the peak of NIMEP limit, which occurs at approximately the same lambda for the reference system. Conversely, the DE mode has practically reached the COV limit at the peak NIMEP limit whereas the reference system has lower COV and ultimately enhanced misfire limit extension (Figure 4.3.1.2). For the enhanced operational sweeps, it is clear that although the Adrenaline DE mode outperforms the CD mode, the reference system is still the best performer with regard to NIMEP, COV, and extension of all three dilution limits. Looking at 0-10% burned interval performance, the Adrenaline DE mode is the fastest burning configuration without enhancement although the reference system does slightly better out near the misfire limit with 20% enhancement (Figure 4.3.1.3). The faster burning tendency of the enhanced mixtures becomes clear for $\lambda > 1.2$. There is far less spread in 10-90% burned performance (Figure 4.3.1.4) than 0-10%. This suggests that the largest impact of the ignition system is seen early in the combustion process when the ignition system is charged with initiating a propagating flame kernel. Once the kernel has developed, the ignition would not be expected to have much impact on flame propagation and the results support this.

Next, we will look at the results of the reference system (0.035 in spark plug gap) compared against an alternate Denso 580 setup with the same Bosch J-plug with a widened 0.070 in gap

and also the MSD Digital 7 Plus ignition with both standard and wide gap Bosch plugs. The widened gap spark plug improves NIMEP output and extension of the misfire and peak NIMEP limits with both the Denso and MSD ignition systems (Figure 4.3.1.5). The improvement is most pronounced with the Denso coil; peak NIMEP with enhanced operation increases by over 2%. Lean extension of the MSD system is quite poor, lagging behind both the Denso and Adrenaline systems. Comparing COV performance, the Denso systems have the leanest extension before reaching the 2% COV limit (Figure 4.3.1.6). COV performance of standard and wide gap plugs is comparable through to the 2% threshold; beyond this, the wide gap plugs have slightly greater extension before reaching the misfire limit. In agreement with the improved NIMEP and COV performance, the wide gap plugs also demonstrate faster 0-10% burn intervals (Figure 4.3.1.7). Below the peak NIMEP limits, the MSD configurations burn slightly faster than the Denso systems, but then more slowly moving out to the misfire limit. Similarly, the MSD systems are faster burning over the 10-90% interval until roughly the peak NIMEP limit, after which the Denso systems burn fastest to the misfire limit (Figure 4.3.1.8). Interestingly, the Denso system has marginally faster 10-90% burn with the narrow gap plug as opposed to the wide gap plug, both with and without enhancement.

Overall, these findings indicate that the Denso system is the best performer with highly diluted mixtures, allowing leaner operation with higher NIMEP and lower COV than the Adrenaline or MSD system. Furthermore, a wide gap Bosch platinum J-plug offers improved performance over the standard gap reference plug. These results support earlier findings that the longer discharge time constant of an inductive coil ignition leads to improved performance over the short duration discharge of higher energy capacitive systems.

4.3.2- Charge Motion Control Findings

First we compare the performance of the reference configuration (2/3 asymmetric restrictor plate) against the extreme turbulence, moderate turbulence, and port deactivation cones. In the absence of enhancement, the reference system offers the greatest peak NIMEP output while the moderate turbulence cone has the greatest extension of all three lean limits (Figure 4.3.2.1). The port deactivation cone sees the earliest peak NIMEP limit while the extreme turbulence cone seems to reach the misfire limit right near the point of peak NIMEP, *before* hitting the 2% COV

threshold (Figure 4.3.2.2). This suggests that as the flow rate increases in the highly dilute regime, the turbulence levels being generated are too high, resulting in quenching of the flame front. Turning toward 20% enhanced performance, we see that the extreme and moderate turbulence cones have a slight edge in misfire limit extension over the reference configuration; however, the reference setup maintains a much higher NIMEP output at the misfire limit. Correspondingly low COV of NIMEP near the misfire limit is also measured. Peak NIMEP output of the reference restrictor and moderate turbulence cone match very closely while the extreme turbulence cone sees the best peak NIMEP performance with the highest output and greatest extension of the peak NIMEP limit. The port deactivation cone is the poorest enhanced operation performer in all respects. With regard to 0-10% burned interval performance, the extreme turbulence cone shows the fastest combustion, followed closely by the moderate cone, then the reference restrictor, and with the port deactivation cone trailing (Figure 4.3.2.3). This same order of performance is seen both with and without enhancement. This data clearly shows how turbulent flow conditions are able to accelerate combustion; even at the misfire limit, the extreme turbulence cone allows the first 10% of air-fuel mixture to be burned in less than 25 CAD. The 0-10% data also provides some insight on the abrupt onset of misfires seen with non-enhanced operation of the extreme turbulence cone. The corresponding 0-10% trace takes a sudden upwards turn right before the misfire limit, affirming the rapid deterioration of combustion stability. The 10-90% burned interval data reveals the same ranking of relative combustion speed seen in the 0-10% data (Figure 4.3.2.4). There is a far greater spread in 10-90% performance between these different charge motion configurations than was seen in comparing different ignition systems in section 4.3.1. This further demonstrates that in-cylinder turbulence affects the entire combustion process while ignition effects primarily impact the early stages of combustion.

Next we move on to a comparison of the reference restrictor plate against the tumble cone and the baseline head without restriction. The reference system shows the greatest non-enhanced lean misfire limit extension while the tumble cone has the greatest peak NIMEP output and leanest peak NIMEP limit (Figure 4.3.2.5). In the case of the tumble cone, the non-enhanced peak NIMEP limit, 2% COV limit, and misfire limit are concurrent (Figure 4.3.2.6). This is similar to the non-enhanced performance of the extreme turbulence cone; perhaps this behavior can also be

attributed to excessive in-cylinder turbulence. With 20% enhancement, the reference system offers more than $\lambda = 0.15$ greater extension of the misfire limit but sees lower NIMEP output than the other two configurations up until $\lambda = 1.8$. These findings are supported by very close matching of the tumble cone and unrestricted head enhanced COV traces, while the reference restrictor maintains low COV out to nearly $\lambda = 2.0$. Examining the 0-10% burned interval data, we see that the reference system is the fastest burning, followed closely by the tumble cone (Figure 4.3.2.7). The baseline head generates far slower combustion; the baseline 0-10% interval with enhancement is approximately 15 CAD slower than the reference restrictor at $\lambda = 1.8$. The same ranking of combustion speed is observed with and without enhancement. The higher combustion speed of the reference case is even more evident in the 10-90% burned interval data (Figure 4.3.2.8). The restrictor plate gives faster 10-90% combustion *without* enhancement than the other two inlet configurations see *with* 20% enhancement. For the tumble cone and baseline head, enhancement does not seem to accelerate 10-90% burn, however it does provide greater misfire extension.

In summary, it is difficult to single out one best performing charge motion configuration. Instead, each configuration must be evaluated against a particular performance criterion. In terms of non-enhanced operation, the tumble cone generates the highest peak NIMEP while the moderate turbulence cone is characterized by the greatest extension of all three dilution limits. In enhanced operation, the best performers are the reference restrictor and the extreme turbulence and moderate turbulence cones. These two cones offer the leanest misfire limit while the restrictor trades only a slight amount of misfire limit extension for a broader, flatter NIMEP curve. In comparison, the highly peaked extreme turbulence cone offers the highest peak NIMEP occurring at the leanest peak NIMEP limit. In terms of combustion speed, the extreme turbulence cone offers the fastest burn in 0-10% and 10-90% intervals, with and without enhancement. The moderate turbulence cone trails as a close second.

4.3.3- Mixture Preparation Findings

The NIMEP trace indicates far better non-enhanced output with the Delphi 12-hole injector compared against the reference Bosch single-hole injector (Figure 4.3.3.1). The Delphi injector also sees corresponding improvement in all three non-enhanced dilution limits. Similarly, the

COV plot shows delayed deterioration of engine stability with the Delphi injector (Figure 4.3.3.2). It should be noted that because of the limitations of the fuel pulse width adjustment in the MoTeC ECU, the actual fuel delivered might have been approximately 2% higher with the Delphi injector, which could explain most of the NIMEP improvement. With 20% enhancement, the Bosch injector has a very slight edge in NIMEP output while the Delphi injector demonstrates slightly greater extension of the misfire and peak NIMEP dilution limits. COV performance is virtually identical. The 0-10% burned interval plot shows a very slight (~ 1 CAD) improvement in non-enhanced combustion speed with the Delphi injector and a more pronounced improvement in 20% enhanced speed (~4 CAD) near the misfire limit (Figure 4.3.3.3). Looking at 10-90% burned interval data, the Delphi injector sees a nearly constant 2 CAD improvement in non-enhanced combustion speed while the enhanced combustion speed is nearly identical for both injectors.

Overall, the Dephi fine-atomizing injector seems to meet or exceed the performance of the reference Bosch injector against all metrics. Although some of the improvements are small and could probably be attributed to the ~2% increase in fuel delivered per cycle with the Delphi injector, the use of a fine-atomizing injector is certainly not detrimental to highly diluted combustion performance.

4.3.4- Composite Findings

For the final set of combustion results, we look at the combined effects of using two different combustion system modifications, in this case the Delphi injector with the extreme turbulence cone. Both of these devices posted good performance as mixture preparation and charge motion control modifications. Plots were prepared showing the reference system (with Bosch injector and 2/3 asymmetric restrictor plate) along with the Delphi-only setup, the extreme turbulence cone-only setup, and then the composite setup with both the Delphi injector and the extreme turbulence cone. NIMEP output of the non-enhanced composite setup closely follows the Delphi-only trace, which far exceeds the performance of the reference setup and the extreme turbulence-only cone (Figure 4.3.3.1). Interestingly, the enhanced NIMEP performance of the composite setup trails behind the other three traces for $\lambda > 1.85$. The peak NIMEP limit of the composite setup closely matches that of the extreme turbulence cone-only setup, which is

slightly better than the corresponding limit of the reference or Delphi-only setups. The composite NIMEP curve is much flatter than the extreme turbulence cone curve and the peak NIMEP output is lower. At the misfire limit, the composite setup gains the improved extension of the extreme turbulence cone without the severe roll off of NIMEP output. The composite setup posts the best COV performance, slightly ahead of the reference or Delphi-only setups and far better than the extreme turbulence cone-only setup (Figure 4.3.3.2). The composite setup also posts the strongest 0-10% performance, burning slightly faster than the already outstanding extreme turbulence cone configuration (Figure 4.3.3.3). In the non-enhanced case, the combustion speed remains extremely fast out to nearly $\lambda = 1.8$ whereas the extreme turbulence cone suffered abrupt degradation just past $\lambda = 1.6$. Performance in the 10-90% burned interval is also best in the comparison, coming out slightly ahead of the extreme turbulence cone-only setup (Figure 4.3.3.4). These extreme turbulence cone-based configurations both burn far faster than the restrictor plate-based reference and Delphi-only setups.

The composite tests point to very promising performance potential for the combination of more than one combustion enhancing technique. The composite setup seemed to combine some of the best performance attributes of the Delphi injector and the extreme turbulence cone. Still, it appears that testing is required to assess the exact performance of a composite setup. As an example, the NIMEP output of the composite setup trailed behind that of the extreme turbulence cone-only setup through to the peak NIMEP limit, but then outperformed the cone-only system close to the misfire limit.

4.3.5- Trend Analysis

A number of trends emerge by comparing the flow bench test results against combustion data from the corresponding charge motion control experiments. Six different charge motion configurations were evaluated in the combustion experiments (the four cones, baseline unrestricted head, and reference 2/3 asymmetric restrictor plate) and there is also flow bench data for all of these setups. All swirl and tumble measurements correspond to 0.350 in valve lift, which is close to the maximum valve lift of the test engine. A scatter plot of normalized swirl torque vs. lambda at both the peak NIMEP limit and the lean misfire limit without plasmatron enhancement does not reveal any correlations (Figure 4.3.5.1). Similarly, plotting the same chart

using 20% enhanced combustion data also fails to revel any trends, although there is greater separation between the NIMEP limit points and the lean misfire limit points (Figure 4.3.5.2). By contrast, a trend begins to emerge when tumble torque moment is plotted against non-enhanced data for lambda at the peak NIMEP limit and the lean misfire limit. The peak NIMEP limit points show a fair amount of scatter whereas the lean misfire limit trend seems to be directly related to tumble torque moment (Figure 4.3.5.3). The configurations with highest tumble also have the most extended lean misfire limit. A tumble moment plot with 20% enhanced combustion data shows the same trend to be unmistakable (Figure 4.3.5.4). At both the peak NIMEP limit and the lean misfire limit, the configurations with the greatest lean extension have the highest tumble torque moments while the worst performers have the lowest tumble torque moments. In particular, the three data points corresponding to the 2/3 asymmetric restrictor plate, extreme turbulence cone and moderate turbulence cone are very closely grouped. These three configurations produce nearly identical levels of tumble and also have very closely matched peak NIMEP and lean misfire limits.

From these results, it appears that swirl turbulence has no identifiable impact on the peak NIMEP limit or the lean misfire limit performance. Conversely, tumble motion coupled with plasmatron enhancement promotes extension of both the peak NIMEP limit and the lean misfire limit. This supports Ed Tully's findings [2], which measured the best limit extension with the 2/3 asymmetric restrictor plate (now known to generate more tumble than the other two plates.) Without enhancement, tumble does not have a clear impact on the peak NIMEP limit but there is a correlation with improvement of the lean misfire limit.

A further series of plots examines how plasmatron enhancement affects a shift in both the peak NIMEP limit and the lean misfire limit. These charts incorporate data for *all* combustion enhancement experiments, not just charge motion control experiments. A scatter plot of the absolute shift in the peak NIMEP limit moving from non-enhanced to 20% enhanced operation vs. the peak NIMEP limit at non-enhanced conditions reveals a downward trend (Figure 4.3.5.5). This means that the test configurations showing the worst baseline non-enhanced performance saw the greatest improvement in the peak NIMEP limit with 20% enhacement. Alternatively, the best performing baseline systems saw the smallest improvements in the peak NIMEP limit. It

remains to be seen if this trend would continue for a baseline combustion system that brings the peak NIMEP limit past $\lambda = 1.8$ (a very formidable challenge.) The results for a similar scatter plot based around lean misfire limit data show a somewhat different trend (Figure 4.3.5.6). Regardless of baseline misfire limit performance, 20% enhancement affects a nearly constant improvement in the misfire limit in the range $\lambda = 0.18 - 0.25$. One outlier, corresponding to the performance of the unrestricted Volvo head, saw an even greater $\lambda = 0.34$ shift in the lean misfire limit. The difference between NIMEP limit and misfire limit behavior with plasmatron addition is best explained by the different mechanisms that govern these limits. Higher NIMEP is achieved when the combustion process is faster. Furthermore, engine efficiency is inversely related to burn duration, with efficiency levels deteriorating more quickly as burn becomes slower. For a poor performing baseline combustion system that is already burning slowly at a less lean peak NIMEP limit, hydrogen enhancement will be able to offer greater improvement than for a faster burning system that sees shorter burn intervals near the peak NIMEP limit. Furthermore, the downward slope in Figure 4.3.5.5 reveals the continuous nature of this limit. In contrast, flame quenching at the misfire limit is more of an abrupt, cutoff-type effect. When the adiabatic flame temperature reaches the quenching temperature ($T_{quench} \sim 1600$K [23]), the thermal gradient between burned and unburned mixture is too small to conduct thermal energy (and diffuse radicals.) Flame reaction kinetics cannot be initiated and combustion will cease. Hydrogen addition promotes thermal and radical diffusion, increasing the laminar (molecular) flame speed and delaying the quenching process. Regardless of baseline performance, the impact of hydrogen addition in preventing quenching should be nearly constant and this is reflected in the constant misfire limit shift seen in experimental results.

In designing future plasmatron enhanced combustion systems, the time and expense spent to improve the performance of the baseline combustion system may depend upon the intended operating point. For operation at the peak NIMEP limit, the trend of diminishing marginal returns raises questions about the ideal balance between baseline combustion performance and combustion enhancement through plasmatron reformate addition. In all cases, the peak NIMEP limit with enhancement falls in the range $\lambda = 1.58 - 1.74$, regardless of baseline performance. Alternatively, for operation close to the lean misfire limit, it seems that a good baseline system is critical because the misfire limit shift promoted by plasmatron enhancement is constant.

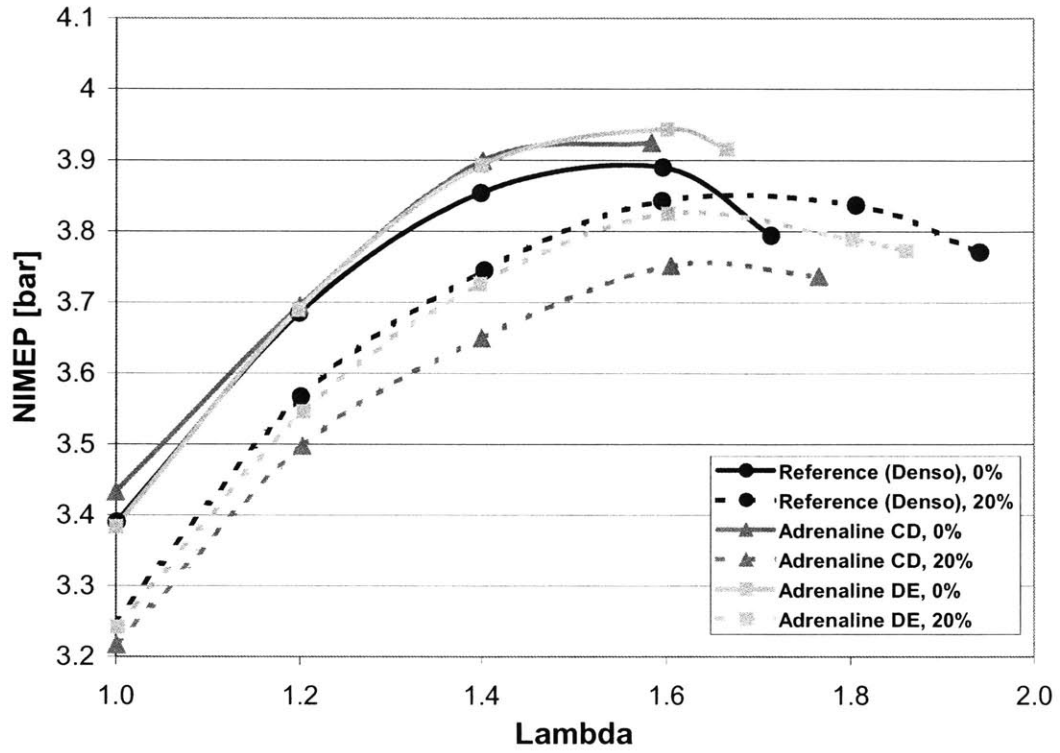

Figure 4.3.1.1- Ignition Results 1: Reference (Denso 580 Ignition) vs. Adrenaline Research Ignition at Low Energy (CD) and High Energy (DE) Settings with 0 and 20% Enhancement

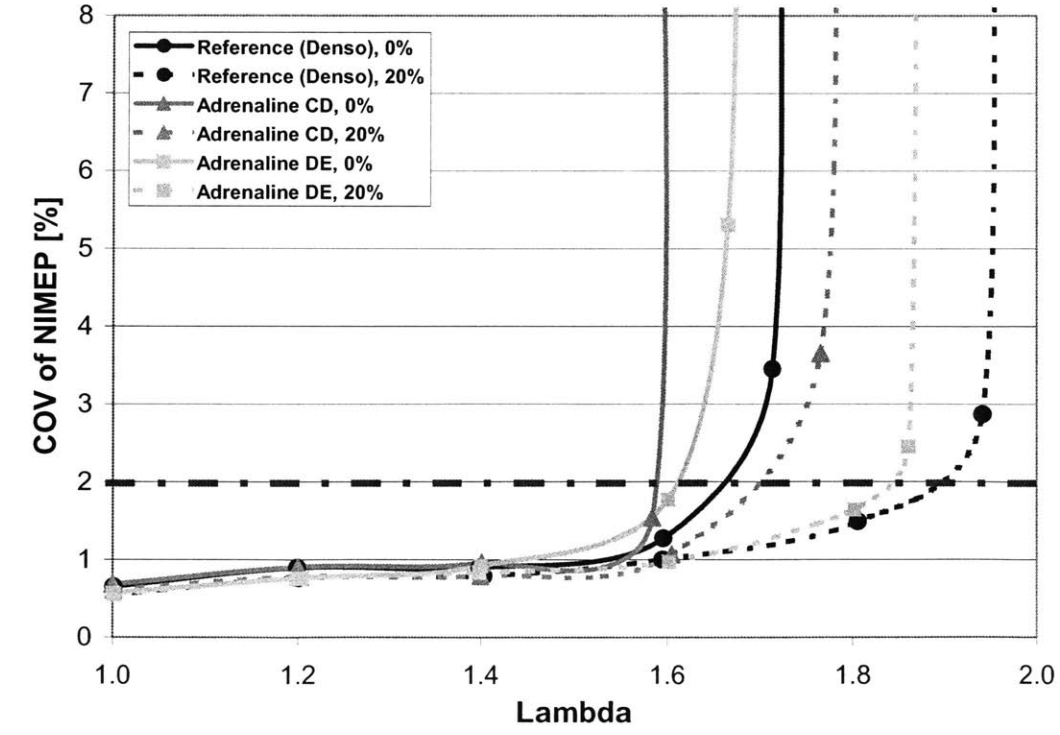

Figure 4.3.1.2- Ignition Results 2: Reference (Denso 580 Ignition) vs. Adrenaline Research Ignition at Low Energy (CD) and High Energy (DE) Settings with 0 and 20% Enhancement

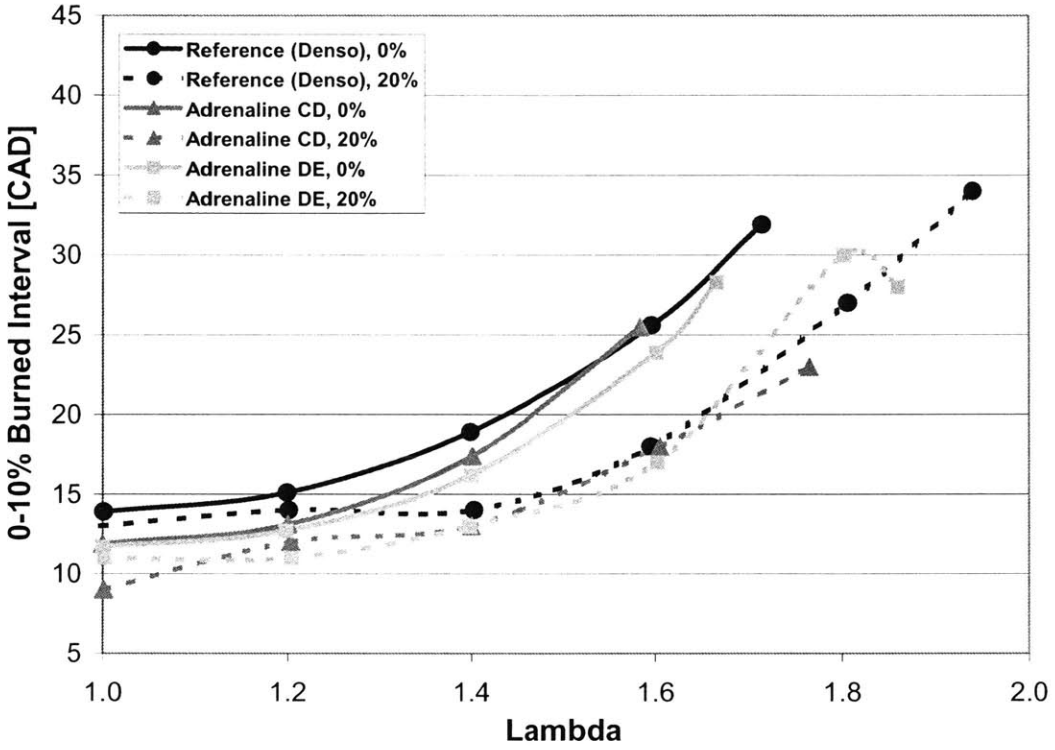

Figure 4.3.1.3- Ignition Results 3: Reference (Denso 580 Ignition) vs. Adrenaline Research Ignition at Low Energy (CD) and High Energy (DE) Settings with 0 and 20% Enhancement

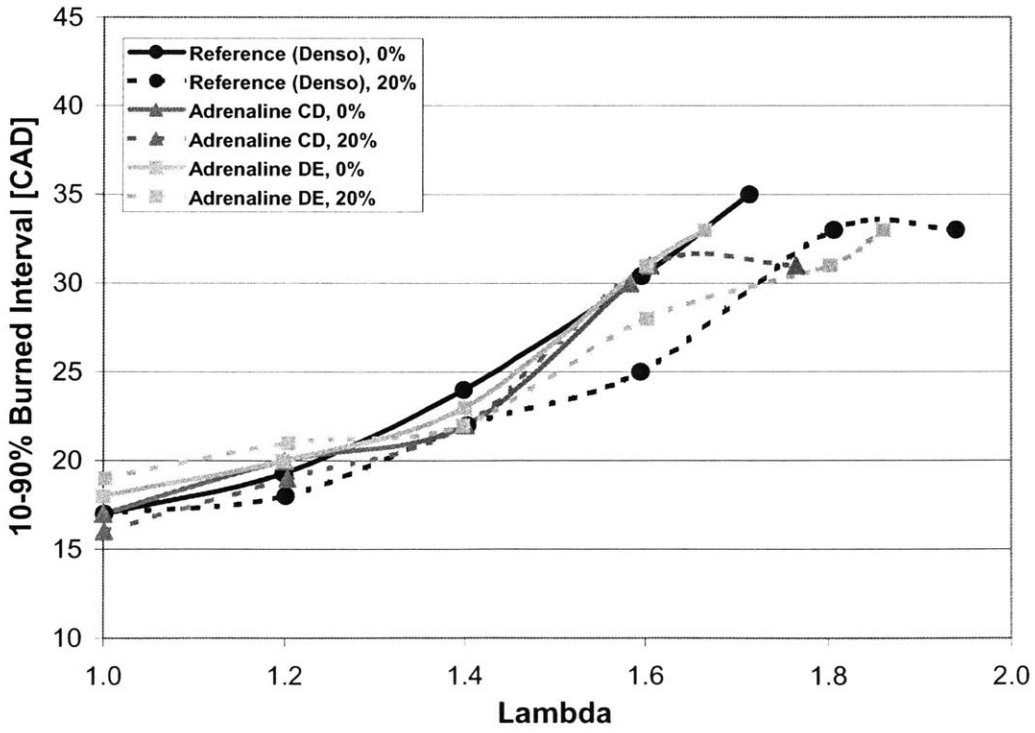

Figure 4.3.1.4- Ignition Results 4: Reference (Denso 580 Ignition) vs. Adrenaline Research Ignition at Low Energy (CD) and High Energy (DE) Settings with 0 and 20% Enhancement

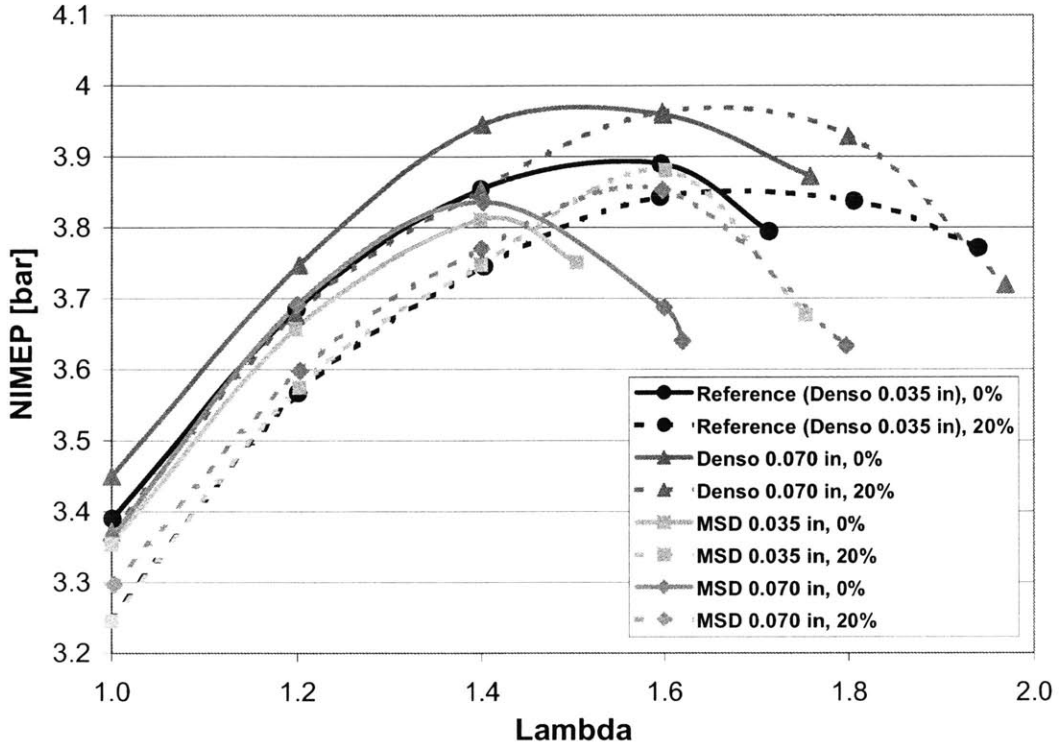

Figure 4.3.1.5- Ignition Results 5: Reference (Denso 580, 0.035 in Plug Gap) vs. Denso 580, 0.070 in Gap and MSD Ignition, 0.035 in or 0.070 in Gap with 0 and 20% Enhancement

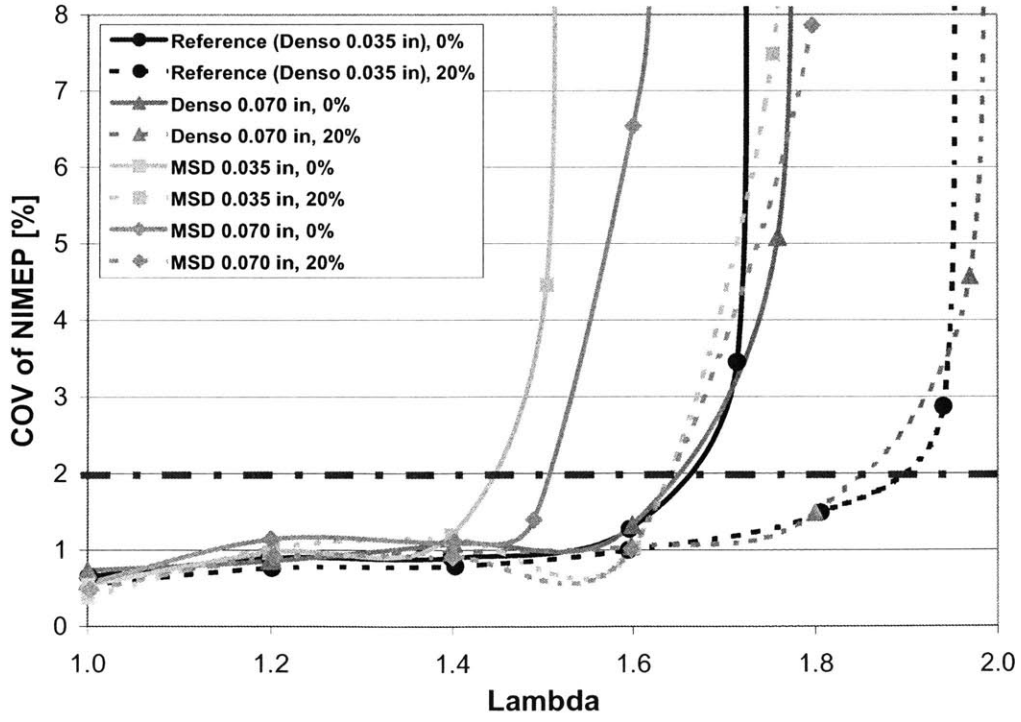

Figure 4.3.1.6- Ignition Results 6: Reference (Denso 580, 0.035 in Plug Gap) vs. Denso 580, 0.070 in Gap and MSD Ignition, 0.035 in or 0.070 in Gap with 0 and 20% Enhancement

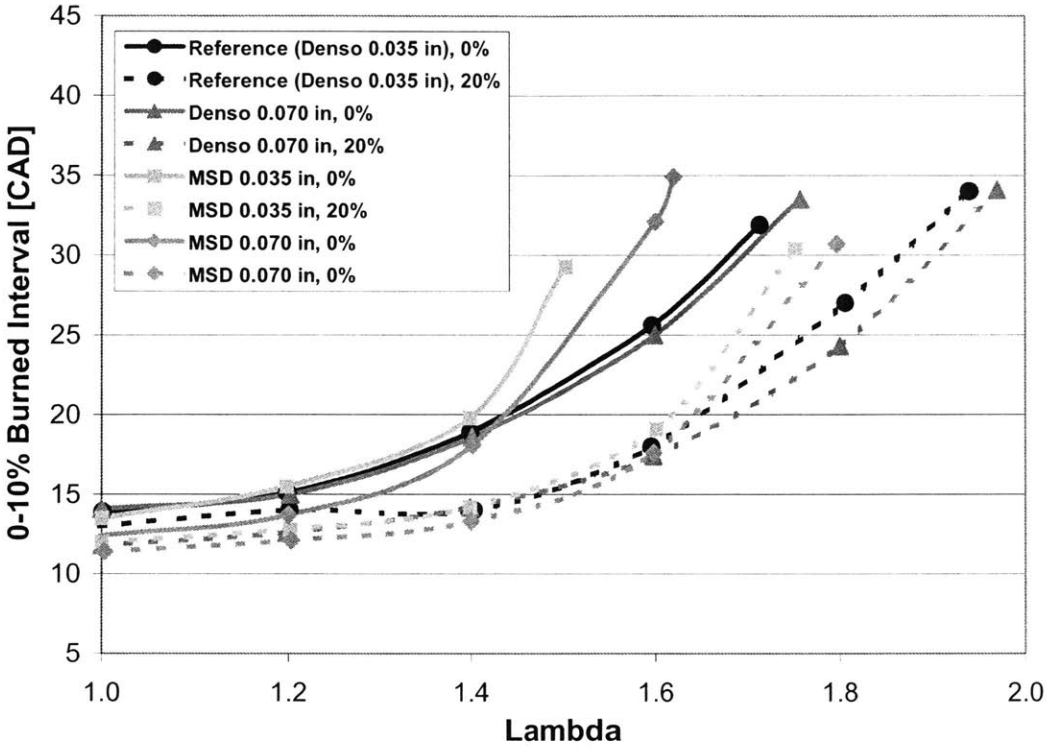

Figure 4.3.1.7- Ignition Results 7: Reference (Denso 580, 0.035 in Plug Gap) vs. Denso 580, 0.070 in Gap and MSD Ignition, 0.035 in or 0.070 in Gap with 0 and 20% Enhancement

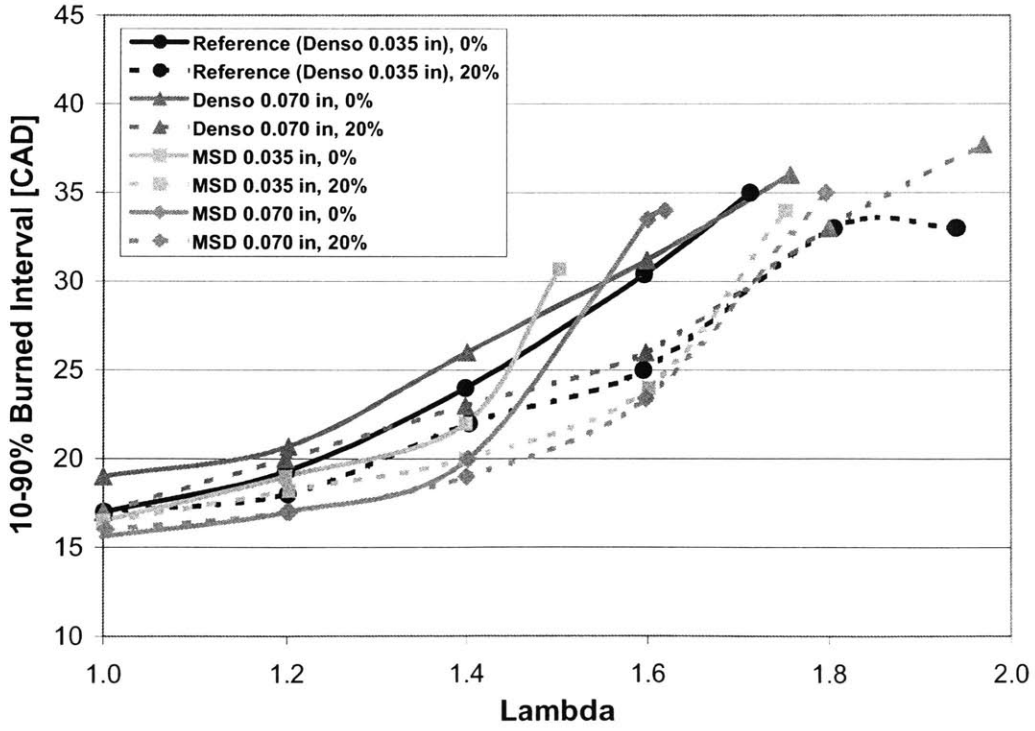

Figure 4.3.1.8- Ignition Results 8: Reference (Denso 580, 0.035 in Plug Gap) vs. Denso 580, 0.070 in Gap and MSD Ignition, 0.035 in or 0.070 in Gap with 0 and 20% Enhancement

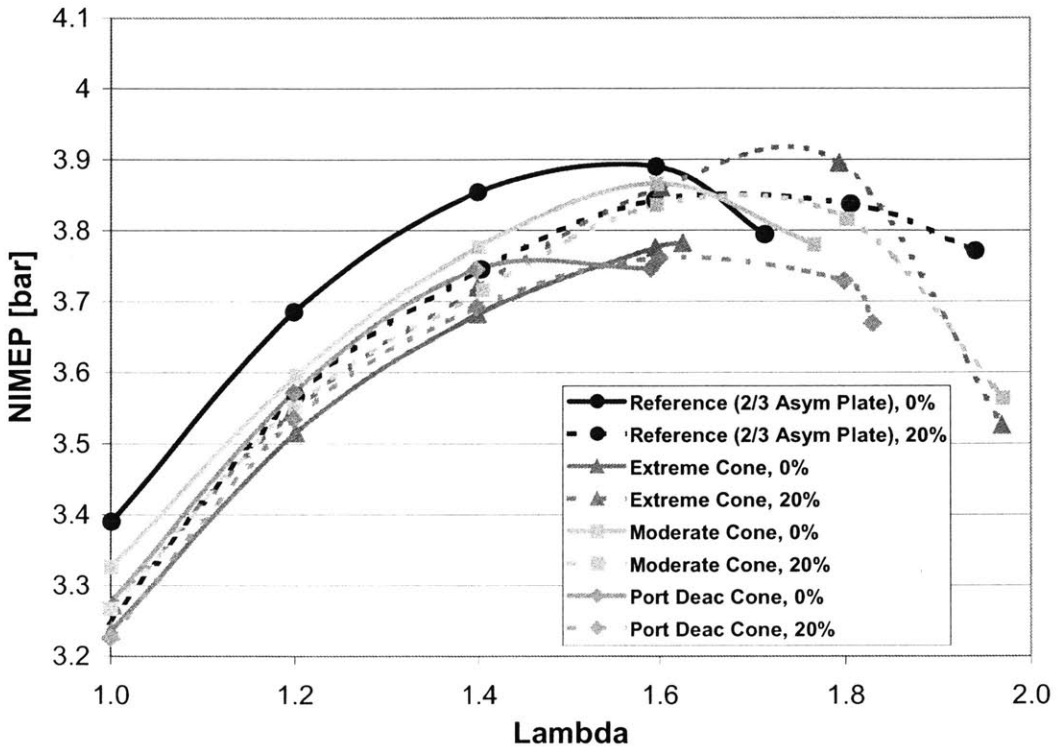

Figure 4.3.2.1- Chg. Motion Results 1: Reference (2/3 Asymmetric Restrictor Plate) vs. Extreme Turbulence, Moderate Turbulence, and Port Deactivation Cones with 0 and 20% Enhancement

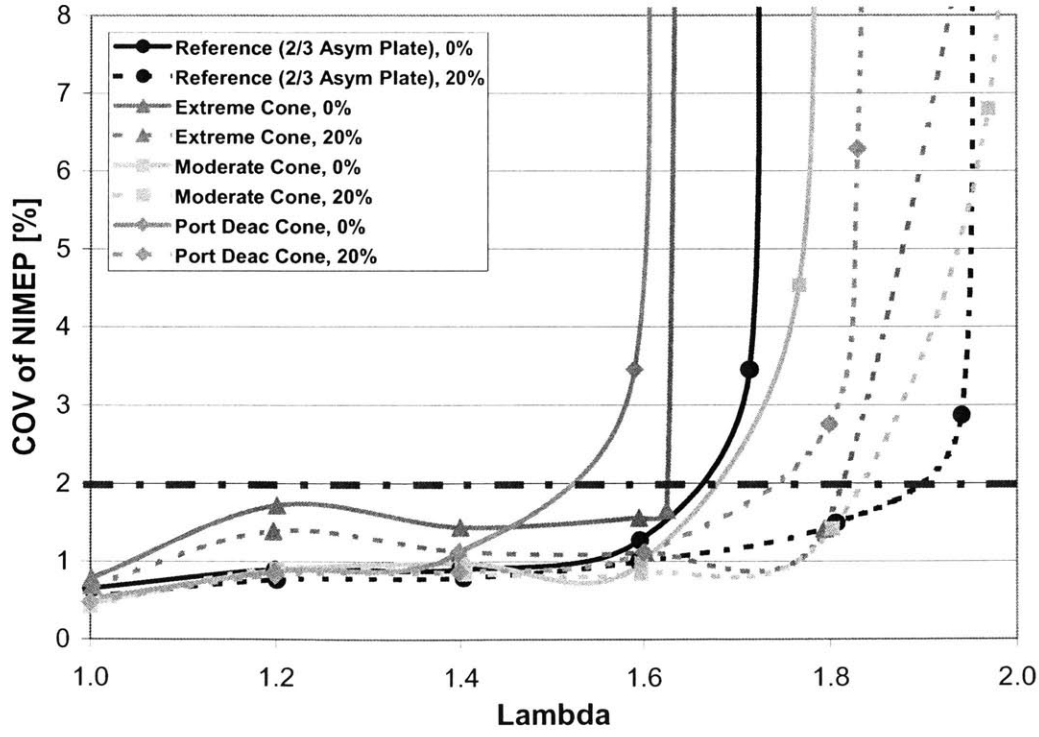

Figure 4.3.2.2- Chg. Motion Results 2: Reference (2/3 Asymmetric Restrictor Plate) vs. Extreme Turbulence, Moderate Turbulence, and Port Deactivation Cones with 0 and 20% Enhancement

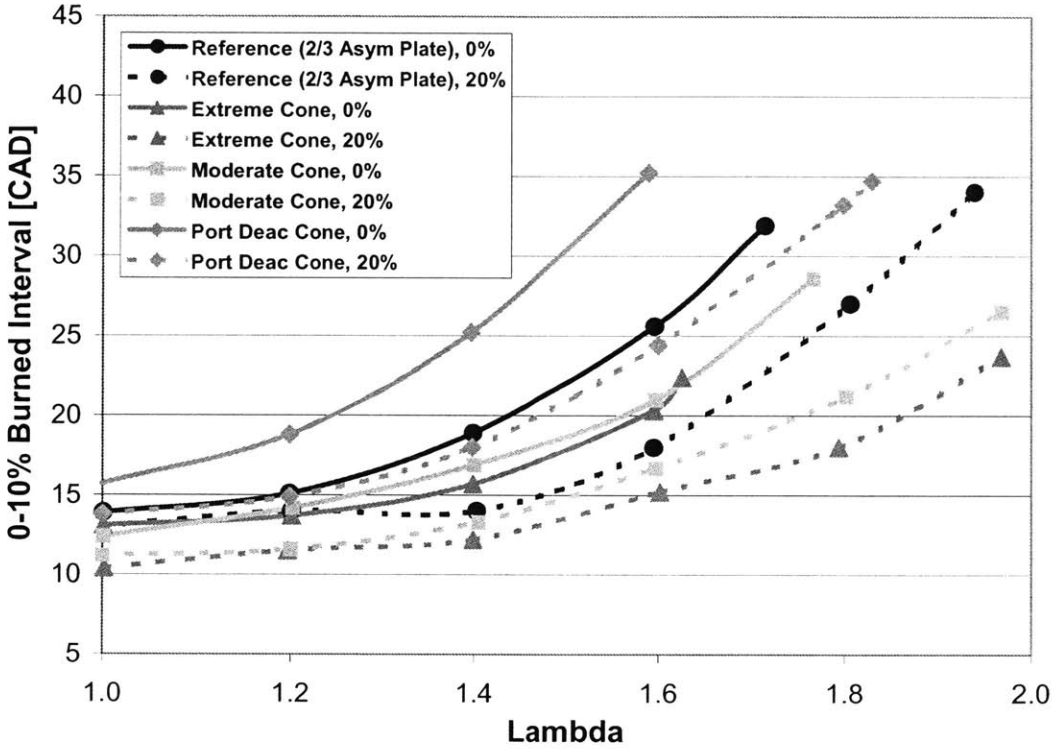

Figure 4.3.2.3- Chg. Motion Results 3: Reference (2/3 Asymmetric Restrictor Plate) vs. Extreme Turbulence, Moderate Turbulence, and Port Deactivation Cones with 0 and 20% Enhancement

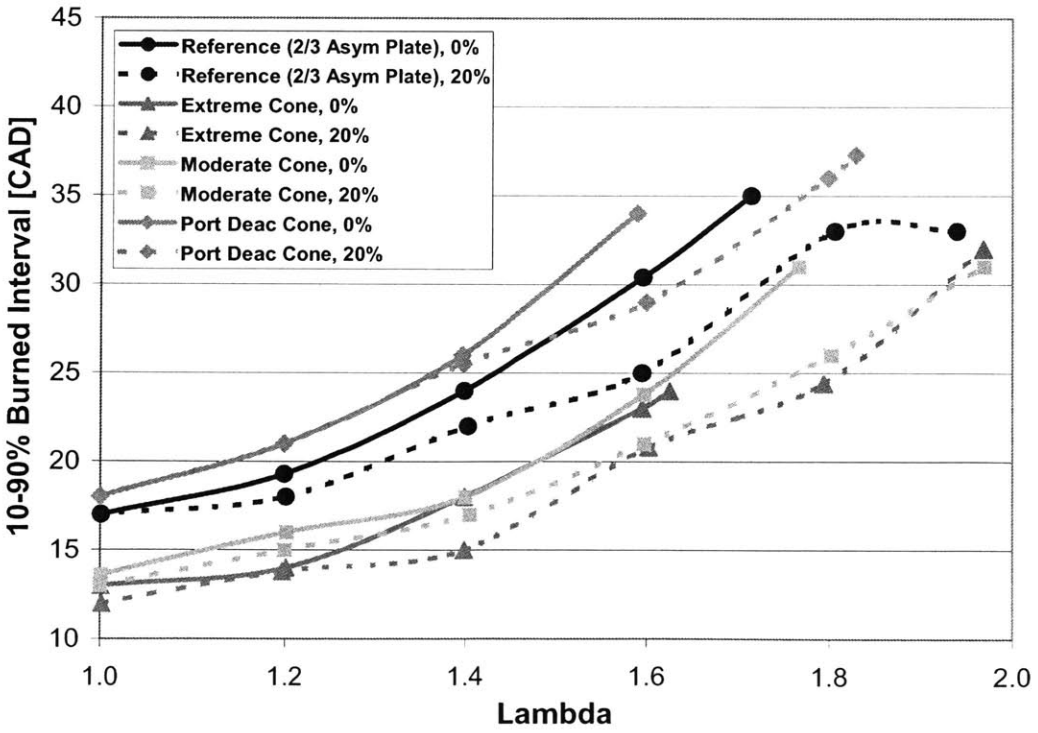

Figure 4.3.2.4- Chg. Motion Results 4: Reference (2/3 Asymmetric Restrictor Plate) vs. Extreme Turbulence, Moderate Turbulence, and Port Deactivation Cones with 0 and 20% Enhancement

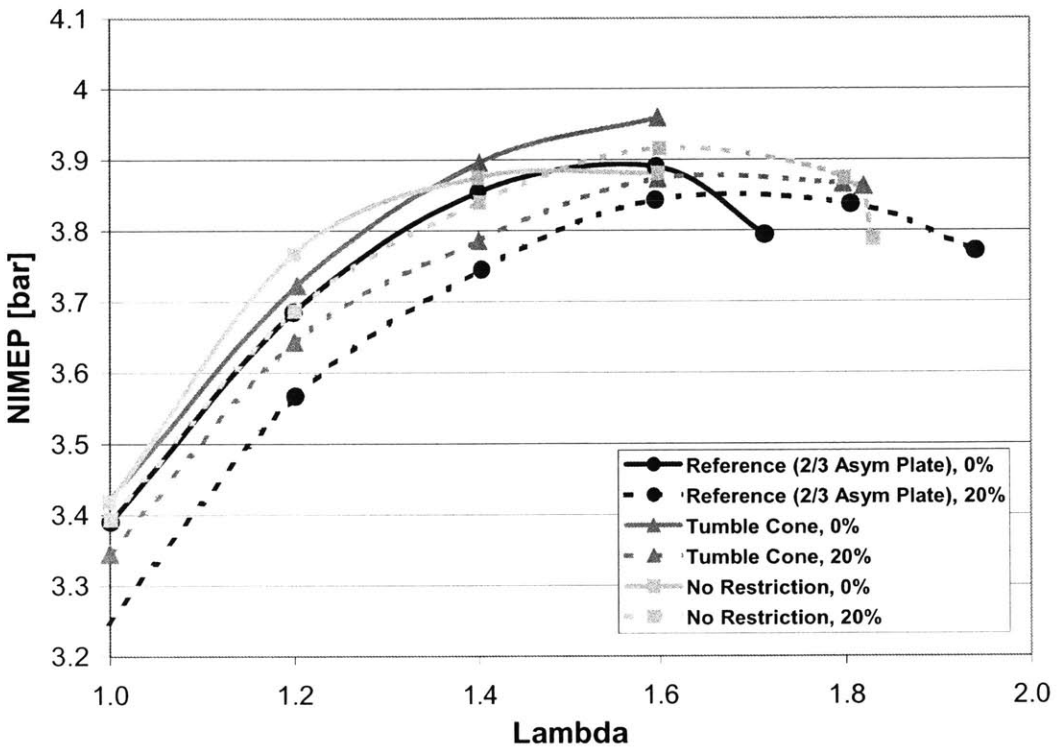

Figure 4.3.2.5- Chg. Motion Results 5: Reference (2/3 Asymmetric Restrictor Plate) vs. Tumble Cone and Baseline Unrestricted Head with 0 and 20% Enhancement

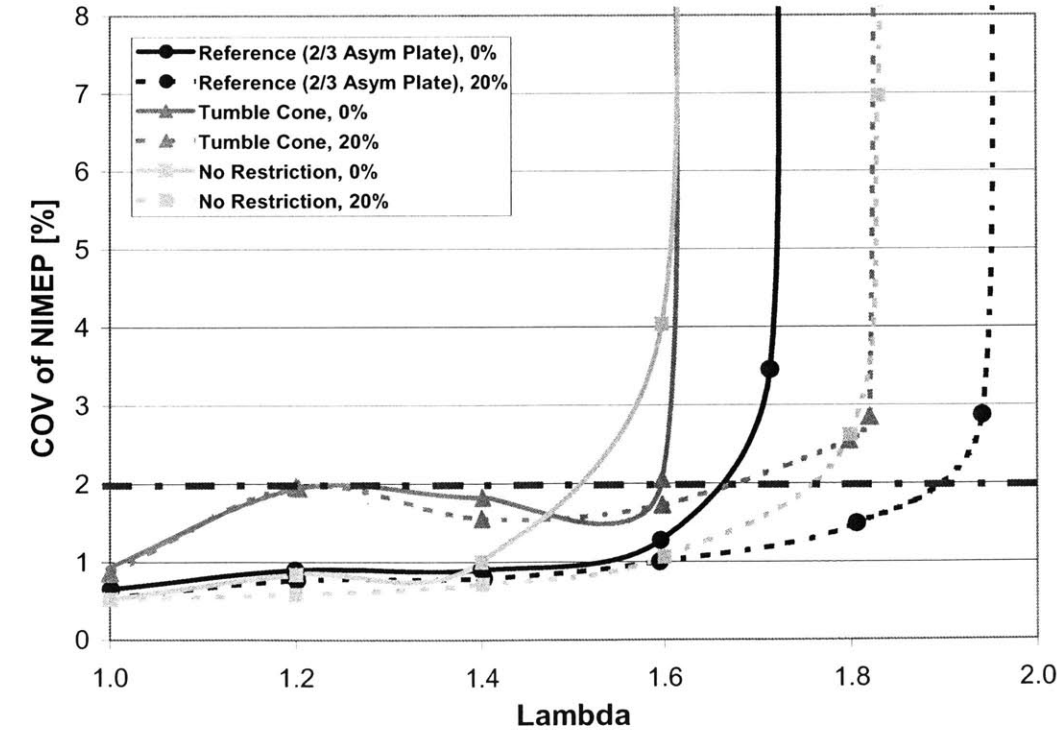

Figure 4.3.2.6- Chg. Motion Results 6: Reference (2/3 Asymmetric Restrictor Plate) vs. Tumble Cone and Baseline Unrestricted Head with 0 and 20% Enhancement

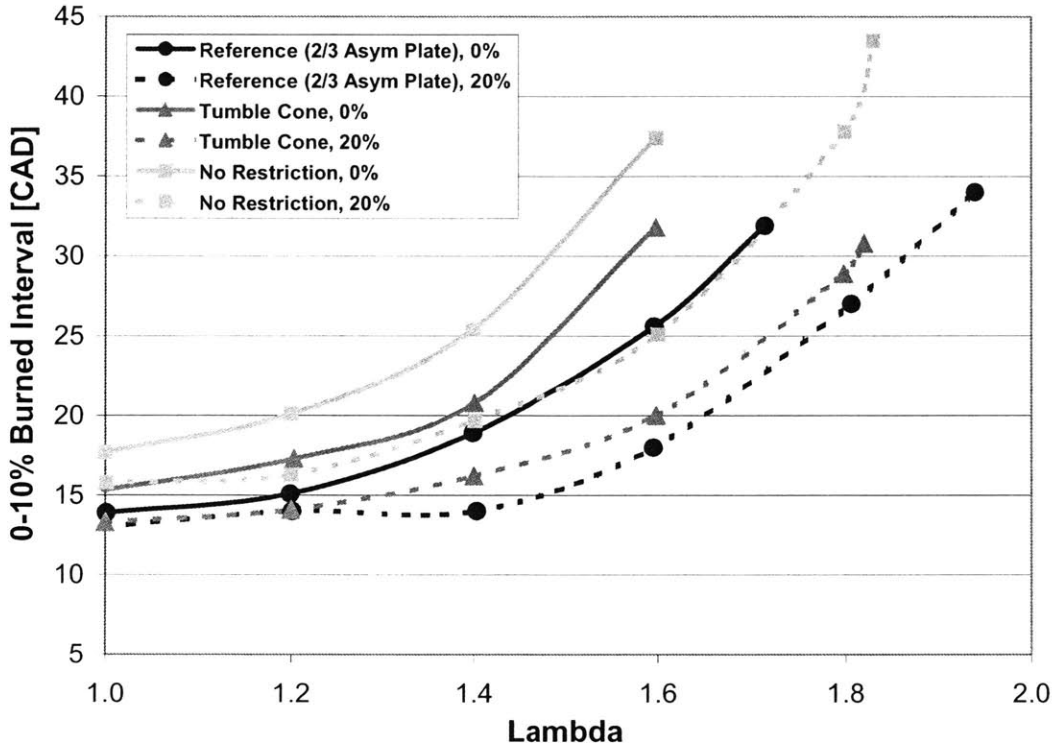

Figure 4.3.2.7- Chg. Motion Results 7: Reference (2/3 Asymmetric Restrictor Plate) vs. Tumble Cone and Baseline Unrestricted Head with 0 and 20% Enhancement

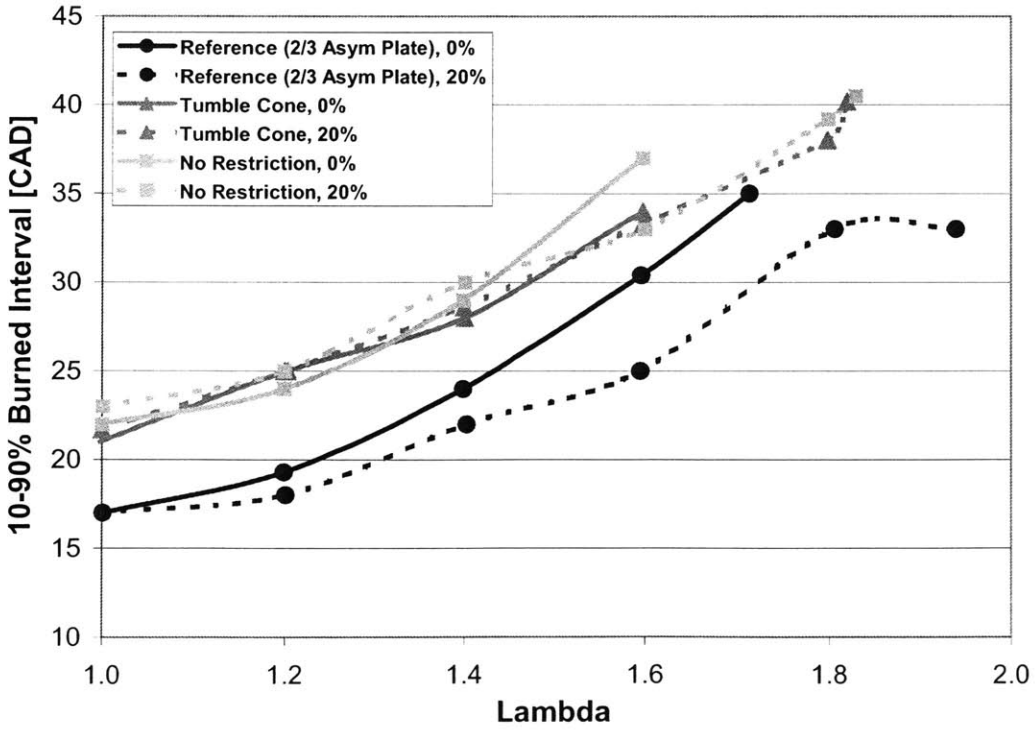

Figure 4.3.2.8- Chg. Motion Results 8: Reference (2/3 Asymmetric Restrictor Plate) vs. Tumble Cone and Baseline Unrestricted Head with 0 and 20% Enhancement

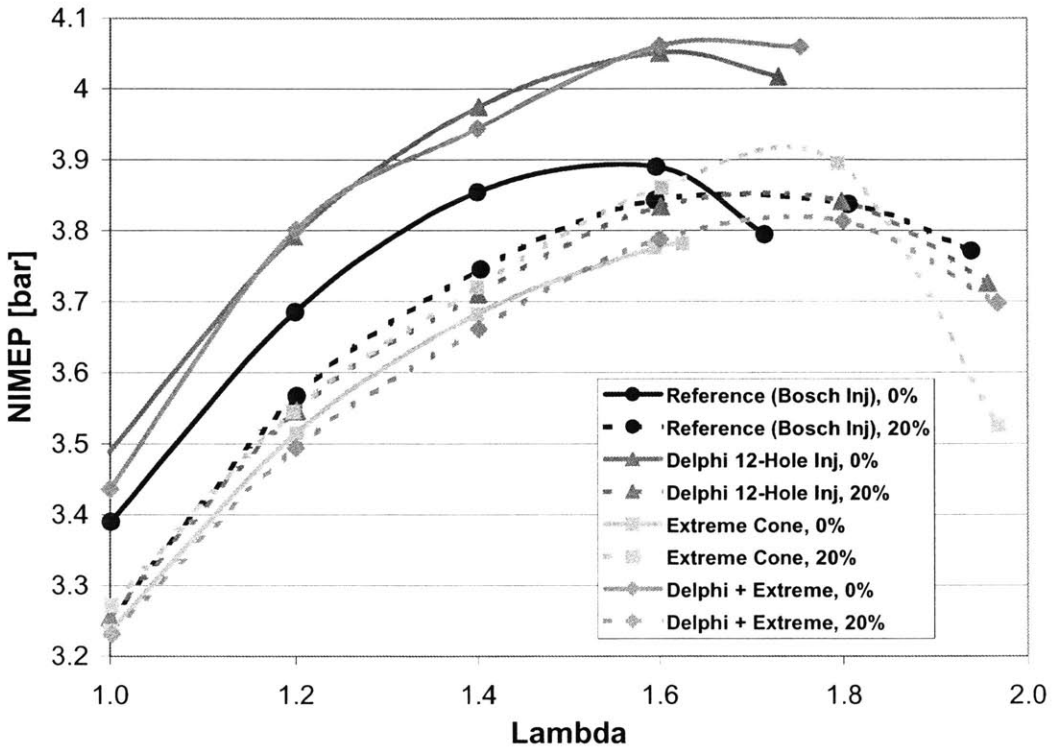

Figure 4.3.3.1- Mixture/ Composite Results 1: Reference (Bosch Injector) vs. Delphi Injector and Delphi Injector + Extreme Cone (Extreme Cone Only also Shown) with 0 and 20% Enhancement

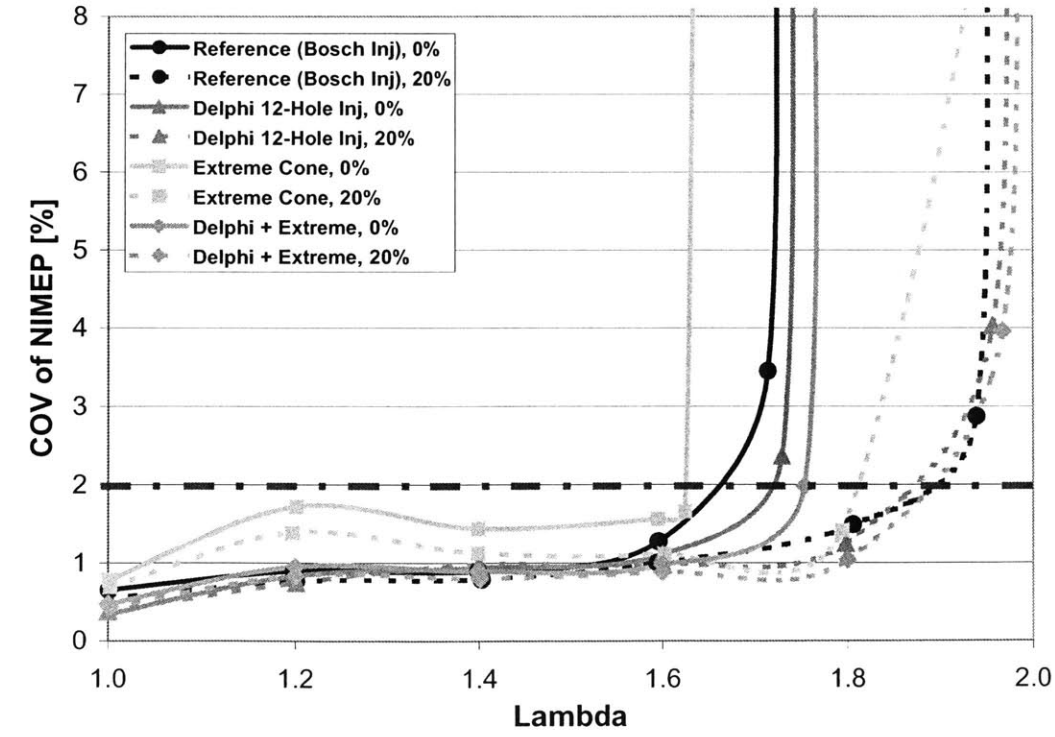

Figure 4.3.3.2- Mixture/ Composite Results 2: Reference (Bosch Injector) vs. Delphi Injector and Delphi Injector + Extreme Cone (Extreme Cone Only also Shown) with 0 and 20% Enhancement

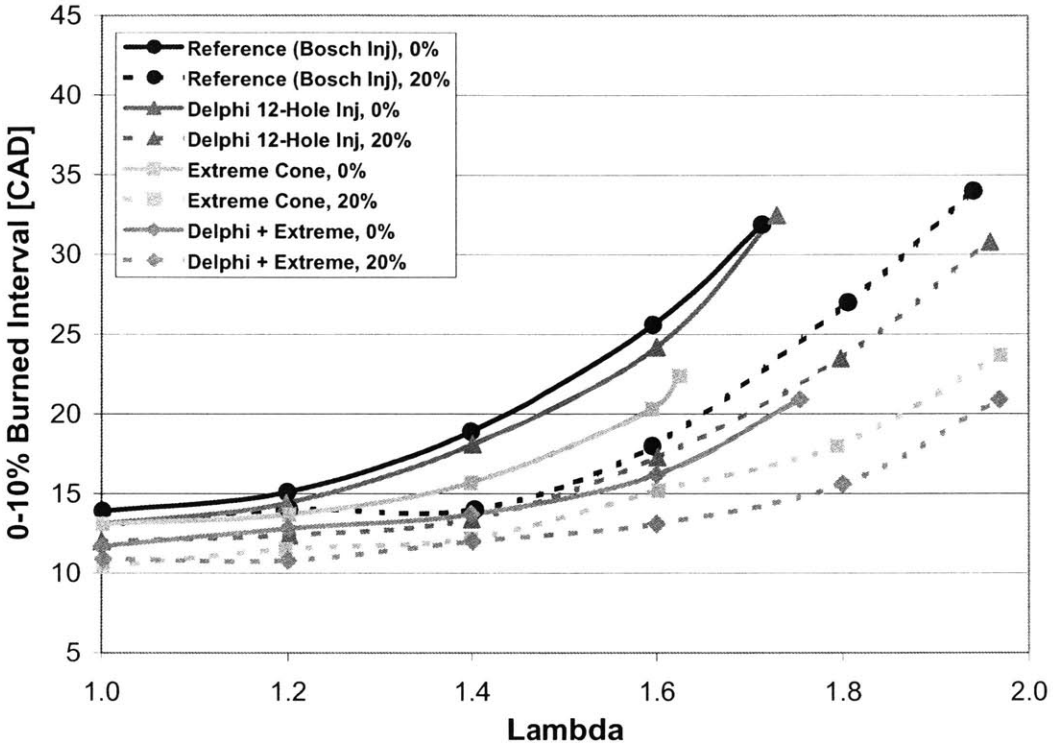

Figure 4.3.3.3- Mixture/ Composite Results 3: Reference (Bosch Injector) vs. Delphi Injector and Delphi Injector + Extreme Cone (Extreme Cone Only also Shown) with 0 and 20% Enhancement

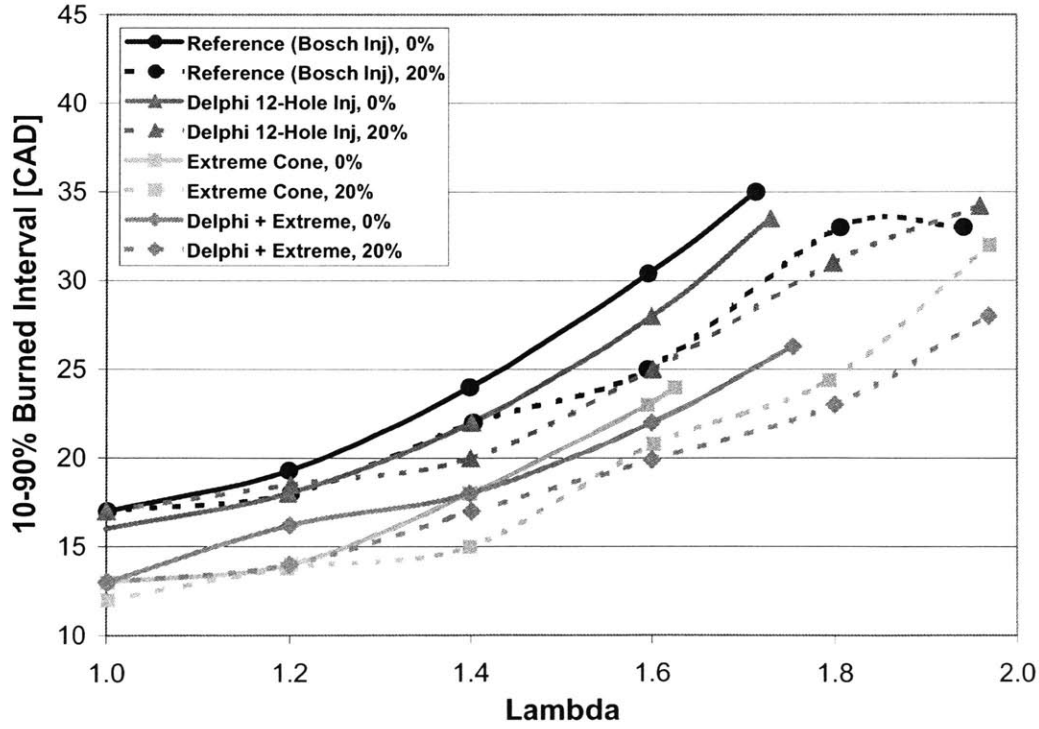

Figure 4.3.3.4- Mixture/ Composite Results 4: Reference (Bosch Injector) vs. Delphi Injector and Delphi Injector + Extreme Cone (Extreme Cone Only also Shown) with 0 and 20% Enhancement

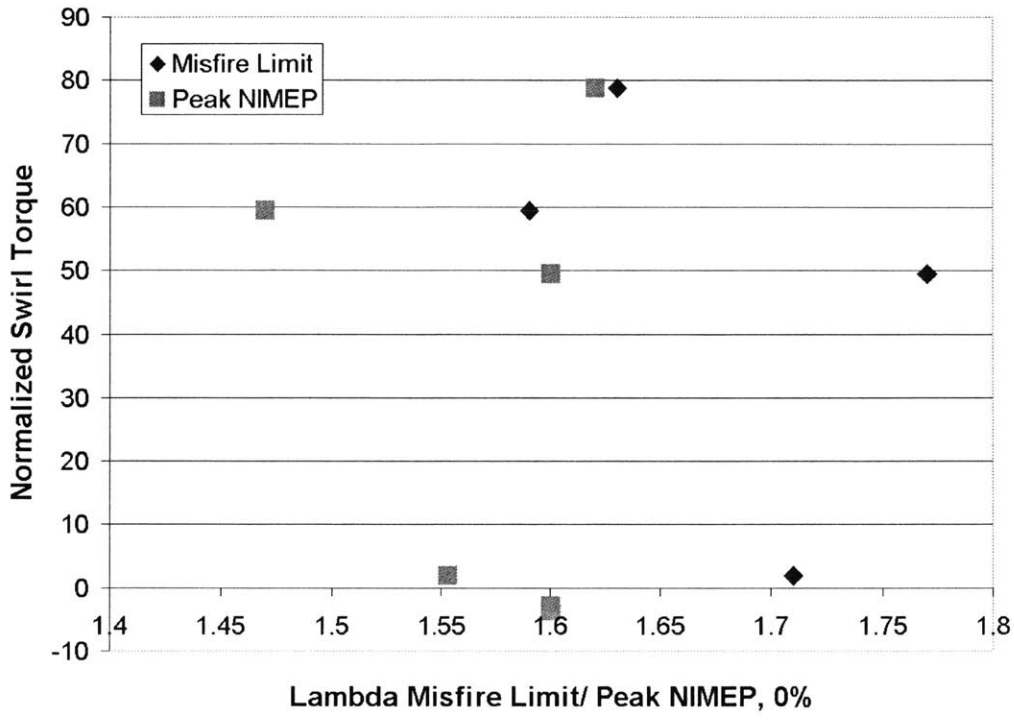

Figure 4.3.5.1- Normalized (to Flow Rate) Swirl Torque vs. Lambda at Lean Misfire Limit and Peak NIMEP Limit without Plasmatron Enhancement

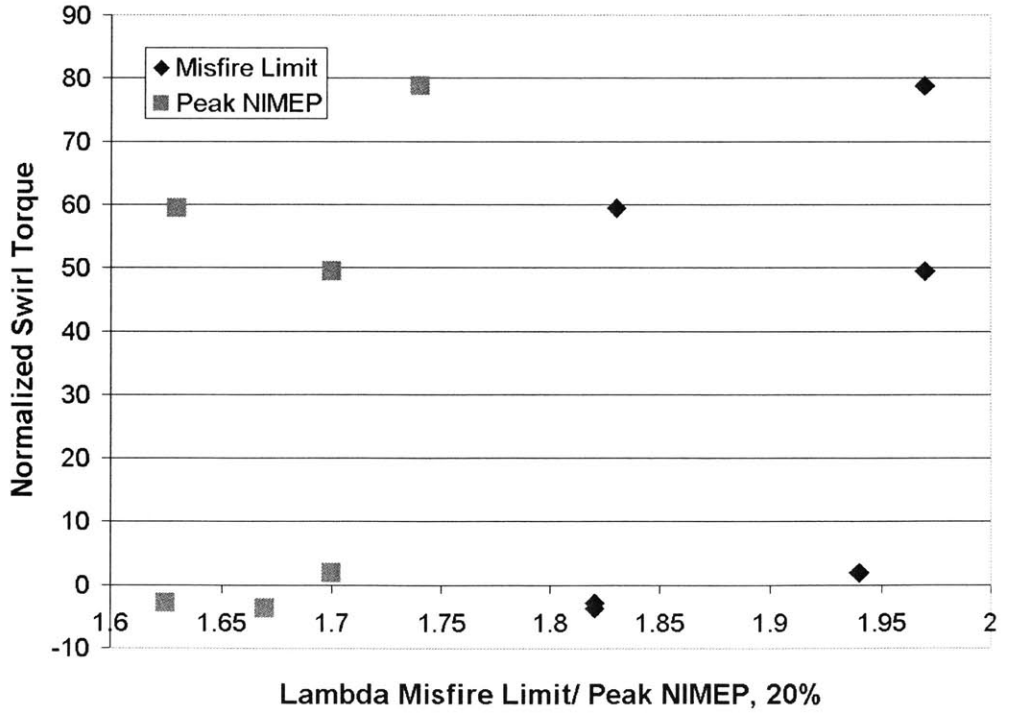

Figure 4.3.5.2- Normalized (to Flow Rate) Swirl Torque vs. Lambda at Lean Misfire Limit and Peak NIMEP Limit with 20% Plasmatron Enhancement

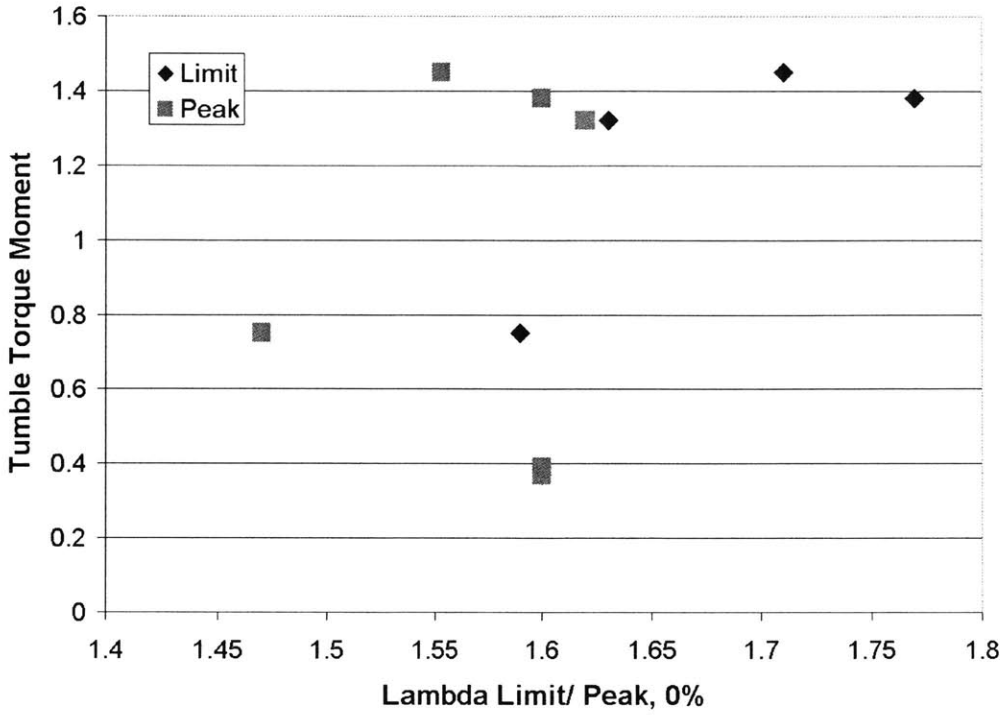

Figure 4.3.5.3- Tumble Torque Moment vs. Lambda at Lean Misfire Limit and Peak NIMEP Limit without Plasmatron Enhancement

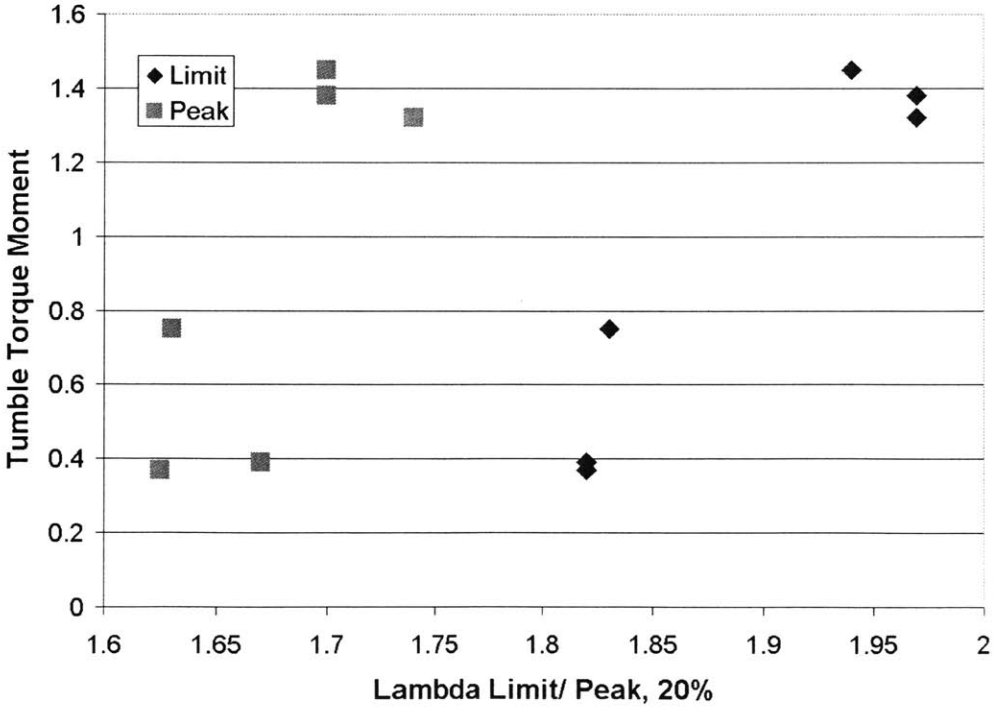

Figure 4.3.5.4- Tumble Torque Moment vs. Lambda at Lean Misfire Limit and Peak NIMEP Limit Point with 20% Plasmatron Enhancement

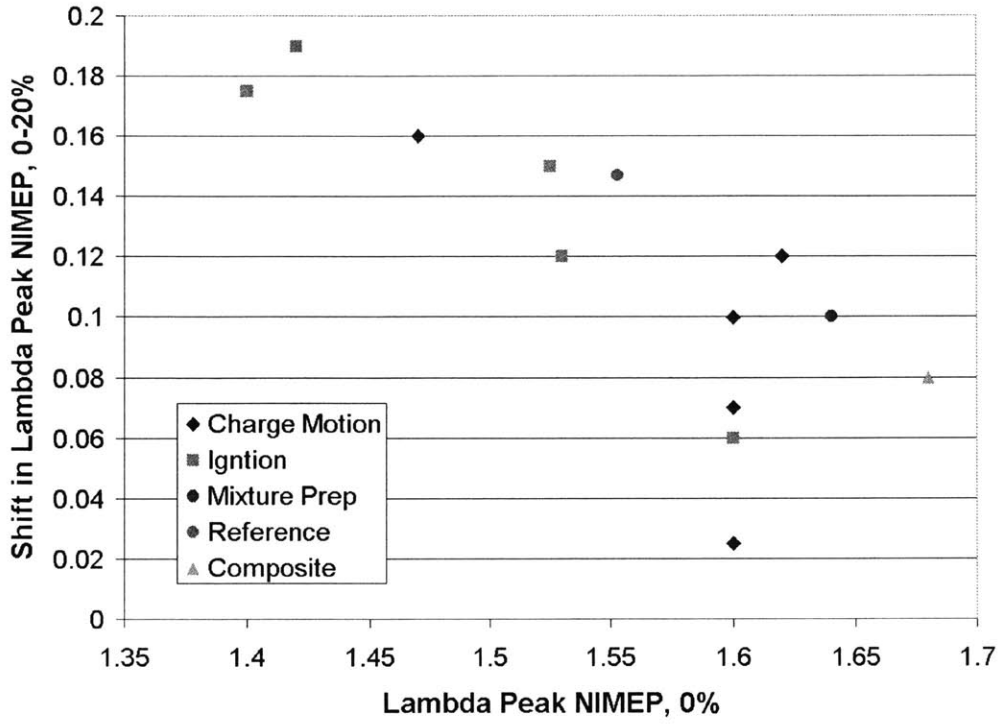

Figure 4.3.5.5- Absolute Shift in Lambda from Peak NIMEP Limit without Enhancement to Peak NIMEP Limit with 20% Enhancement vs. Peak NIMEP Limit without Enhancement

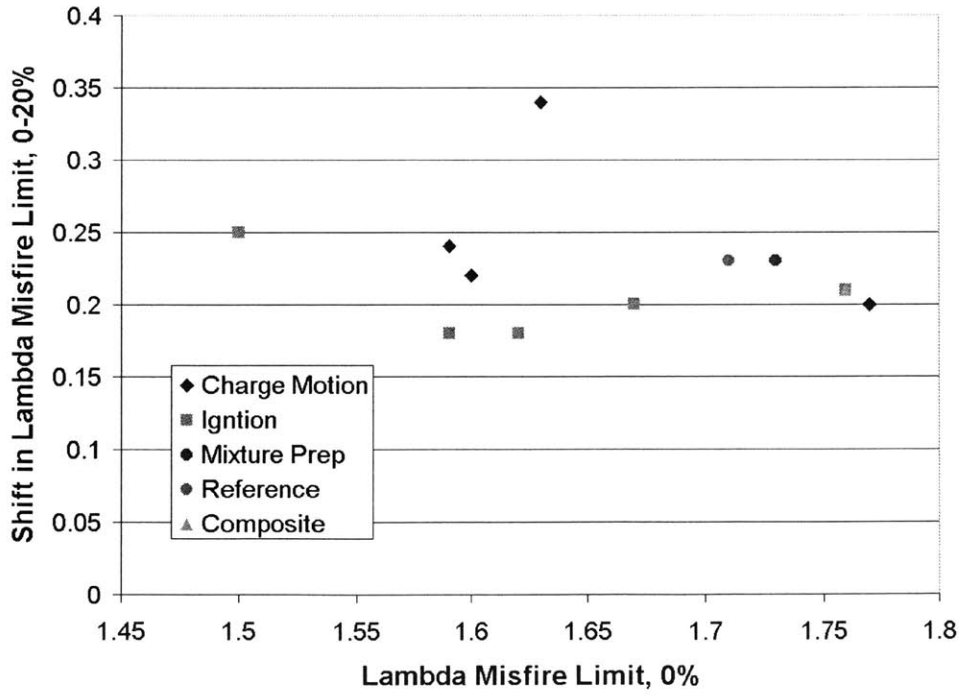

Figure 4.3.5.6- Absolute Shift in Lambda from Lean Misfire Limit without Enhancement to Lean Misfire Limit with 20% Enhancement vs. Lean Misfire Limit without Enhancement

4.4 EGR Experimental Results

One of the key benefits of EGR dilution is a dramatic reduction in engine-out NO_x emissions, and experimental results verify this trend (Figure 4.4.1). Regardless of engine load or plasmatron enhancement fraction, the greatest reduction in NO_x is seen with the first 10% of EGR fraction. Not surprisingly, NO_x concentrations are higher during high load operation, when combustion temperatures are greatest. Plasmatron addition also has a positive effect on NO_x levels, with lower concentrations measured at each EGR fraction for both high and low load conditions. This is largely explained by the chemical behavior of the CO molecules that are introduced through plasmatron addition. During the combustion process, these CO molecules oxidize before N_2, reducing the availability of free O_2 molecules that would promote NO_x formation.

Other combustion metrics reveal that EGR dilution impacts combustion performance in a manner similar to lean dilution with air. Engine stability behavior is comparable with the COV of NIMEP tending to remain below the 2% threshold until close to the misfire limit, at which point COV increases very rapidly (Figure 4.4.2). Plasmatron enhancement serves to improve combustion stability by delaying the EGR diluted misfire limit. The effect is greater with 30% enhancement than with 15% enhancement. Furthermore, EGR dilution tolerance is greater at high load operation, as prior research has also found [24]. MIT Sloan Laboratory colleague Ziga Ivanic has observed a similar trend in tests that characterize lean dilution tolerance at varied load conditions. It was not possible to reach the EGR dilution misfire limit for the higher load operating point with 30% plasmatron addition because the installed EGR system cannot deliver more than 46% EGR fraction under these conditions. Even at this extreme dilution level, combustion remains stable with COV < 1%. The 10-90% burned interval data also leads to some interesting conclusions. Without any enhancement, both the low load and higher load data indicate very similar combustion speed with the higher load points having a slight edge at high dilution (Figure 4.4.3). With plasmatron enhancement, combustion becomes progressively faster as 15 and 30% reformate fractions are added. The noteworthy trend is that these combustion speeding effects are more pronounced at higher loads, with the 5.2 bar NIMEP points seeing the greatest improvement. Even out at close to 50% EGR fraction, the high load 30% enhanced condition sees a 0-10% interval of just over 20 CAD, affirming that combustion remains stable.

Lastly, the 10-90% burned interval data show similar trends with progressively higher enhancement fractions speeding combustion (Figure 4.4.4). Again, these improvements are more pronounced at higher load operation, where overall duration of the 10-90% interval is shorter than at low load 3.5 bar NIMEP conditions.

In summary, these EGR results affirm the NO_x reducing effects of recirculated exhaust gas. Furthermore, EGR dilution behavior closely matches lean dilution behavior in that high dilution fractions lead to degraded combustion stability and slower burn intervals. Plasmatron enhancement is able to reverse these effects and promote stable operation at higher dilution rates. This similar behavior encourages the use of TDP as a means for comparing EGR diluted operation with lean diluted operation. In this way, the lean combustion optimization results may be extended to suggest means for improving EGR diluted combustion systems.

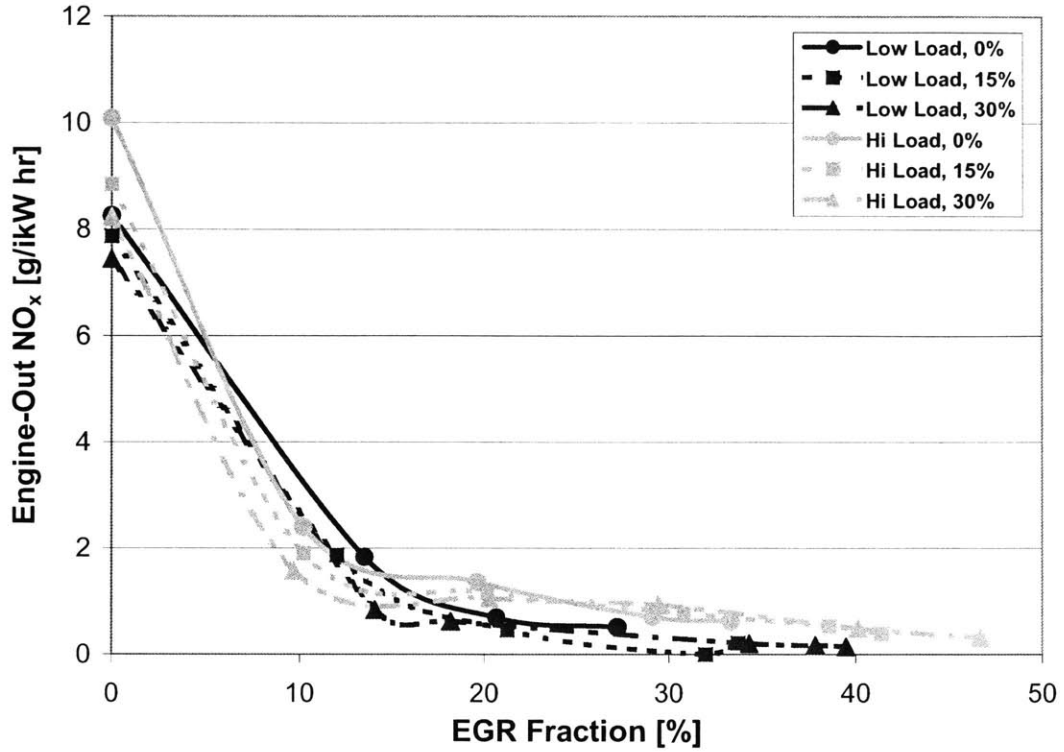

Figure 4.4.1- EGR Results 1: Engine Out-NO_x vs. EGR Fraction at Low Load (3.5 bar NIMEP) and High Load (5.2 bar NIMEP) Conditions with 0, 15, and 30% Enhancement

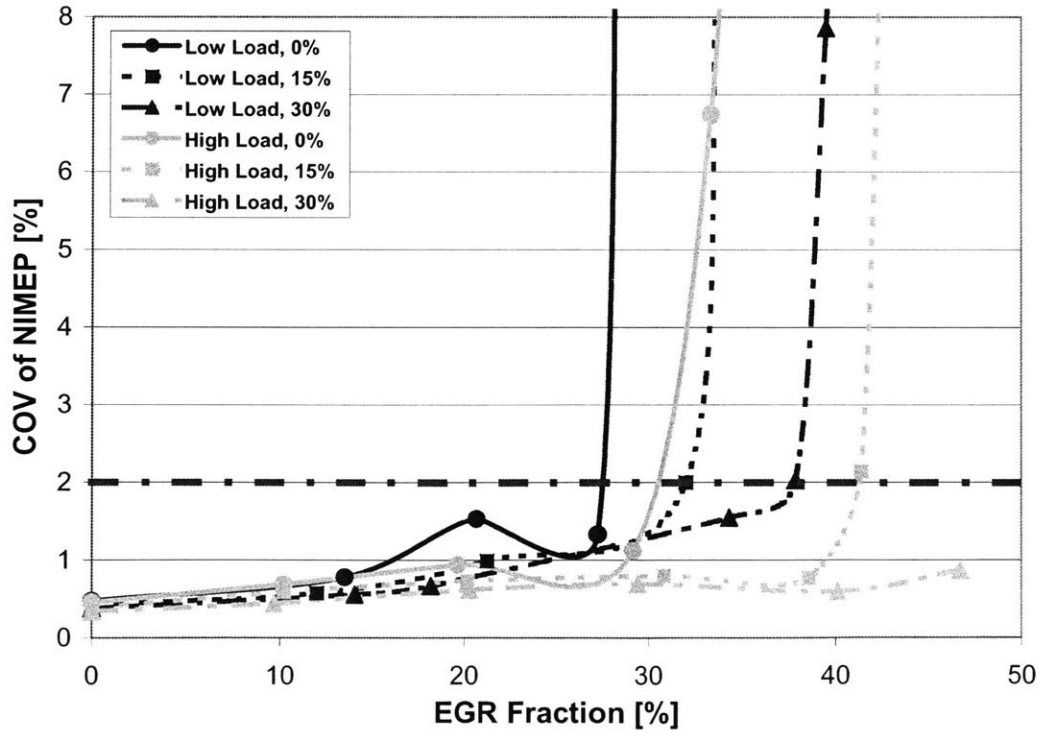

Figure 4.4.2- EGR Results 2: COV of NIMEP vs. EGR Fraction at Low Load (3.5 bar NIMEP) and High Load (5.2 bar NIMEP) Conditions with 0, 15, and 30% Enhancement

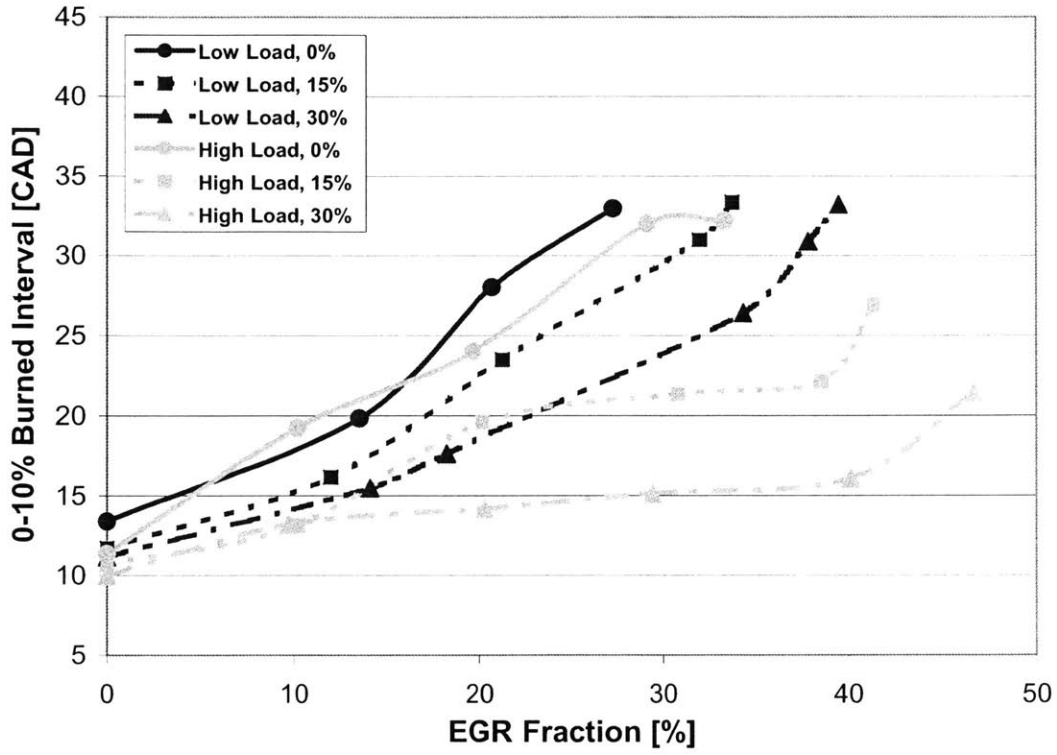

Figure 4.4.3- EGR Results 3: 0-10% Burned Interval vs. EGR Fraction at Low Load (3.5 bar NIMEP) and High Load (5.2 bar NIMEP) Conditions with 0, 15, and 30% Enhancement

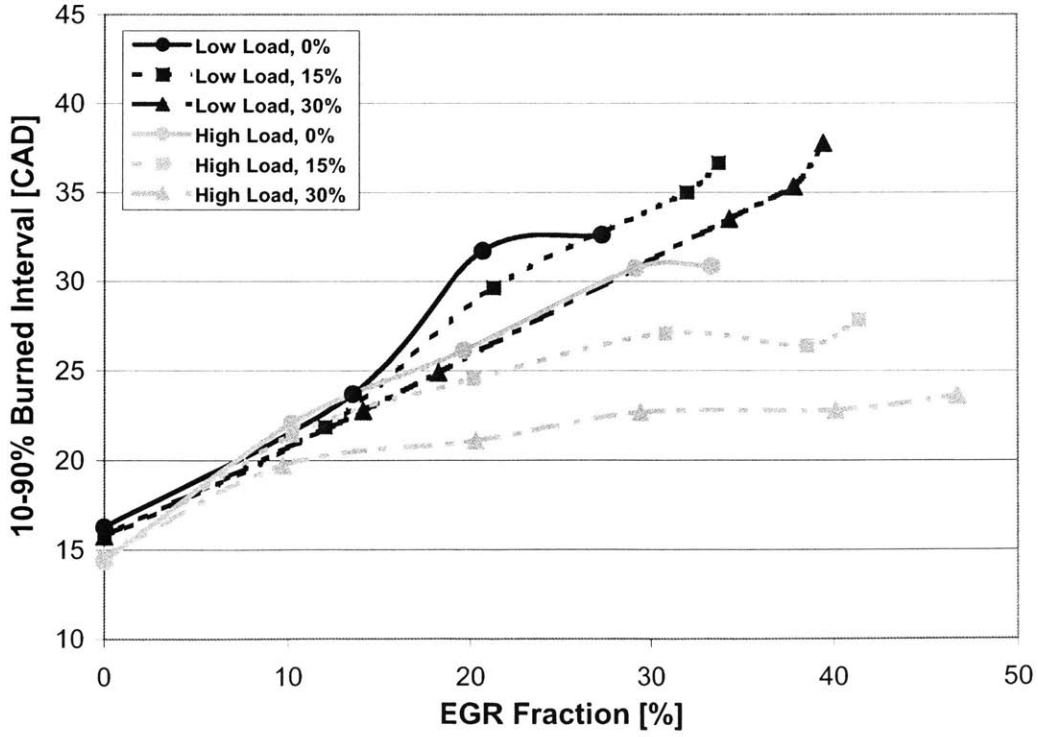

Figure 4.4.4- EGR Results 4: 10-90% Burned Interval vs. EGR Fraction at Low Load (3.5 bar NIMEP) and High Load (5.2 bar NIMEP) Conditions with 0, 15, and 30% Enhancement

4.5 TDP Correlation

Using the TDP parameter, it is possible to plot lean diluted experimental data together with EGR diluted experimental data to make useful comparisons. Charts have been prepared to show combustion performance data for the reference lean combustion system (the same setup used during the EGR tests) at both 0 and 20% enhancement fractions, along with low and higher load EGR diluted data at 0, 15, and 30% enhancement fractions. Considering the different test conditions used to obtain the data (varying low load for the lean data, fixed 3.5 and 5.2 bar NIMEP load for the EGR data,) and the varied enhancement fractions used, it may be difficult to make direct comparisons; however these charts still illustrate the potential of TDP. At non-enhanced conditions, lean operation seems to allow for higher dilution before the sharp increase of COV that accompanies the misfire limit (Figure 4.5.1). With 20% enhancement, lean diluted performance seems to fall between 15 and 30% enhanced higher load EGR dilution. Similar results are also seen in the 0-10% burned interval data. The non-enhanced lean diluted trace has faster burn than the EGR diluted traces, however, the 20% enhanced lean performance seems to fall between the 15 and 30% enhanced high load EGR performance until TDP = 1.5, after which is trails both (Figure 4.5.2). Similar performance is again observed in the 10-90% burned interval with lean dilution outperforming under non-enhanced conditions. At 20% enhancement, the lean condition again demonstrates combustion speed between the 15 and 30% enhanced high load EGR conditions until about TDP = 1.5, after which performance deteriorates (Figure 4.5.3).

In order to show which EGR fractions and lambda values represent comparable levels of dilution, a scatter plot has been prepared using data from experimental operating points (Figure 4.5.4). The vertical axes show measured EGR fraction (EGR diluted points) or equivalence ratio (lean diluted points) against calculated TDP. Equivalence ratio ($\phi = 1 / \lambda$) is used to indicate leanness because it allows the lean data to collapse with the EGR data. This chart can be used as a guideline for estimating either the EGR or air dilution tolerance of a particular combustion system if data is available for one form of dilution but not the other. Furthermore, the figure can be used to estimate how the various optimized combustion systems explored in section 4.3 would perform under high EGR dilution operation.

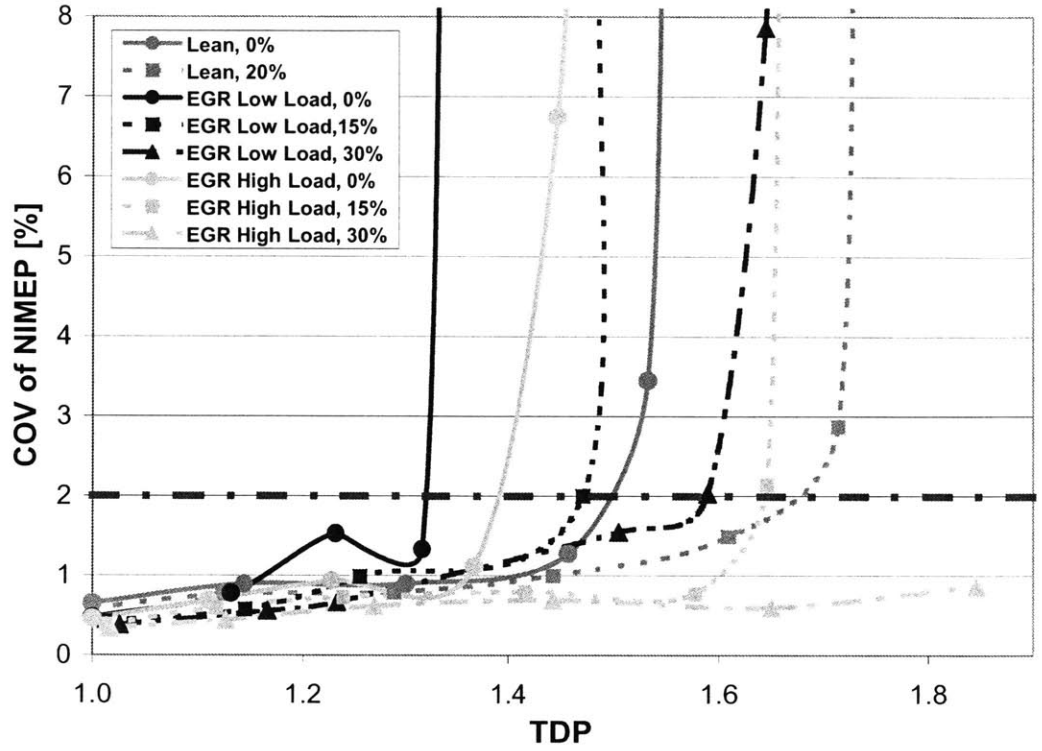

Figure 4.5.1- COV of NIMEP vs. TDP at Lean-Diluted and Low (3.5 bar NIMEP) and High (5.2 bar NIMEP) Load EGR-Diluted Conditions with Varied Fractions of Enhancement

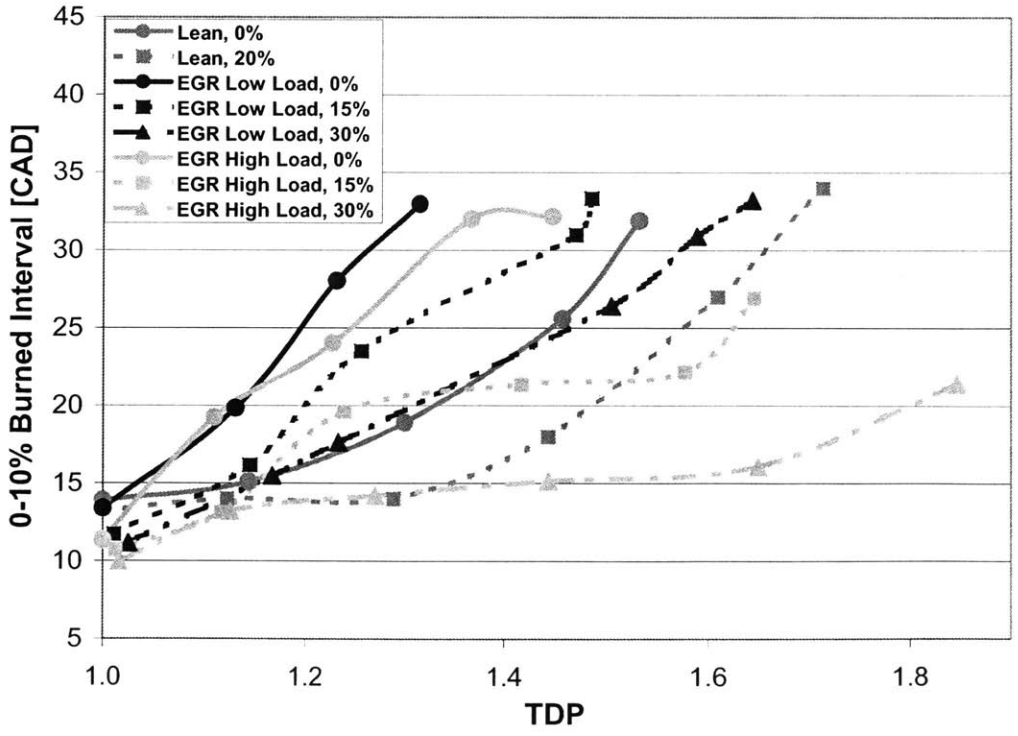

Figure 4.5.2- 0-10% Burned Interval vs. TDP at Lean-Diluted and Low (3.5 bar NIMEP) and High (5.2 bar NIMEP) Load EGR-Diluted Conditions with Varied Fractions of Enhancement

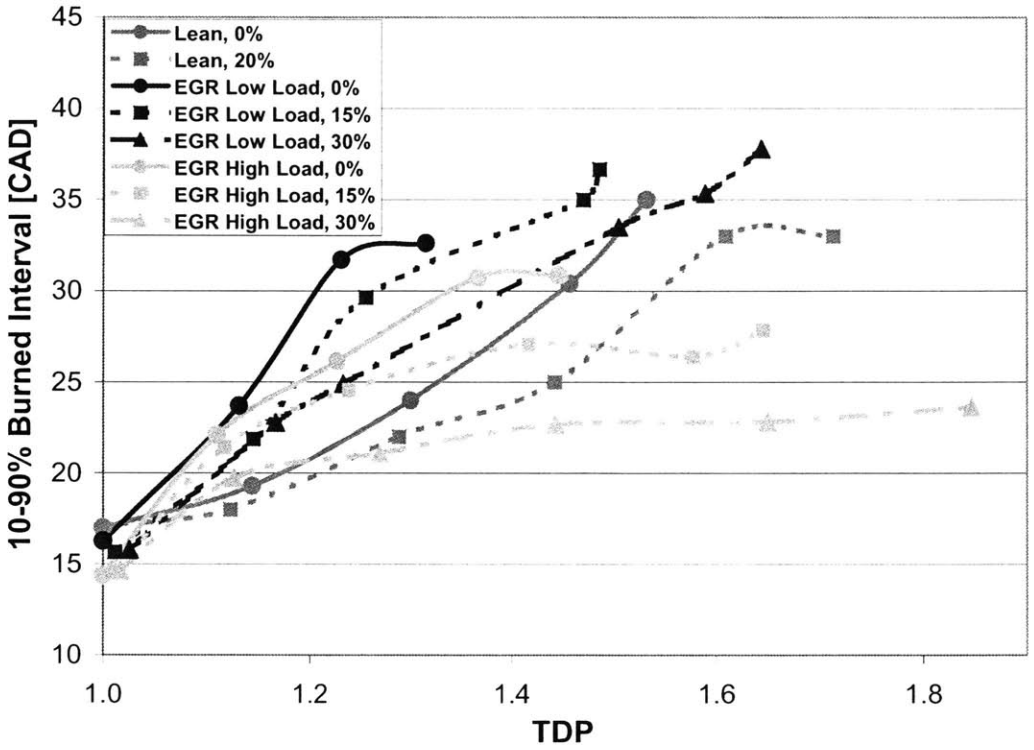

Figure 4.5.3- 10-90% Burned Interval vs. TDP at Lean-Diluted and Low (3.5 bar NIMEP) and High (5.2 bar NIMEP) Load EGR-Diluted Conditions with Varied Fractions of Enhancement

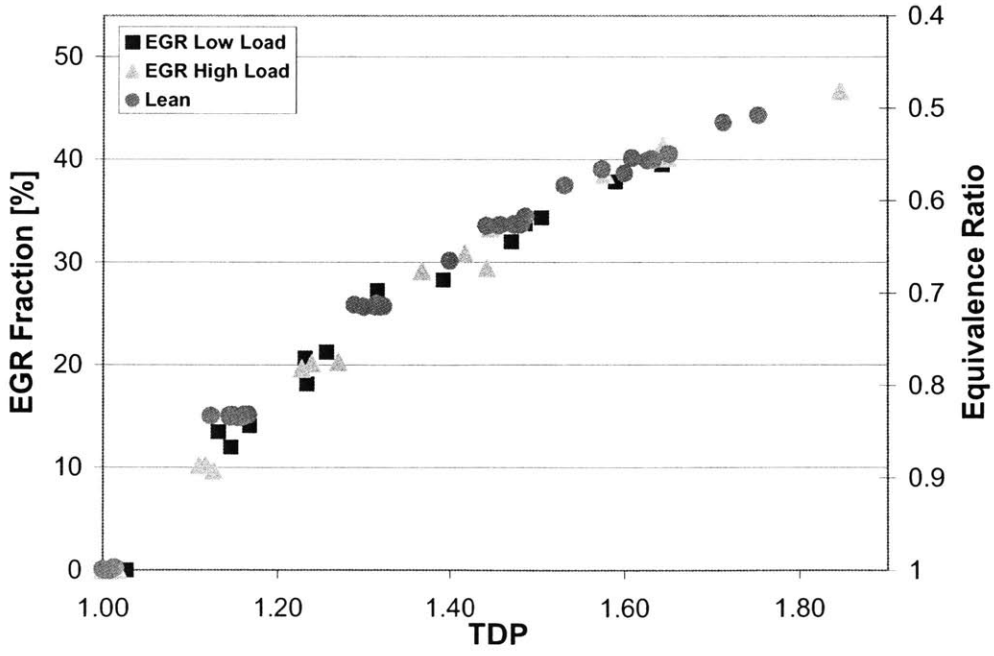

Figure 4.5.4- Correlation of Experimentally Obtained Low and High Load EGR-Diluted Data Points (EGR Fraction) and Lean-Diluted Data Points (Equivalence Ratio, $\phi = 1/\lambda$) vs. TDP

(This page was intentionally left blank.)

Chapter 5: Conclusions

The findings of this thesis may be summarized in a few concise statements:

1) Inlet restrictor plates and inlet port cones are a useful tool for quickly modifying the in-cylinder flow patterns of a given test engine. These devices may be tailored to allow different amounts of swirl and tumble, along with varied degrees of flow restriction. A properly designed plate or cone can be used to effectively simulate the charge motion control schemes used in series production engines, such as tumble control valves or inlet valve deactivation.

2) Optimizations of the combustion system coupled with hydrogen enhancement lead to significant improvements in lean combustion performance. Modifications to the combustion system in conjunction with 20% plasmatron addition produced a range of peak NIMEP limits between $\lambda = 1.58 - 1.74$ and a range of lean misfire limits between $\lambda = 1.75 - 1.97$. A series of trials has identified some of the best performing combustion system components. An inductive coil ignition with a wide gap J-plug helps to extend the three lean limits and encourages a fast 0-10% burned interval. High tumble charge motion configurations such as the 2/3 asymmetric restrictor plate, or the extreme or moderate turbulence cones encourage fast 0-10 and 10-90% burned intervals with good combustion stability. A fine-atomizing injector like the tested Delphi unit can also encourage faster burn. Finally, combining these different enhancements may lead to the best overall system performance.

3) No clear correlation has emerged between swirl generated in-cylinder motion and extension of the peak NIMEP limit or lean misfire limit. Conversely, high tumble in-cylinder motion configurations promote extension of both of these limits, particularly in combination with plasmatron addition. Experimental results show that the most extended lean limits are all achieved by configurations that generate large amounts of tumble motion.

4) Comparing different combustion systems, the improvement in peak NIMEP limit with 20% plasmatron enhancement declines linearly against the corresponding peak NIMEP limit of non-enhanced operation. The shift in the enhanced peak NIMEP limit ranges between $\lambda = 0.19 - 0.02$ over a range of non-enhanced peak NIMEP limits between $\lambda = 1.4 - 1.62$. In contrast, the improvement in the lean misfire limit with 20% plasmatron enhancement remains fairly constant and ranges between $\lambda = 0.18 - 0.25$. The difference in behavior may be explained by the different principles that govern the two limits. NIMEP output follows the trend behavior of engine efficiency with burn duration, which sees non-linear improvement due to the increase in combustion speed from hydrogen addition. The misfire limit is governed by flame quenching, which is a cutoff-type behavior that sees a nearly constant shift due to the effects of hydrogen addition on the molecular flame propagation process.

5) Dilution of air-fuel mixtures with EGR leads to a pronounced decline in NO_x emission. Over 75% of the reduction in engine-out NO_x concentration is achieved with a 10% EGR fraction. Highly EGR diluted mixtures behave similarly to lean diluted mixtures with decreased combustion speed leading to eventual instability and the onset of misfires and partial burns. Plasmatron enhancement can suppress these tendencies by promoting faster burn and the extension of the 2% COV of NIMEP and misfire dilution limits. Higher load conditions encourage faster and more stable combustion and magnify the improvements of adding progressively higher fractions of plasmatron reformate.

6) Thermal dilution parameter (TDP) can be used as a basis for comparing EGR and lean diluted data sets. Experimental results show that non-enhanced lean mixtures burn with slightly greater speed and stability than similarly diluted EGR mixtures while the 20% enhanced lean mixture behavior can be characterized as somewhere between the 15 and 30% enhanced high load EGR behavior. A correlation curve has been constructed to enable an approximation of which EGR fractions and lean equivalence ratios should result in similar combustion performance. This curve may also be used to predict the EGR dilution tolerance of the various combustion configurations studied during the optimization experiments.

References

[1] Heywood, J.B., Internal Combustion Engine Fundamentals, McGraw-Hill, Inc., New York, 1988.

[2] Tully, E.J., Heywood, J.B., "Lean-Burn Characteristics of a Gasoline Engine Enriched with Hydrogen From a Plasmatron Fuel Reformer," SAE 2003-01-0630.

[3] Kido, H., Huang, S., Tanoue, K., Nitta, T., "Improvement of Lean Hydrocarbon Mixtures Combustion Performance by Hydrocarbon Addition and Its Mechanisms," International Symposium, COMODIA 94, Yokohama, Japan, 1994.

[4] Tully, E.J., "Lean-Burn Characteristics of a Gasoline Engine Enriched with Hydrogen from a Plasmatron Fuel Reformer," SM Thesis, MIT Department of Mechanical Engineering, 2002.

[5] Topinka, J.A., Gerty, M.D., Heywood, J.B., Keck, J.C., "Knock Behavior of a Lean-Burn, H_2 and CO-Enhanced, SI Gasoline Engine Concept," SAE 2004-01-0975.

[6] Stokes, J., Lake T.H., Osbore, R.J., "A Gasoline Engine Concept for Improved Fuel Economy-The Lean Boost System," SAE 2000-01-2902.

[7] Glassman, I., Combustion, Academic Press, Inc., California, 1996.

[8] Geiger, J., Pischinger, S., Böwing, R., Koß, H.-J., Thiemann, J., "Ignition Systems for Highly Diluted Mixtures in SI-Engines," SAE 1999-01-0799.

[9] Lee, Y.G., Grimes, D.A., Boehler, T.A., Sparrow, J., Flavin, C., "A Study of the Effects of Spark Plug Electrode Design on 4-Cycle Spark-Ignition Engine Performance," SAE 2000-01-1210.

[10] Pischinger, S., Heywood, J.B., "How Heat Losses to the Spark Plug Electrodes Affect Flame Kernel Development in an SI-Engine," SAE 900021.

[11] Rivin, B., Dulger, M., Sher, E., "Extending Lean Misfire Limit of Methane-Air Mixtures by Means of an Enhanced Spark Discharge," SAE 1999-01-0573.

[12] Shen, H., Hinze, P.C., Heywood, J.B., "A Study of Cycle-to-Cycle Variations in SI Engines Using a Modified Quasi-Dimensional Model," SAE 961187.

[13] Heywood, J.B., "Combustion and its Modeling in Spark-Ignition Engines," International Symposium, COMODIA 94, Yokohama, Japan, 1994.

[14] Pajot, O., Mounaïm-Rouselle, C., Queiros-Conde, D., "New Data on Flame Behaviour in Lean Burn S.I. Engine," SAE 2001-01-1956.

[15] Fekete, N., et al., "Advanced Engine Control and Exhaust Gas Aftertreatment of a Leanburn SI Engine," SAE 972873.

[16] Endres, H., Neußer, H.-J., Wurms, R., "Influence of Swirl and Tumble on Economy and Emissions of Multi Valve SI Engines," SAE 920516.

[17] Stein, R.A., Chou, T., Lyjak, J.C., "The Combustion System of the Ford 5.4L 3-Valve Engine," Powertrain Conference, Dearborn, MI, September 2003.

[18] Matsuki, M., et al., "Development of a Lean Burn Engine with a Variable Valve Timing Mechanism," SAE 960583.

[19] Kobayashi, K., et al., "Effect of Fuel Atomization on the Lean-Burn Characteristics Under Steady Condition in a Spark-Ignition Engine," SAE 960460.

[20] Chevron Phillips Chemical Company LP, UTG-96 Specification Sheet, Specialty Chemicals Product Number: 10211671, Rev. 6/18/02.

[21] Balles, E.N., VanDyne, E.A., Wahl, A.M., Ratton, K., and Lai, M.C., "In-Cylinder Air/Fuel Ratio Approximation Using Spark Gap Ionization Sensing," SAE 980166.

[22] Chun, K., Heywood, J.B., "Estimating Heat-Release and Mass-of-Mixture Burned from Spark-Ignition Engine Pressure Data," Combustion Science and Technology, Vol. 54, pp. 133-143, 1987.

[23] Pischinger, S., Heywood, J.B., "A Model for Flame Kernel Development in a Spark-Ignition Engine," 23rd Symposium (International) on Combustion, The Combustion Institute, pp. 1033-1040, 1990.

[24] Shayler, P.J., Winborn, L.D., Hill, M.J., Eade, D., "The Influence of Gas/Fuel Ratio on Combustion Stability and Misfire Limits of Spark Ignition Engines," SAE 2000-01-1208.

[25] "Specification for Thesis Preparation, 2003-2004," MIT Libraries, Cambridge, MA, Summer 2003.

(This page was intentionally left blank.)

Appendix

Table A.1- Flow Bench Testing Results

Trial/	Inlet Valves		Volume	Swirl Torque		Tumble
Charge Motion Device	Left	Right	Flow	Absolute	Normalized	Moment
	[in]	[in]	[CFM]	[in oz]	[in oz/CFM]	
	0.050	0.050	36.1	0.2	5.5	0.84
Baseline/	0.100	0.100	75.1	-0.2	-2.7	0.25
Unrestricted B5254 Head	0.150	0.150	112.7	-0.6	-5.3	0.13
	0.200	0.200	139.4	-0.1	-0.7	0.41
	0.250	0.250	155.4	-0.5	-3.2	0.36
	0.300	0.300	165.9	-0.3	-1.8	0.43
	0.350	0.350	171.7	-0.5	-2.9	0.53
	0.400	0.400	175.0	-0.5	-2.9	0.56

Trial/	Inlet Valves		Volume	Swirl Torque		Tumble
Charge Motion Device	Left	Right	Flow	Absolute	Normalized	Moment
	[in]	[in]	[CFM]	[in oz]	[in oz/CFM]	
	0.050	0.050	36.1	-0.1	-2.8	0.69
Baseline Deactivated/	0.100	0.050	55.9	0.9	16.1	0.64
Unrestricted B5254 Head	0.150	0.050	75.2	1.7	22.6	0.71
	0.200	0.050	88.8	2.7	30.4	0.56
	0.250	0.050	97.3	3.5	36.0	0.48
	0.300	0.050	99.1	4.5	45.4	0.60
	0.350	0.050	100.9	5.3	52.5	0.72
	0.400	0.050	103.1	5.7	55.3	0.78

Trial/	Inlet Valves		Volume	Swirl Torque		Tumble
Charge Motion Device	Left	Right	Flow	Absolute	Normalized	Moment
	[in]	[in]	[CFM]	[in oz]	[in oz/CFM]	
	0.050	0.050	22.7	0.2	8.8	0.86
Extreme Turbulence/	0.100	0.100	32.5	1.0	30.8	1.06
Extreme Turbulence Cone	0.150	0.150	35.4	1.9	53.7	1.05
	0.200	0.200	36.2	2.4	66.3	1.23
	0.250	0.250	36.5	2.6	71.2	1.38
	0.300	0.300	36.6	2.8	76.5	1.35
	0.350	0.350	36.8	2.9	78.8	1.32
	0.400	0.400	36.8	2.9	78.8	1.27

Table A.1- Flow Bench Testing Results (continued)

Trial/	Inlet Valves		Volume	Swirl Torque		Tumble
Charge Motion Device	Left	Right	Flow	Absolute	Normalized	Moment
	[in]	[in]	[CFM]	[in oz]	[in oz/CFM]	
	0.050	0.050	22.7	0.2	8.8	1.04
Extreme Deactivated/	0.100	0.050	32.4	1.0	30.9	0.96
Extreme Turbulence Cone	0.150	0.050	35.3	1.9	53.8	0.97
	0.200	0.050	36.1	2.4	66.5	1.14
	0.250	0.050	36.4	2.6	71.4	1.22
	0.300	0.050	36.6	2.8	76.5	1.23
	0.350	0.050	36.7	2.9	79.0	1.18
	0.400	0.050	36.7	3.0	81.7	1.13

Trial/	Inlet Valves		Volume	Swirl Torque		Tumble
Charge Motion Device	Left	Right	Flow	Absolute	Normalized	Moment
	[in]	[in]	[CFM]	[in oz]	[in oz/CFM]	
	0.050	0.050	27.1	0.2	7.4	1.06
Moderate Turbulence/	0.100	0.100	36.2	0.7	19.3	1.09
Moderate Turbulence	0.150	0.150	39.4	1.0	25.4	1.34
Cone	0.200	0.200	40.0	1.3	32.5	1.23
	0.250	0.250	40.4	1.5	37.1	1.29
	0.300	0.300	40.4	1.8	44.6	1.35
	0.350	0.350	40.4	2.0	49.5	1.38
	0.400	0.400	40.4	2.2	54.5	1.39

Trial/	Inlet Valves		Volume	Swirl Torque		Tumble
Charge Motion Device	Left	Right	Flow	Absolute	Normalized	Moment
	[in]	[in]	[CFM]	[in oz]	[in oz/CFM]	
	0.050	0.050	29.6	0.3	10.1	1.38
Port Deactivation/	0.100	0.100	49.6	0.9	18.1	0.40
Port Deactivation Cone	0.150	0.150	67.2	2.4	35.7	0.79
	0.200	0.200	75.7	3.1	41.0	0.59
	0.250	0.250	81.1	3.6	44.4	0.66
	0.300	0.300	82.5	4.3	52.1	0.73
	0.350	0.350	84.2	5.0	59.4	0.75
	0.400	0.400	85.9	5.7	66.4	0.84

Table A.1- Flow Bench Testing Results (continued)

Trial/	Inlet Valves		Volume	Swirl Torque		Tumble
Charge Motion Device	Left	Right	Flow	Absolute	Normalized	Moment
	[in]	[in]	[CFM]	[in oz]	[in oz/CFM]	
	0.050	0.050	35.0	-0.1	-2.9	0.73
Tumble Motion/	0.100	0.100	62.1	-0.1	-1.6	0.21
Tumble Cone	0.150	0.150	75.5	0.1	1.3	0.35
	0.200	0.200	78.9	0.1	1.3	0.46
	0.250	0.250	79.2	-0.1	-1.3	0.41
	0.300	0.300	79.5	-0.2	-2.5	0.39
	0.350	0.350	80.0	-0.3	-3.8	0.39
	0.400	0.400	80.2	-0.3	-3.7	0.44

Trial/	Inlet Valves		Volume	Swirl Torque		Tumble
Charge Motion Device	Left	Right	Flow	Absolute	Normalized	Moment
	[in]	[in]	[CFM]	[in oz]	[in oz/CFM]	
	0.050	0.050	31.5	0.2	6.3	0.44
2/3 Asymmetric Plate/	0.100	0.100	47.4	0.3	6.3	0.59
2/3 Asymmetric Restrictor	0.150	0.150	51.0	0.2	3.9	1.19
Plate (Reference)	0.200	0.200	52.0	0.1	1.9	1.31
	0.250	0.250	52.1	0.2	3.8	1.42
	0.300	0.300	52.3	0.0	0.0	1.43
	0.350	0.350	52.3	0.1	1.9	1.45
	0.400	0.400	52.3	0.0	0.0	1.42

Trial/	Inlet Valves		Volume	Swirl Torque		Tumble
Charge Motion Device	Left	Right	Flow	Absolute	Normalized	Moment
	[in]	[in]	[CFM]	[in oz]	[in oz/CFM]	
	0.050	0.050	31.9	0.0	0.0	0.47
2/3 Symmetric Plate/	0.100	0.100	49.7	0.0	0.0	0.41
2/3 Symmetric Restrictor	0.150	0.150	53.6	-0.1	-1.9	1.35
Plate	0.200	0.200	54.6	-0.1	-1.8	1.33
	0.250	0.250	55.0	-0.2	-3.6	1.29
	0.300	0.300	54.8	-0.3	-5.5	1.24
	0.350	0.350	54.9	-0.4	-7.3	1.19
	0.400	0.400	54.9	-0.3	-5.5	1.13

Table A.1- Flow Bench Testing Results (continued)

Trial/ Charge Motion Device	Inlet Valves		Volume	Swirl Torque		Tumble
	Left [in]	Right [in]	Flow [CFM]	Absolute [in oz]	Normalized [in oz/CFM]	Moment
	0.050	0.050	35.7	0.2	5.6	0.41
1/3 Symmetric Plate	0.100	0.100	71.4	-0.2	-2.8	0.21
1/3 Symmetric Restrictor	0.150	0.150	99.2	-0.2	-2.0	0.40
Plate	0.200	0.200	114.6	-0.5	-4.4	0.55
	0.250	0.250	122.3	-0.6	-4.9	0.61
	0.300	0.300	127.2	-0.8	-6.3	0.64
	0.350	0.350	129.1	-1.0	-7.7	0.67
	0.400	0.400	129.9	-1.1	-8.5	0.69

Table A.2- Experimental Lean Misfire Limit and Peak NIMEP Limit Results

Configuration	Lean Misfire Limit [lambda]		Peak NIMEP Limit [lambda]		Peak NIMEP [bar]	
	Enhancement		Enhancement		Enhancement	
	0%	20%	0%	20%	0%	20%
Reference	1.71	1.94	1.55	1.70	3.88	3.85
Denso 580 Ignition, 0.070 in Gap	1.76	1.97	1.53	1.68	3.97	3.97
Adrenaline Ignition CD (Low Energy)	1.59	1.77	1.53	1.65	3.93	3.75
Adrenaline Ignition DE (High Energy)	1.67	1.87	1.60	1.66	3.95	3.83
MSD Digital 7 Ignition, 0.035 in Gap	1.50	1.75	1.42	1.61	3.82	3.88
MSD Digital 7 Ignition, 0.070 in Gap	1.62	1.80	1.40	1.58	3.83	3.86
Extreme Turbulence Cone	1.63	1.97	1.62	1.74	3.78	3.92
Moderate Turbulence Cone	1.77	1.97	1.60	1.70	3.87	3.85
Port Deactivation Cone	1.59	1.83	1.47	1.63	3.75	3.76
Tumble Cone	1.60	1.82	1.60	1.67	3.95	3.88
Baseline Unrestricted Head	1.60	1.82	1.60	1.63	3.88	3.92
Delphi Injector	1.73	1.96	1.64	1.74	4.05	3.86
Delphi Injector + Moderate Cone	1.76	1.97	1.68	1.76	4.07	3.83